THE UNIVERSITY OF CHICAGO

COMPUTATIONAL BENEFITS AND BEHAVIORAL IMPLICATIONS OF MULTIDIMENSIONAL SENSORY TUNING

A DISSERTATION SUBMITTED TO

THE FACULTY OF THE DIVISION OF THE BIOLOGICAL SCIENCES

AND THE PRITZKER SCHOOL OF MEDICINE

IN CANDIDACY FOR THE DEGREE OF

DOCTOR OF PHILOSOPHY

COMMITTEE ON NEUROBIOLOGY

BY

MATTHEW MACELLAIO

CHICAGO, ILLINOIS

JUNE 2018

Copyright

Dedication

To my dad, Joe Macellaio; Josephine; and Mario.

Life would be tragic if it weren't funny.
Be curious. And however bad life may seem,
there is always something you can do, and succeed at.
– Stephen Hawking

Acknowledgments

Advisor

Leslie Osborne

Thesis Committee

Nicho Hatsopoulos

Stephanie Palmer

Jason Maclean

Osborne Lab, past and present

Trishna Mukherjee

Bing Liu

Sangwook Alex Lee

Claudio Simoncini

Stephanie Thomas

Erika Aitken

George Zakhary

Amedeo, Burrhus, Copernicus, Diogenes, Erasmus, Fermi, Galileo

ARC Veterinary and Husbandry Staff

Neuroscience Department Administration

My family and friends

Table of Contents

List of Figures

Abstract

Organisms' behaviors and perceptions are shaped by the manner in which the brain processes incoming sensory information. Different sensory streams of the brain manage and process disparate types of inputs from sensory receptors in order to transform sensory information into decision and action. To adequately achieve this goal, neurons in many areas simultaneously encode multiple features of the outside world. Jointly encoding various features can, however, lead to ambiguity in the decoding process: single-trial fluctuations in the spike rate of a neuron can represent a change in any or all of the encoded stimulus features. To explore the benefits and impacts of joint coding, we probed the macaque visuomotor pathway. In the first study, we used information theoretic methods to quantify the benefit of joint coding of direction and speed in single neurons in extrastriate area MT, in small simulated populations, and in smooth pursuit eye movements. We found that there is a consistent benefit to encoding multiple stimulus features jointly rather than separately, which we call stimulus synergy. Additionally, we determined that the scale of stimulus synergy can be altered by the tuning bandwidth and the number of stimulus features encoded. The observation of stimulus synergy in pursuit eye movements implies that the MT population is being read out jointly, as a motion vector. In the second study, we further investigated the interaction of direction and speed in pursuit eye movements. We found that single-trial direction and speed errors are correlated, bolstering our claim that fluctuations in the MT population response are jointly decoded to generate direction and speed estimates. Finally, we confirm using simulated MT responses that such correlations can only occur when

decoding motion estimates from MT as a motion vector, not as direction and speed separately.

CHAPTER I

Introduction

Overview

Viewed from the perspective of systems neuroscience, the brain's function is to generate behavior and perception by efficiently transforming incoming sensory information. The localized areas of the brain form a recurrently connected hierarchy that can quickly process many aspects of the environment. Each area of the brain may be described to handle one category of processing, but even neurons involved in early processing respond to many low-level sensory features from the periphery. Therefore, understanding how single neurons encode multiple features simultaneously, and the impact of that joint coding on behavior and perception, is critical to fully grasping information processing.

Joint encoding of multiple features of a stimulus causes ambiguity in decoding. Specifically, trial-to-trial fluctuations in a neuron's spike rate can be interpreted as representing a change in any or all of the stimulus features encoded. However, the brain manages to overcome this ambiguity, encoding multiple features and reading them out to drive behavior with high levels of precision. The details of how cortical circuits manage to achieve this are still poorly known. To explain the process of transformation of jointly tuned features requires a multi-pronged approach: probing neural responses in sensory areas, analyzing behavioral output, and combining results from both ends with simulations to test competing theories. By doing so, we can glean insight into how fundamental transformations occur in sensorimotor processing.

Joint encoding of multiple features in cortex

What is the best way to understand what a single neuron, or a population of neurons, is communicating about a stimulus? Some of the most evocative early studies of visual neuroscience, by Hubel and Weisel, focused on single features of a neuron's response to a stimulus. By sweeping a bright bar across a screen and recording the number of spikes fired by a neuron, they could describe the spatial range to which a neuron would fire spikes (its receptive field), the neuron's response to different orientations of the bar, and how the response was modulated based on the contrast of that bar against the background [1,2]. The neuron's modulation to each feature can be systematically probed, and described in terms of the stimulus to which the neuron responds most strongly, or tuning preference, and the range of that feature to which it responds. Neurons in macaque primary visual cortex, V1, are tuned to low-level visual features such as color, orientation, and contrast [3,4]. Similarly, primary auditory cortical neurons in A1 are tuned to pitch and intensity, among other features [5]. Since many neurons in early cortical areas smoothly change the magnitude of their responses across the range of a stimulus feature, categorizing tuning along one feature allows downstream brain areas as well as researchers to easily translate a spike count or pattern into a stimulus.

Early sensory feature representations are decoded to drive behavior and generate perceptual judgments, and are further transformed by combining them with other features to generate new features. This process requires integrating responses across many neurons, producing secondary sensory areas that can be invariant to

low-level sensory features but are tuned to higher-level features. For example, V1 simple cells that respond to the static orientation of bars provide input to V1 complex cells in such a circuit that the complex cells are tuned to the orientation of a bar regardless of its location in their receptive field [6,7]. One step further in the stream of processing are cells in the middle temporal area, or MT, that are driven by motion direction and speed of a variety of stimuli, as well as three-dimensional motion and binocular disparity [8–10].

A widespread feature of sensory cortical areas is that neurons modulate their responses to multiple features of their sensory modalities. Each of the sensory representations in primary cortical areas is a transformation of the information transmitted via subcortical pathways from the sensory periphery, whether it be retina, cochlea, or stretch and pressure receptors in skin. Low-level features of the sensory modality from the periphery, such as the on/off activity of rods and cones, has been transformed into basic features of vision by the time they are represented in cortex [11,12]. Tuning to multiple features can exist such that the neuron's tuning to feature A does not substantially change as a function of feature B: although the amplitude of the tuning curve may be scaled, the tuning preference remains stable [13–15]. Such tuning to multiple features is called "separable": the tuning curves for A and B are independent, and the mean spike count for the joint tuning curve can be fully described by the product of the tuning curves for A and B [16–18]. In contrast, inseparable tuning describes the condition in which feature B and feature A's tuning curves are linked in such a way that one must know the value of one feature to properly determine the other purely from spike count. A benefit that separable tuning

affords the brain over inseparable tuning is the ability to integrate spikes over a population to read out, or decode, feature A without being concerned about their tuning to feature B or the value of feature B of the stimulus [19]. Separable tuning therefore is compatible with simpler downstream readout and transformation circuitry. Inseparable tuning, on the other hand, requires downstream readout to take both features into account, functionally forcing the downstream area to consider the neurons' responses not in relation to the individual features but instead in relation to a single feature.

One way to grasp this re-interpretation of a unit's stimulus tuning is to consider neurons in MT, which are tuned for features of image motion on the retina [10,14,20]. If we consider direction and speed of motion as the axes along which MT neurons modulate their firing rates, MT neurons exhibit separable tuning, in that the preferred direction of a cell does not significantly change as a function of the stimulus speed tested. They can also be described as being inseparably tuned, though, for the spatial frequency and the temporal frequency of motion [21,22]. The latter interpretation is most useful when integrating MT responses from V1 neurons modeled as banks of spatiotemporal filters [23–27], a conceptualization that has been particularly apt for considering encoding of natural scenes that can be well-described with three-dimensional spatiotemporal receptive fields [24].

Integration of multiple stimulus features has been shown to affect task performance, pointing to the benefit of jointly tuned neurons and to reading out neural responses with respect to the joint stimulus. One way to show how stimulus features become intertwined during cortical processing is to inject noise into the

presentation of one feature and observe how behavioral output is affected for each feature. When joint tuning to both features is present, the amplification of noise to one feature will cause fluctuations in the neural response in a jointly tuned area, and the downstream interpretation of any co-encoded features would be thereby affected as well [28]. When variance of either the direction or speed of dot motion was increased, variance of both direction and speed of smooth pursuit eye movements was altered, showing the joint neural encoding of direction and speed but also the joint readout [28]. Similar effects were also observed in spatial grouping, using a behavioral task of detecting curved "paths" formed by an array of oriented Gabor patches [29]. Interaction between the orientation and change of orientation features that constituted the "paths" allowed task performance to increase above that expected by the combined task performance using the individual features, highlighting the importance of using both features for optimal perceptual judgments.

In addition to integration of stimulus features within a single sensory modality, both cortical and subcortical areas combine information between different sensory modalities [30]. One such circuit is the multisensory integration of the visual and vestibular systems in order to create a holistic representation in areas such as the medial superior temporal area (MST) and the frontal eye fields (FEF) of the organism's movement in space [31–35]. The key component signals involved in these particular joint multisensory representations are visual and vestibular. Visual responses derived from the dorsal motion pathway represent the movement of the head relative to objects in the field of view[34,36,37]. Vestibular signals originate from the otolith organs of the ears that encode static tilt - head position relative to

gravity - and acceleration in head-centered coordinates [38]. MST responses have been modeled as a the combined movement vector generated from the integration of visual and vestibular information [37], suggesting that other areas encoding multiple features or multisensory information could also be modeled as a joint representation of their component features. Joint coding, and the potential for sequential processing steps, can serve as a scaffold for further hierarchical processing via similar repeated integration of lower-level sensory features [39]. The integration of multiple senses is critical for making sense of the constant streams of sensory information entering the cortex, and can inform our understanding of the sequential, hierarchical integration of lower-level sensory features as well.

Information theory

As experimenters, we aim to quantify neural coding to understand the fundamental limits of how the brain works, given the transformation of sensory information at the periphery from forms such as photons, chemicals, pressure, and sound waves to the electrochemical language of neurons. In the 1940s, Claude Shannon laid mathematical frameworks that are as useful today for neuroscience as when he formulated them for signal transmission on a noisy channel [40]. He described the entropy S of the system in two ways: the response entropy and the noise entropy. Response entropy is the amount of information available from observations of each possible response r of the encoding unit:

$S[P(r)] = -\sum_r P(r) \log_2 P(r)$. Noise entropy is the amount available from the likelihood of stimulus s given an observed response value r: $S[P(r|s)] = -\sum_s P(s) \sum_r P(r|s) \log_2 P(r|s)$ To determine how useful the encoding unit is about

the signal it is transmitting, we use the difference between the response entropy and the noise entropy [41]. This quantity, the Shannon information or mutual information, is the amount our uncertainty about the stimulus is reduced by observing the response of the encoding unit. When the encoding unit is more precise, the noise entropy decreases, so the mutual information of the stimulus and response increases, which matches our intuition that a more precise unit is more informative about the stimulus[42,43].

Mutual information has been used widely in helping to elucidate the neural code in a range of systems. A great deal of work has been performed on the representational capacity of the H1 motion-sensitive neuron of the blowfly, which encodes horizontal movement across the fly visual field [44]. The fly is affixed to a pedestal and shown patterns on a screen while the experimenter records from one of the two H1 neurons, one for each hemifield. Early work showed that the estimates of velocity recreated from H1 spike trains approached optimal computation given the physical limits of the system, showing that the representational capacity could be comparable to the maximum amount of information available to the H1 neuron [45]. Further work showed that patterns of spikes encoded more information than individual spikes and that information increased with greater temporal resolution, highlighting the importance of temporal coding in this system[46–48]. The H1 neuron also exhibits adaptation, matching its response to the range of the stimulus in order and maximizing information transmission [49,50]. The middle temporal area of the macaque is a similar system to which we can compare these results, specifically its capability to represent motion information about drifting dot patches and natural

scenes in anesthetized and awake animals. MT neurons have also been shown to encode more motion information in patterns of spikes than in total count, indicating the potential for complex temporal encoding [51]. Adaptation has also been explored in MT: neurons manipulate the range of their response to fit the range of the stimulus on very fast timescales (<40ms) in order to maintain their level of information transmission [52]. Given that these two systems are far removed from each other in an evolutionary sense, it is striking how both systems have both managed to efficiently encode motion information, and speaks to the ubiquity of efficient processing across neural systems. In chapter II of this thesis, I apply information theoretic methods to quantify the benefit of joint encoding in area MT, and extend the analysis to include small populations of simulated neurons and smooth pursuit eye movements.

The power of mutual information has also been leveraged to understand more about joint encoding [16,17]. The information in jointly tuned units in V1 and MT about each stimulus separately was summed and compared to the information about the joint stimulus. The V1 population exhibited inseparable tuning to orientation and binocular disparity [17], while the MT population was separably tuned to direction and binocular disparity [16]. Neurons in both populations encoded more information about the joint stimulus than the sum of both stimulus features s_1 and s_2 separately. An increase of information is perhaps expected for the inseparable neurons: they would exhibit greater noise entropy than separable units. The tuning curve of the unit to stimulus feature s_1, expressed as $\sum_n nP(n|s_1)$, varies more across different values of s_2 for inseparable neurons, in turn leading to a more diffuse $P(s_1|n)$ and a larger

noise entropy than for separable neurons. The result that information from spike count about the joint stimulus exceeds that about the component stimuli for both types of neurons points to a more fundamental property of jointly tuned neurons, namely that joint coding provides a coding advantage that downstream decoding could exploit.

Smooth pursuit in the macaque

Given that the conventional job of the brain is to process information for action, careful examination of the output of cortical circuits is useful for a complete understanding of them. To this end, we turn to the smooth pursuit system of the macaque, in which the eyes are smoothly rotated to follow a target by minimizing retinal image slip [53]. MT provides estimates of target motion to drive smooth pursuit, and there is minimal noise added between the representation of visual motion in MT and smooth pursuit eye movements [54]. After information about retinal image motion arrives in V1, it is quickly transmitted to MT directly, and indirectly via secondary visual cortex (V2) [55]. MT responses are read out, transformed, and integrated with other visual and vestibular information in MST and the frontal eye fields (FEF)[34,56–58]. Motion information for motor drive from MST and FEF neurons travels via the pontine nuclei to the flocculus of the cerebellum [57]. At this point, the direction-speed coordinate frame of cortical motion responses has been transformed into head-centered, Cartesian coordinate frame to correspond to the horizontal and vertical axes along which 4 of the 6 extraocular muscles move the eyes [59]. Motor signals then are sent to brainstem premotor nuclei, which drive the extraocular muscles of the eye. These muscle pairs approximately rotate the eye in

the orbit along horizontal, vertical, and diagonal axes. The very few (<6) synapses between MT and the eye muscles underscore the tight connection that exists between MT readout and eye movements. For this reason, among others described above, we can treat smooth pursuit eye movements as a faithful representation of the output of MT.

Smooth pursuit eye movements and their link to MT readout have been used to shed light on a variety of cortical mechanisms. MT neurons have been shown to adapt to the statistics of visual motion, altering their gain in order to more efficiently encode the stimuli with the range of their responses, and smooth pursuit reflected the cortical adaptation [52]. Evidence for integration of direction and speed at the level of neural populations was also found via smooth pursuit experiments [28]. In this study, the variance of either the direction or speed of dots in a random-dot patch was manipulated and compared to the variance of eye movements. In each condition, the direction and speed of eye movements were both impacted, indicating that stimulus variance about both stimulus features was represented in the neural population and read out jointly. A different way of directly comparing neurons and behavior was to use the correlation between neuron fluctuation and behavioral fluctuation in simultaneously recordings [60]. By simulating MT population responses and treating estimates from decoding models as the output of the population that would drive eye movements, investigators could test a variety of decoding models to predict which one matched the observed neuron-behavior correlation.

Noise correlations and impact on coding

Although smooth pursuit behavior and the estimate in MT have been shown to be tightly linked [52,54,28,60], the question remains of how cortical circuitry is organized to make this happen. One way we test competing theories of cortical readout methods is to simulate responses from populations of MT neuron-like units and compare the readout of our candidate decoding methods. To do so requires that our testbed of MT-like units is similar to MT in its tuning preferences, spike probability, tuning bandwidth, and other properties of MT. One such property is the noise correlation between units, which can significantly impact the output of the population[61–63]. Since the redundancy of cortex means that a number of cells will have similar preferences, it is expected that the mean response change of two similarly tuned cells to a change in stimulus will be correlated. In comparison to this "signal correlation", cells may also exhibit a correlation in the trial-by-trial fluctuations from their mean responses to a single stimulus, deemed noise correlations[61]. Depending on the direction of the noise correlation compared to the direction of the signal correlation, the noise correlation can significantly reduce the discriminability of the stimulus change, possibly hindering the brain's ability to decode activity from a population of noise-correlated neurons[64,65]. Recent investigation into the properties of noise correlations in the visual system has begun to clarify their sources and mechanisms of modulation.

The magnitude of noise correlations is dependent on the orientation preference similarity and the physical distance between cells. When the responses of mouse primary visual cortex cells were averaged across all orientation preferences,

spontaneous noise correlations and noise correlations evoked by drifting sinusoidal gratings decreased exponentially as a function of electrode distance[66]. Evoked noise correlations also decreased in an inversely proportional manner to the difference between the cells' orientation preferences, with the dependence of noise correlations on orientation tuning similarity being especially strong at shorter electrode distances (< 0.5mm)[66]. Since V1 orientation tuning is a result of summation of inputs from LGN cells with adjacent receptive fields[2], cells with similar orientation tuning would necessarily be receiving input from LGN cells whose spike trains would be highly correlated. Taken together with the expectation that cells in close proximity are more likely to be synaptically connected, these results indicate that noise correlation magnitude may be a function of shared inputs between cells.

Since the activity of cells across the cortex is correlated to varying degrees based on the cells' tuning properties and their location, the brain's task of separating signal correlation from noise correlation is simplified somewhat through the reduction of noise correlations by attention. This phenomenon was studied in the V4 extrastriate area[67,68], responsible for shape recognition[69]. Attentional modulation in a direction discrimination task was shown to improve behavioral performance via an increase in firing rate and decrease in mean-matched Fano factor during the sustained period of the response, as well as a reduction in noise correlations[67] that was inversely proportional to the change in firing rate[68]. The change in noise correlations was correlated with the magnitude of attentional modulation when cells' activity was modulated in the same direction, while opposite

attentional modulation of the cells effectively abolished noise correlations[68], further suggesting that comodulated cells share a common input.

Noise correlations' importance in population coding is still under debate. Shared variability has been shown to impair perceptual performance [64,68], and reduction of noise correlations can recover some precision [70,71], but some have determined that noise correlations may be beneficial to decoding in certain situations[64,72,73,62]. Specifically, models that include a diversity of tuning curve widths and magnitudes have shown that a population with limited noise correlations can encode more information than a population of independent units, especially at large population sizes[62,74]. Others have shown that increased noise correlations between excitatory and inhibitory units contribute to improved stimulus encoding by a downstream excitatory cell via an increase in the signal-noise ratio and sharpening of its tuning curve [72]. Considering the diverse range of findings on the impact of noise correlations on efficient population coding [74–78], continued examination is certainly warranted and necessary in order to gain a more complete understanding of how the brain reads out population activity to successfully interpret sensory inputs and generate precise behaviors. In Chapter III of this thesis, I implement noise correlations that decay with reduced tuning similarity between units in a simulation of responses from a population of MT cells, and use the resulting spike counts as inputs to population decoding models to match our observations from smooth pursuit experiments.

Summary

The brain is a system based on hierarchical processing of sensory input, transformed in series and in parallel to generate action and perception. A key component of the transformation is that neurons modulate their firing rates in response to multiple stimulus features, creating the potential for ambiguity but also for increased overall efficiency. One question that remains to be fully answered is how the system benefits from and manages joint coding at all levels, from sensory cortex to behavior. Gaining a better understanding of joint coding can be especially useful in the future in the field of brain-computer interfaces, which are applied from the sensory periphery (retinal implants) to motor output (manipulation of prosthetics via motor cortex).

In this thesis, I apply information theoretic methods to help elucidate joint processing in single neurons in extrastriate area MT, small simulated populations of neurons, and smooth pursuit behavior as a readout of neural population estimates. I also analyze the variance of smooth pursuit behavior to constrain population decoding models and predict how jointly encoded cortical estimates are read out. I find evidence that joint encoding is beneficial for sensory processing, and that behavior is best predicted by decoders that read out stimulus features jointly, not separately. These results can provide insight into visual motion processing specifically, but can also improve understanding of joint coding across the brain.

References

1. Hubel D, Wiesel TN. Receptive fields, binocular interaction and functional architecture in the cat's visual cortex. J Physiol. Not Available; 1962;160: 106–154.

2. Hubel DH, Wiesel TN. Receptive fields and functional architecture of monkey striate cortex. J Physiol . 1968;195: 215–243. Available: http://jp.physoc.org/content/195/1/215.abstract

3. Snowden R, Treue S, Andersen R. The response of neurons in areas V1 and MT of the alert rhesus monkey to moving random dot patterns. Exp Brain Res. 1992; Available: http://link.springer.com/article/10.1007/BF02259114

4. Sincich LC, Horton JC. The circuitry of V1 and V2: integration of color, form, and motion. Annu Rev Neurosci. 2005;28: 303–26. doi:10.1146/annurev.neuro.28.061604.135731

5. Brugge JF, Merzenich MM. Responses of neurons in auditory cortex of the macaque monkey to monaural and binaural stimulation. J Neurophysiol. 1973;36: 1138–58. doi:10.1152/jn.1973.36.6.1138

6. Chance FS, Nelson SB, Abbott LF. Complex cells as cortically amplified simple cells. Nat Neurosci. 1999;2: 277–282. doi:10.1038/6381

7. Mechler F, Ringach DL. On the classification of simple and complex cells. Vision Res. Pergamon; 2002;42: 1017–1033. doi:10.1016/S0042-6989(02)00025-1

8. Albright T. Direction and orientation selectivity of neurons in visual area MT of the macaque [Internet]. Journal of Neurophysiology. 1984. pp. 1106–1130. Available: http://jn.physiology.org/content/52/6/1106.short

9. DeAngelis GC, Uka T. Coding of horizontal disparity and velocity by MT neurons in the alert macaque. J Neurophysiol. 2003;89: 1094–1111. doi:10.1152/jn.00717.2002

10. Maunsell JHR, Van Essen DC. Functional properties of neurons in middle temporal visual area of the macaque monkey . I . Selectivity for stimulus direction, speed, and orientation. J Neurophysiol. 1983;49: 1127–1147.

11. Barberini CL, Cohen MR, Wandell B a, Newsome WT. Cone signal interactions in direction-selective neurons in the middle temporal visual area (MT). J Vis. 2005;5: 603–21. doi:10:1167/5.7.1

12. Horwitz GD, Chichilnisky EJ, Albright TD. Cone Inputs to Simple and Complex Cells in V1 of Awake Macaque. J Neurophysiol. American Physiological Society; 2007;97: 3070–3081. doi:10.1152/jn.00965.2006

13. Nover H. A Logarithmic, Scale-Invariant Representation of Speed in Macaque

Middle Temporal Area Accounts for Speed Discrimination Performance. J Neurosci. 2005;25: 10049–10060. doi:10.1523/JNEUROSCI.1661-05.2005

14. Priebe NJ, Cassanello CR, Lisberger SG. The neural representation of speed in macaque area MT/V5. J Neurosci. 2003;23: 5650–5661. doi:23/13/5650 [pii]

15. Sunkara A, DeAngelis GC, Angelaki DE. Joint representation of translational and rotational components of optic flow in parietal cortex. Proc Natl Acad Sci U S A. 2016;113: 5077–82. doi:10.1073/pnas.1604818113

16. Smolyanskaya A, Ruff DA, Born RT. Joint tuning for direction of motion and binocular disparity in macaque MT is largely separable. J Neurophysiol. 2013;110: 2806–16. doi:10.1152/jn.00573.2013

17. Grunewald A, Skoumbourdis EK. The integration of multiple stimulus features by V1 neurons. J Neurosci. 2004;24: 9185–9194. doi:10.1523/JNEUROSCI.1884-04.2004

18. Baker C, Cynader M. Space-time separability of direction selectivity in cat striate cortex neurons. Vision Res. 1988;28: 239–246.

19. Kim HR, Pitkow X, Angelaki DE, DeAngelis GC. A simple approach to ignoring irrelevant variables by population decoding based on multisensory neurons. J Neurophysiol. 2016; jn.00005.2016. doi:10.1152/jn.00005.2016

20. Newsome W, Wurtz R, Dürsteler M, Mikami a. Deficits in visual motion processing following ibotenic acid lesions of the middle temporal visual area of the macaque monkey. J Neurosci. 1985;5: 825–40.

21. Rust NC, Mante V, Simoncelli EP, Movshon JA. How MT cells analyze the motion of visual patterns. Nat Neurosci. 2006;9: 1421–31. doi:10.1038/nn1786

22. Simoncelli EP, Heeger DJ. A Model of Neuronal Responses in Visual Area MT. Vision Res. 1998;38: 743–761.

23. Pack CC, Conway BR, Born RT, Livingstone MS. Spatiotemporal structure of nonlinear subunits in macaque visual cortex. J Neurosci. 2006;26: 893–907. doi:10.1523/JNEUROSCI.3226-05.2006

24. Nishimoto S, Gallant JL. A Three-Dimensional Spatiotemporal Receptive Field Model Explains Responses of Area MT Neurons to Naturalistic Movies. J Neurosci. 2011;31: 14551–14564. doi:10.1523/JNEUROSCI.6801-10.2011

25. Priebe NJ, Lisberger SG, Movshon JA. Tuning for spatiotemporal frequency and speed in directionally selective neurons of macaque striate cortex. J Neurosci. 2006;26: 2941–2950. doi:10.1523/JNEUROSCI.3936-05.2006

26. Rust NC, Schwartz O, Movshon JA, Simoncelli EP. Spatiotemporal elements of macaque V1 receptive fields. Neuron. 2005;46: 945–956. doi:10.1016/j.neuron.2005.05.021

27. Bradley DC, Goyal MS. Velocity computation in the primate visual system. Nat Rev Neurosci. 2008;9: 686–95. doi:10.1038/nrn2472

28. Osborne LC, Lisberger SG. Spatial and temporal integration of visual motion signals for smooth pursuit eye movements in monkeys. J Neurophysiol. 2009;102: 2013–25. doi:10.1152/jn.00611.2009

29. Lee SH, Blake R. Neural synergy in visual grouping: When good continuation meets common fate. Vision Res. 2001;41: 2057–2064. doi:10.1016/S0042-6989(01)00086-4

30. Stein BE, Stanford TR. Multisensory integration: current issues from the perspective of the single neuron. Nat Rev Neurosci. Nature Publishing Group; 2008;9: 255–266. doi:10.1038/nrn2331

31. Xu J, Yu L, Stanford TR, Rowland B a., Stein BE. What does a neuron learn from multisensory experience? J Neurophysiol. 2014; 883–889. doi:10.1152/jn.00284.2014

32. Seilheimer RL, Rosenberg A, Angelaki DE. Models and processes of multisensory cue combination. Curr Opin Neurobiol. 2014;25: 38–46. doi:10.1016/j.conb.2013.11.008

33. Drugowitsch J, DeAngelis GC, Klier EM, Angelaki DE, Pouget A. Optimal multisensory decision-making in a reaction-time task. Elife. 2014;2014: 1–19. doi:10.7554/eLife.03005.001

34. Gu Y, Cheng Z, Yang L, DeAngelis GC, Angelaki DE. Multisensory Convergence of Visual and Vestibular Heading Cues in the Pursuit Area of the Frontal Eye Field. Cereb Cortex. 2015; doi:10.1093/cercor/bhv183

35. Angelaki DE, Gu Y, DeAngelis GC. Multisensory integration: psychophysics, neurophysiology, and computation. Curr Opin Neurobiol. 2009;19: 452–8. doi:10.1016/j.conb.2009.06.008

36. Lagae L, Maes H, Raiguel S, Xiao DK, Orban G a. Responses of macaque STS neurons to optic flow components: a comparison of areas MT and MST. J Neurophysiol. 1994;71: 1597–1626.

37. Gu Y. Visual and Nonvisual Contributions to Three-Dimensional Heading Selectivity in the Medial Superior Temporal Area. J Neurosci. Society for Neuroscience; 2006;26: 73–85. doi:10.1523/JNEUROSCI.2356-05.2006

38. Fernandez C, Goldberg JM. Physiology of peripheral neurons innervating otolith organs of the squirrel monkey. I. Response to static tilts and to long-duration centrifugal force. J Neurophysiol. 1976;39: 970–984. doi:10.1152/jn.1976.39.5.970

39. Zeki S, Shipp S. The functional logic of cortical connections. Nature. Nature Publishing Group; 1988;335: 311–317. doi:10.1038/335311a0

40. Shannon CE. A mathematical theory of communication. Bell Syst Tech J. 1948;27: 379–423. doi:10.1145/584091.584093

41. Cover TM, Thomas JA. Information Theory and Statistics. Elements of Information Theory. John Wiley & Sons, Inc.; 2005. pp. 347–408. doi:10.1002/047174882X.ch11

42. Bialek W, de Ruyter van Steveninck R, Rieke F, Warland D. Spikes: Exploring the Neural Code. Boston: MIT Press; 1997.

43. Brunel N, Nadal JP. Mutual information, Fisher information, and population coding. Neural Comput. 1998;10: 1731–57. Available: http://www.ncbi.nlm.nih.gov/pubmed/9744895

44. van Steveninck RDR, Borst A, Bialek W. Real time encoding of motion: Answerable questions and questionable answers from the fly's visual system. 2000; 28. Available: http://arxiv.org/abs/physics/0004060

45. Bialek W, Rieke F, de Ruyter van Steveninck RR, Warland D. Reading a neural code. Science. 1991;252: 1854–1857. doi:10.1126/science.2063199

46. de Ruyter van Steveninck RR, Bialek W. Real-Time Performance of a Movement-Sensitive Neuron in the Blowfly Visual System: Coding and Information Transfer in Short Spike Sequences. Proc R Soc B Biol Sci. The Royal Society; 1988;234: 379–414. doi:10.1098/rspb.1988.0055

47. de Ruyter van Steveninck RR, Lewen GD, Strong SP, Koberle R, Bialek W. Reproducibility and variability in neural spike trains. Science. 1997;275: 1805–1808. doi:10.1126/science.275.5307.1805

48. Strong SP, Koberle R, de Ruyter van Steveninck RR, Bialek W. Entropy and Information in Neural Spike Trains. Phys Rev Lett. 1998;80: 197–200. Available: http://arxiv.org/abs/cond-mat/9603127v2

49. Safran MN, Flanagin VL, Borst A, Sompolinsky H. Adaptation and information transmission in fly motion detection. J Neurophysiol. 2007;98: 3309–3320. doi:10.1152/jn.00440.2007

50. Borst A, Flanagin VL, Sompolinsky H. Adaptation without parameter change: Dynamic gain control in motion detection. Proc Natl Acad Sci U S A. 2005;102: 6172–6176. doi:10.1073/pnas.0500491102

51. Osborne LC, Palmer SE, Lisberger SG, Bialek W. The neural basis for combinatorial coding in a cortical population response. J Neurosci. 2008;28: 13522–13531. doi:10.1523/JNEUROSCI.4390-08.2008

52. Liu B, Macellaio M V., Osborne LC. Efficient sensory cortical coding optimizes pursuit eye movements. Nat Commun. Nature Publishing Group; 2016;7: 12759. doi:10.1038/ncomms12759

53. Rashbass C. The relationship between saccadic and smooth tranking eye

movement. J Neurophysiol. 1961; 326–338.

54. Osborne LC, Lisberger SG, Bialek W. A sensory source for motor variation. Nature. 2005;437: 412–6. doi:10.1038/nature03961

55. Born RT, Bradley DC. Structure and function of visual area MT. Annu Rev Neurosci. 2005;28: 157–89. doi:10.1146/annurev.neuro.26.041002.131052

56. Schmolesky MT, Wang Y, Hanes DP, Thompson KG, Leutgeb S, Schall JD, et al. Signal timing across the macaque visual system. J Neurophysiol. 1998;79: 3272–8. Available: http://www.ncbi.nlm.nih.gov/pubmed/9636126

57. Krauzlis RJ. Recasting the Smooth Pursuit Eye Movement System. J Neurophysiol. 2003;91: 591–603. doi:10.1152/jn.00801.2003

58. Grossberg S, Srihasam K, Bullock D. Neural dynamics of saccadic and smooth pursuit eye movement coordination during visual tracking of unpredictably moving targets. Neural Networks. 2012;27: 1–20. doi:10.1016/j.neunet.2011.10.011

59. Krauzlis RJ, Lisberger SG. Directional organization of eye movement and visual signals in the floccular lobe of the monkey cerebellum. Exp Brain Res. Springer-Verlag; 1996;109: 289–302. doi:10.1007/BF00231788

60. Hohl SS, Chaisanguanthum KS, Lisberger SG. Sensory population decoding for visually guided movements. Neuron. Elsevier Inc.; 2013;79: 167–79. doi:10.1016/j.neuron.2013.05.026

61. Josić K, Shea-Brown E, Doiron B, de la Rocha J. Stimulus-Dependent Correlations and Population Codes. Neural Comput. MIT Press; 2009;21: 2774–2804. doi:10.1162/neco.2009.10-08-879

62. Ecker AS, Berens P, Tolias AS, Bethge M. The effect of noise correlations in populations of diversely tuned neurons. J Neurosci. 2011;31: 14272–83. doi:10.1523/JNEUROSCI.2539-11.2011

63. Kohn A, Coen-cagli R, Kanitscheider I, Pouget A. Correlations and Neuronal Population Information. Annu Rev Neurosci. 2016;39. doi:10.1146/annurev-neuro-070815-013851

64. Abbott LF, Dayan P. The effect of correlated variability on the accuracy of a population code. Neural Comput. 1999;11: 91–101. Available: http://www.ncbi.nlm.nih.gov/pubmed/9950724

65. Averbeck BB, Latham PE, Pouget A. Neural correlations, population coding and computation. Nat Rev Neurosci. 2006;7: 358–66. doi:10.1038/nrn1888

66. Denman DJ, Contreras D. The Structure of Pairwise Correlation in Mouse Primary Visual Cortex Reveals Functional Organization in the Absence of an Orientation Map. Cereb Cortex. 2013; 1–14. doi:10.1093/cercor/bht128

67. Cohen MR, Maunsell JHR. Attention improves performance primarily by

reducing interneuronal correlations. Nat Neurosci. 2009;12: 1594–600. doi:10.1038/nn.2439

68. Cohen MR, Maunsell JHR. Using neuronal populations to study the mechanisms underlying spatial and feature attention. Neuron. Elsevier Inc.; 2011;70: 1192–204. doi:10.1016/j.neuron.2011.04.029

69. Pasupathy A, Connor CE. Shape Representation in Area V4: Position-Specific Tuning for Boundary Conformation. J Neurophysiol . 2001;86: 2505–2519. Available: http://jn.physiology.org/content/86/5/2505.abstract

70. Cohen M, Kohn A. Measuring and interpreting neuronal correlations. Nat Neurosci. 2011;14: 811–819. doi:10.1038/nn.2842.Measuring

71. Gutnisky D a, Dragoi V. Adaptive coding of visual information in neural populations. Nature. 2008;452: 220–4. doi:10.1038/nature06563

72. Cafaro J, Rieke F. Noise correlations improve response fidelity and stimulus encoding. Nature. Nature Publishing Group; 2010;468: 964–7. doi:10.1038/nature09570

73. Ecker AS, Berens P, Keliris G a, Bethge M, Logothetis NK, Tolias AS. Decorrelated neuronal firing in cortical microcircuits. Science. 2010;327: 584–7. doi:10.1126/science.1179867

74. Berens P, Ecker AS, Cotton RJ, Ma WJ, Bethge M, Tolias AS. A fast and simple population code for orientation in primate V1. J Neurosci. 2012;32: 10618–26. doi:10.1523/JNEUROSCI.1335-12.2012

75. Huang X, Lisberger SG. Circuit mechanisms revealed by spike-timing correlations in macaque area MT. J Neurophysiol. 2013;109: 851–66. doi:10.1152/jn.00775.2012

76. Lee J, Lisberger SG. Gamma Synchrony Predicts Neuron-Neuron Correlations and Correlations with Motor Behavior in Extrastriate Visual Area MT. J Neurosci. 2013;33: 19677–88. doi:10.1523/JNEUROSCI.3478-13.2013

77. Huang X, Lisberger SG. Noise correlations in cortical area MT and their potential impact on trial-by-trial variation in the direction and speed of smooth-pursuit eye movements. J Neurophysiol. 2009;101: 3012–30. doi:10.1152/jn.00010.2009

78. Carnevale F, De Lafuente V, Romo R, Parga N. An Optimal Decision Population Code that Accounts for Correlated Variability Unambiguously Predicts a Subjects Choice [Internet]. Neuron. Cell Press,; 2013. pp. 1532–1543. Available: http://linkinghub.elsevier.com/retrieve/pii/S0896627313008544

CHAPTER II

Why sensory neurons are tuned to multiple stimulus features

Abstract

Many sensory neurons encode information about more than one stimulus parameter even though multidimensional representations seem to complicate the brain's decoding task by creating ambiguous stimulus-response relationships. We find that multidimensional tuning functions may in fact offer a computational advantage, allowing the brain to better reconstruct sensory stimuli. We analyze both idealized sensory neurons and extracellular recordings from motion selective units in area MT, which are tuned for the direction and speed of retinal image motion. The brain derives estimates of object direction and speed from MT activity to perceive and track moving targets.

We find that at the level of single neurons, populations, and eye movement behavior, more information can be recovered about the motion vector than about direction and speed individually. We term this coding advantage "stimulus synergy" and show that it arises from inseparability of the response conditioned stimulus distribution along individual stimulus dimensions, rather than from inseparable direction-speed tuning functions. Stimulus synergy is distinct from previously described coding synergies that arise from selectivity differences in nominally redundant populations or spiking interactions that arise between neurons or over time. Downstream processing also benefits from cortical stimulus synergy: the increased information at the single neuron level is preserved in the population

response and is reflected in the precision of pursuit eye movements, a behavior driven by the MT population.

Introduction

Sensory signals are multiplexed throughout the brain such that spike trains encode information about more than one stimulus feature: sound frequency and intensity, color and orientation, odor identity and concentration, body acceleration and retinal motion [1–4]. Sensory multiplexing might arise naturally from correlations in the environment, yet even nominally independent parameters, such as motion direction and speed, are jointly represented by visual sensory neurons. The computational advantage offered by multidimensional sensory representations is not obvious. When two or more stimulus dimensions modulate neural responses, stimulus-response relationships become ambiguous, seemingly complicating the recovery of veridical estimates of each stimulus dimension. The problem is particularly acute in low signal to noise conditions or when rapid motion estimates are required but spike counts are low and population activity is sparse [5,6].

Why then are multidimensional sensory maps so ubiquitous in the brain? In addition to the obvious benefits of reducing metabolic cost, we find that multidimensional sensory representations offer a computational advantage. More information can be recovered about a multidimensional stimulus from a multidimensional map, improving stimulus estimation and the performance of sensory-guided behavior. The computational advantage is greatest when encoding 2-3 dimensions, and gradually decreases with increasing dimensionality. This finding is consistent with previous suggestions that only 3-5 dimensions of the response from a population of V1 neurons would likely be used to decode stimuli based on

discrimination thresholds [7]. The stimulus we consider is constant retinal image motion, which has two independent features --- direction and speed. Our test bed comprises extracellular recordings in motion-selective primate middle temporal extrastriate cortical area (MT), smooth pursuit eye movements, and simulations of Poisson model neurons. Many MT neurons respond selectively to retinal image motion with Gaussian shaped tuning functions for direction and speed [8–10]. MT mediates the perception of motion [11,12] and provides the visual drive to initiate pursuit [13,14]. Pursuit is a visual tracking response to image motion on the retina. By rotating the eye along with a moving target, pursuit stabilizes the retinal image and thereby improves visual acuity. Perhaps because of the need to minimize motion blur, pursuit has evolved to be both rapid and precise[15]. In monkeys, pursuit is initiated about 100ms after target motion begins, about 45ms after MT begins to respond [16,17]. The short integration time is offset by combining responses from the population evidenced by the ~10 fold improvement of direction precision in pursuit compared to MT neurons [17]. Feedback signals that provide error-correction arrive about 125ms after pursuit begins, such that any errors in target motion estimation persist throughout the initiation period [15,16,18,19]. Fluctuations in pursuit during the open-loop interval have the form and scale expected of motion estimation errors, and perceptual and pursuit errors are correlated [15,18,19]. Taken together the evidence suggests that little noise is added between motion estimates and pursuit initiation, and that the eye movement represents a reasonable lower bound on the information recovered from MT population activity.

Studies of multidimensional coding have largely focused on the discriminability of each dimension of a continuously valued stimulus and how that depends on the sharpness of feature tuning [5,6,20–23], population size and response overlap [5,22,24–26], heterogeneity [5,27–29], and correlations between neurons [30,31]. Implicit in single-feature discriminability analysis is the supposition that the brain estimates each stimulus dimension separately. In the motion example, a direction decoder would only interpret responses in the context of each unit's direction selectivity, ignoring its speed tuning, and vice versa. Another possibility is that sensory estimates are decoded in the same (or higher) dimensionality as the map. In the motion example, $\vec{\boldsymbol{s}} = \vec{\mathbf{v}} = ve^{i\theta}$. Instead of decoding scalar direction (θ) and speed (v) independently, the brain could recover a motion vector, $\vec{\mathbf{v}}$, directly. Is one strategy computationally superior to the other? The answer depends in part on whether the population encodes more information about the multidimensional stimulus than about its features taken individually.

$$I(\vec{\boldsymbol{n}}, \vec{\mathbf{v}}) \geq I(\vec{\boldsymbol{n}}, \theta) + I(\vec{\boldsymbol{n}}, v) \tag{1}$$

The terms in Equation 1 represent the mutual information between neural responses and stimulus [32,33]. In laboratory conditions for which stimuli take on discrete values, information theory is well suited to quantify coding performance [5]. We will call conditions for which the inequality in Equation 1 holds "stimulus synergy", a different sense to the term's usual application to coding comparisons between multi-cell response patterns vs. pooled responses [34–36] or patterns of spike times vs.

counts in a time window [35,37,38]. But like the more familiar coding synergy, stimulus synergy arises from a non-linear stimulus-response relationship.

We show that cortical neurons encode stimulus dimensions synergistically, both individually and collectively as a population. We also find that the impact of synergistic sensory encoding is observable in sensory-guided movements. Smooth pursuit reflects the same information advantage observed in cortex, suggesting that multidimensional stimulus representations may enhance motor as well as sensory behaviors.

Materials and Methods

We recorded single-unit MT responses and eye movements in 3 adult male rhesus macaques (*Macaca mulatta*). Prior to these experiments, the monkeys had been extensively trained in pursuit and fixation tasks. We fit each monkey with a head restraint and sclerally-implanted eye coil under general anesthesia, using sterile surgical technique and post-operative analgesics. All study methods were approved in advance by University of Chicago's *Institutional Committee for the Care and Use of Animals* (IACUC), and were in full compliance with guidelines from the National Institutes of Health.

Visual stimuli

For both the physiology and pursuit experiments, monkeys viewed bright visual stimuli against the dark screen of a fast CRT display (SGI GDM-FW9011 or Dell X1250) at a 100Hz frame rate and 1024x768 pixel resolution at a distance of 48.5 or 51.5 cm in a dimly lit room. Full field stimuli subtended 53° by 36° (SGI) or 36° by 33° (Dell). For physiology experiments (Fig 2-1A), stimuli consisted of bright random dot kinetograms (1 dot = 2 pixels; 2 dots/deg^2) with constant speed and direction displayed against the dark background of the screen. Dots moved coherently in a stationary rectangular aperture matched to the preferred size of the recorded cell. Pursuit experiments employed the same dot motion stimuli with matching center of mass motion such that the dot pattern translated across the screen as a cohesive object. For some pursuit experiments we used a uniformly illuminated circular spot

target subtending 0.4° of spatial arc (Fig 2-9A). Trial time courses are defined for the physiology and pursuit experiments below.

Physiological recording

We recorded single units in area MT using a 3-electrode array (TREC, Germany) of high-impedance microelectrodes. Our data acquisition system (Plexon Omniplex, Blackrock Cerebus) sampled neural activity at 30kHz, and stored each channel's waveform for offline spike sorting. We identified area MT based on stereotactic coordinates along with online testing of direction and speed tuning and classical receptive field size. We confirmed our isolation of single units through principal component analysis of spike waveforms in tandem with inspection of inter-spike interval (ISI) distributions. We initially mapped each unit's motion selectivity online using steps of full field (50° by 50°) coherent dot motion in 8 directions (45° increments) and 8 speeds (1-96°/s in powers of 2). Using the coarsely determined preferred speed and direction, we mapped the receptive field (RF) location with dot motion in 5°-square apertures that appeared at pseudo-random positions at 5° spacing on an 8 by 6 grid, covering 20° by 15° of visual space. We interpolated the RF center and remapped the RF in a similar way, using 2°-square apertures at 2° spacing on an 8 by 6 grid, covering 8° by 6° of visual space. We tested a range of aperture sizes (1-40°) and selected the size that drove the maximal firing rate to use for our experiments. Finally, we remapped the unit's direction tuning at 15° intervals before proceeding with the experiment.

We organized the physiology experiments into trials of 1-2s duration during which monkeys maintained fixation within 2° of a spot target. After a 200ms fixation interval, we projected random dot patterns in square apertures scaled to the preferred size in each unit's RF. The dots remained stationary for 200ms to allow firing rates to return to baseline, then stepped to move in a constant direction and speed for 200ms, then remained stationary for another 300ms (see Fig 2-2B). Inter-trial intervals were approximately 2-3s. For the physiology task, trials were initiated with a 200ms fixation interval. We aligned the stimuli set with each unit's preferred direction (see above) and recorded responses to motion at 45° increments with around the circle at speeds of 1, 2, 4, 8, 16, 32, 64, or 96°/s, comprising 64 motion stimuli. Directions of ±75°, ±60° were added for 4 cells to verify that the distribution of chosen directions did not affect analysis (96 stimuli). For 16 cells, trials were concatenated to include 3 motion steps in different directions at a single speed, each step interleaved with a 200ms stationary period. Other neurons in the data sample were recorded with a single stimulus motion per trial as described above. Trial types were pseudo-randomly interleaved in blocks. Monkeys were rewarded following each trial for maintaining fixation within 2° of the target. We presented each stimulus an average of 36 times (range 15-87 repetitions). Single unit isolation was confirmed with Plexon's off-line spike sorter using principal component analyses of the recorded waveforms. We only report data from clearly isolated waveforms. 30 out of 40 recordings met our subjective criteria for isolation.

Pursuit experiments

We trained 3 adult male macaques (M1-3) to fixate and pursue moving targets for a juice reward prior to data collection. We sampled the horizontal and vertical position of one eye at 1ms intervals and then filtered, differentiated, and digitized the signals [18]. During pursuit experiments, animals were required to maintain fixation within 2° for 500-1000ms to begin a trial and during the final 200ms of the pursuit interval and for 400ms at the end of the trial. Accuracy windows were relaxed during pursuit initiation. Pursuit trials were ~2 seconds in duration. The fixation point appeared at the center of the screen for a randomly selected interval from 500-1000ms. The fixation point then disappeared, and a target appeared ~3° eccentric to screen center and immediately moved at a constant direction and speed toward the point of fixation. For each monkey, we selected the eccentricity of target appearance to minimize the occurrence of saccades during pursuit initiation. Targets moved for 600ms then jumped 1° in the direction of motion, remaining stationary a final fixation period of 300ms (Fig 2-8B). Spot targets moved in 8 directions (0°, 45°, 135°, 180°, 225°, and 315° relative to rightward motion) and 8 speeds (14, 16, 18, 20, 22, 24, 26, or 28°/s) for 64 different target motions (Fig 2-8). We did not analyze trials with saccades or eye blinks during a 500ms interval from target motion onset. We collected 20-176 repetitions (average 49) of each target motion for each pursuit data set across multiple sessions.

To measure the period over which pursuit is under open-loop control, we compared eye velocities for trials with and without retinal stabilization for each

monkey [15,16,19]. We stabilized a spot target on the retina by adding the eye velocity to the target velocity at each time step, effectively holding the control loop open. Before pursuit begins, the target translates at 20°/s for both stabilized and non-stabilized trials. But as the eye begins to pursue on stabilized trials, target speed increases to maintain a 20°/s image velocity on the retina. The arrival of feedback is seen with the divergence of the eye speed in the normal vs. stabilized trials. We defined the duration of the open loop interval as the time point with respect to pursuit onset that mean eye speeds diverged by 1 SD. The open-loop interval was 146ms (M1), 135ms (M2), and 138ms (M3), consistent with past studies [15,19].

Analytical methods

We quantified the relationship between motion stimuli and MT response with the mutual information [32,17], which captures in bits the average reduction in uncertainty about stimulus identity from the observation of a neuron's response. We define the neural response as the total number of spikes fired in a time window beginning at motion onset up to some time, T – i.e. the cumulative spike count. The rate at which the count increases changes over time based on dynamics in the firing rate and is highly dependent on the direction and speed of the motion stimulus. We sampled the cumulative count at 1ms resolution to form response distributions and entropies. We computed information values (see Equation 2 below) with 50 random draws of different fractions of our data sample, computing the means and standard deviations (SD) of all quantities. We corrected for finite sample effects by inspecting and fitting a linear function to each fraction's information value as a function of 1/(no.

of trials) and extrapolating to an infinite sample size [39,17]. All reported values had finite size corrections of less than 10%.

Stimulus synergy

Synergy is typically defined as the excess of information available from a pattern of responses (across cells or over time) compared to the sum of the information contributed by each [34,37,38]. Here we consider the relationship between coding of different stimulus parameters, and so we define stimulus synergy as an excess of mutual information about a motion vector - direction and speed jointly – compared to the sum of the individual direction and speed information values [40,41]. The mutual information in bits between a set of stimuli *s* and responses *r* is defined as

$$I(s,r) = \sum_s \sum_r P(s,r) \log_2 \frac{P(s,r)}{P(s)P(r)} \quad (2)$$

where *P(s,r)* is the joint probability distribution between the stimuli and responses and the sums are taken across all stimulus and response values. Equation 2 is equivalent to the Kullback-Leibler divergence between the joint stimulus-response distribution and the product of the marginals, $D_{KL}[P(s,r)||P(s)P(r)]$. Here we define the response, *r*, to be the number of spikes fired as a function of time since stimulus onset, *n(T),* i.e. the cumulative spike count [42]. Thus, the joint distribution of stimulus and response values and the information will generally change over time. We define the stimulus as either a motion vector comprising a speed and direction, $\vec{v} = ve^{-i\theta}$, or the speed *v* and direction □□individually. We define stimulus synergy

in bits to be the (positive) difference between the joint and summed individual information values, i.e.

$$I_{\text{synergy}} = I(\vec{\text{v}}, n) - \big(I(\theta, n) + I(v, n)\big). \tag{3}$$

If coding for direction and speed is independent, Equation 2 will have a value of 0. To illustrate the link between our definition of synergy with the more usual definition [34,37], we rewrite Equation 1 in terms of the stimulus vector $\vec{\text{v}}$ and count n, indicating the cumulative spike count at a particular time with respect to stimulus onset,

$$I(\vec{\text{v}}, n) = \sum_n \sum_{\theta,v} P(\vec{\text{v}}, n)\ \log_2 \frac{P(\vec{\text{v}}, n)}{P(\vec{\text{v}})P(n)}$$

$$= \sum_n \sum_{\theta,v} P(\vec{\text{v}}, n)\ \log_2 \frac{P(\vec{\text{v}}|n)}{P(\vec{\text{v}})}$$

$$\equiv \left\langle \log_2 \frac{P(\vec{\text{v}}|n)}{P(\vec{\text{v}})} \right\rangle_{n,\theta,v} \tag{4}$$

where the angle brackets <…> represent the average over all motion directions, speeds, and counts and $P(\vec{\text{v}}|n)$ is the stimulus distribution given a particular value of the spike count. The expression for synergy in Equation 3 can be rewritten as

$$I_{\text{synergy}} = \left\langle \log_2 \frac{P(\vec{\text{v}}|n)}{P(\vec{\text{v}})} \right\rangle_{n,\theta,v} - \left\langle \log_2 \frac{P(\theta|n)}{P(\theta)} \right\rangle_{n,\theta} - \left\langle \log_2 \frac{P(v|n)}{P(v)} \right\rangle_{n,v} \tag{5}$$

If $P(\vec{\text{v}}|n) = P(\theta|n)P(v|n)$, then the terms in Equation 5 cancel and there is no stimulus synergy. However, if the conditional stimulus vector distribution is not the outer product of its marginals, stimulus synergy is possible. Like more traditional forms of synergy, stimulus synergy arises from a divergence between a vector

distribution and its scalar components, but that vector is the stimulus rather than the response [34,36–38,43–45].

Poisson model simulations

We used several types of Poisson model neurons to determine the statistical origin of stimuli synergy in our data. To investigate the role of separability in direction and speed tuning functions to stimulus synergy we created data-driven model MT neurons with homogeneous Poisson spike statistics. We fit 1D Gaussian functions to the peak firing rate, tuning width and baseline rate to each neuron's spike count in a 200ms window with respect to stimulus motion onset. We used responses to preferred speed to fit the direction tuning curve and vice versa. We measure speed tuning in $\log_2$ units of stimulus speed. The outer product of each model neuron's direction and speed tuning curves provided the mean spike rate λ for a Poisson count distribution for each stimulus condition $s = \vec{\mathbf{v}}$:

$$P(n|s) = \frac{(\lambda(s)T)^n e^{-\lambda(s)T}}{(\lambda(s)T)!} \quad (6)$$

To analyze the role that tuning curve separability plays in generating stimulus synergy, we interpolated the 2D tuning curve to 5° spacing around the circle and 0.2-unit spacing in $\log_2$ speed (i.e., 5, 5.2, 5.4 in $\log_2$ spacing = 32, 36.8, 42.2 in degrees/s). We manipulated the direction-speed separability by rotating the ellipsoidal 2D tuning curve about its preferred stimulus in 1° steps. At a rotation angle of 0°, the tuning curve is perfectly separable, with an SI of 1. At a rotation angle of 45°, the tuning curve has an SI of 0.88, and the direction and speed tuning functions are not independent, i.e. inseparable [46,40,41]. We use the definition that a separable distribution is one

where the second SVD mode does not reach statistical significance ($p < 0.01$) using a permutation test. We randomly permuted the elements of each tested matrix 1000 times and used the distribution of the separability values to determine whether the second SVD mode was above chance [41]. Rotating a separable 2D Gaussian tuning function by >20° increases the second SVD mode above chance levels. The SI at a 20° rotation is 0.95, so any SI below 0.95 is inseparable.

Separability analysis

We used SVD analysis to characterize the degree of separability of the 2D direction-speed tuning functions of our MT sample [41]. The relative squared weight or fractional power of the first singular value s_1 with respect to the other i modes, i.e. $s_1^2 / \sum_i s_i^2$ quantifies the degree to which the 2D tuning function, $f(\theta,v)$ is captured by the outer product of a direction-only and speed-only curves, $f(\theta)\, g(v)^T$. This value defines a separability index (SI) for each neuron [41,47]. An SI of 1 indicates that variance in the filter form is perfectly captured by a single mode and hence, its space-time separability is exact.

Population information from pooled counts

To study information encoded by pooled spike counts, we treated our MT neurons as if they had identical preferred directions, but did not adjust their speed tuning. This created a pool of responses with overlapped direction selectivity but only partially overlapping speed selectivity. For each unit in a coding pool, we randomly selected a trial to include in a pseudo-population response to a stimulus presentation. We created 100 different cell groups for each population size (2-28) and 100 synthetic

population responses for each of 64 stimulus conditions. We measured the cumulative spike count at 1 millisecond intervals from motion onset for all units in a group. Thereafter, we computed information quantities and bias-corrected for sample size as described for single units.

The pooled count analysis of the MT data necessarily ignored stimulus conditioned correlations between neurons because the units were not recorded simultaneously. To analyze how correlations between neurons affect information representation in cortical populations, we made Poisson models based on the tuning parameters of our MT neurons and generated population responses using different correlation models. For each model unit, we generated spike counts with homogeneous Poisson statistics from a separable tuning function:

$$r(\theta, v) = r_{\max} e^{-0.5\left(\frac{\log_2(v-v_p)}{\sigma_v}\right)^2} e^{-0.5\left(\frac{\theta-\theta_p}{\sigma_\theta}\right)^2}, \quad (7)$$

where r_{max}, v_p, σ_v, and σ_θ were drawn randomly from normal distributions with mean and SD roughly comparable to our sample of neurons (r_{max} = 42 ± 36 Hz, v_p = 4 ± 1 $\log_2$(°/s), σ_v = 2.9 ± 0.7 $\log_2$(°/s), and σ_θ = 60° ± 50°) and θ_p was 0° for all units. Spiking was defined, for a population of size N, by an N x N covariance matrix, $\boldsymbol{C}$, of pair-wise stimulus-conditioned correlations. We constructed either uniform correlation between neurons, i.e. all non-diagonal elements were set to the same value in the range 0 - 0.6, or structured correlation that decayed as a function of the separation between units' preferred stimuli:

$$C_{ij} = \rho_{\max} e^{-\left(\frac{\log_2(v_i-v_j)}{\tau_v}\right)^2} e^{-\left(\frac{\theta_i-\theta_j}{\tau_\theta}\right)^2}, \quad (8)$$

where v_i and θ_i are the preferred speed and direction of neuron i, ρ_{max} is the maximum pairwise correlation, and τ_v and τ_θ scale the widths of the correlation tuning function with respect to similarity in preferred speed and direction. The values of τ_v = 1.35 and τ_θ = 45 were selected based on data from [48], however in our case the preferred directions were identical so only the speed preferences modulated correlations. Using the Matlab function mvnrnd, we generated a matrix of Gaussian distributed values with a zero mean and pairwise correlations across trials defined by Equation 8. For each unit, we computed the cumulative probability of those random events and used the Matlab function icdf to evaluate a Poisson distribution to fit those values when scaled to the appropriate firing rate defined in Equation 7. We summed counts over populations of 2 – 32 model neurons on each of 2000 trials and 64 stimulus conditions and then calculated information values using Equation 2.

Combinatorial population information

When neurons are not identical copies of each other, patterns of spikes and silences across a population can encode substantially more information about a stimulus than the summed spike count [34,36,38]. To test whether the fractional stimulus synergy encoded in response patterns is comparable to that in the pooled count, we analyzed model MT neurons described above, but used different coding symbols. Our coding symbols were patterns of spike counts across neurons, $\{n_1, n_2, \ldots, n_N\}$ where n could take on a range of integer values from 0 to a maximum count, rather than the more familiar binary words of 1s and 0s [34]. The number of observable words, $(n_{\max}+1)^N$, scales rapidly with the population size (N) and the maximum count ($n_{\max}$), precluding

direct sampling of the recorded data. Rather, we used Poisson model MT neurons, as previously described, which allowed us to construct the probability of occurrence of each response pattern directly. We analyzed conditionally independent populations of 2-9 cells. Preferred directions were aligned to 0°; preferred speeds spanned 8-64°/s (e.g. 2^3, $2^{4.5}$, and 2^6°/s, for a 3-cell population) such that spacing depended on population size. Tuning parameters were identical among neurons in the pattern and were comparable to the average values in the recorded data with the exception of firing rate. To keep the simulations tractable, we selected the peak firing rate such that the probability of observing a response >5 spikes per neuron in 250ms was below 4%. The cut-off in maximum count had a negligible effect on entropy estimates. A 5-spike cut-off underestimates the word entropy by 2% and the information by 0.8% in a 4-cell population. We constructed the probability of each word as:

$$p(\{n_1, n_2, \ldots, n_N\} | \vec{\mathbf{s}}) = \prod_{i=1}^{N} p(n = n_i | \vec{\mathbf{s}}) \quad (9)$$

where N is the number of cells, and n_i is the count for neuron i. Each conditional count distribution, $p(n = n_i|\vec{\mathbf{s}})$ is given by Equation 6 recognizing that the mean spike count for each stimulus condition $\bar{n}(\vec{\mathbf{s}}) = \lambda(\vec{\mathbf{s}})T$. Motion stimuli were identical to the pooled count analysis described previously. We calculated the mutual information between stimulus and population word from the joint probability distribution $P(\vec{\mathbf{s}}, \{n_1, n_2, \ldots, n_N\})$ between the motion vector $\vec{\mathbf{s}}$ and the count pattern:

$$I(\vec{\mathbf{s}}, \{n_1, n_2, \ldots, n_N\}) = \sum_n \sum_{\theta,v} P(\vec{\mathbf{s}}, \{n_1, n_2, \ldots, n_N\}) \log_2 \frac{P(\vec{\mathbf{s}}, \{n_1, n_2, \ldots, n_N\})}{P(\vec{\mathbf{s}}) P(\{n_1, n_2, \ldots, n_N\})} \quad (10)$$

which is analogous to Equation 2. Because we can express the probability of occurrence for each symbol given the motion stimulus, there was no need to correct for sampling bias.

Multidimensional encoding

Cortical neurons are generally tuned for more than 2 stimulus features, so we extend the two-dimensional Poisson unit to up to 8 dimensions. We used a normalized stimulus range (in arbitrary units) of -0.5 to 0.5 for all dimensions, and simulated rates for up to 8 dimensions by taking the outer products of all 1-dimensional Gaussian tuning curves:

$$r(x_1, x_2, \dots x_n) = r_{\max} e^{-0.5\left(\frac{x_1 - x_{1p}}{\sigma_{x_1}}\right)^2} e^{-0.5\left(\frac{x_2 - x_{2p}}{\sigma_{x_2}}\right)^2} \dots e^{-0.5\left(\frac{x_n - x_{np}}{\sigma_{x_n}}\right)^2} \quad (11)$$

This does assume separable tuning, since we examine the outcomes of non-separable tuning in the 2D case only. To test the effect of sensitivity on the multidimensional information, we varied the tuning bandwidth σ of dimensions from 4% to 50% of the arbitrary stimulus range.

Results

The essence of the sensory coding dilemma posed by multidimensional stimulus representations is a credit assignment problem. Firing rate modulations of a neuron tuned to more than one stimulus dimension cannot be uniquely associated with a stimulus value. Given that multidimensional representations are ubiquitous in the brain, how do they impact sensory function? We can illustrate the problem, and a potential solution, with an idealized example. Consider a Poisson sensory neuron with a constant firing rate that is scaled by identical, independent Gaussian tuning functions for n = 1-8 independent stimulus dimensions (Fig 2-1A). Downstream circuits could interpret this neuron's spikes as signaling the superposition of features from all n tuning dimensions jointly (Fig 2-1B, right) or one can imagine n independent downstream circuits each interpreting spikes as arising from a single stimulus dimension (Fig 2-1B, left). The comparative efficiency of the joint, n-dimensional decoder vs. n 1-dimensional (1-D) decoders will be limited by whether the multidimensional sensory neuron encodes more information about all n stimulus dimensions jointly compared to the sum of the information encoded about each dimension individually.

For each number of dimensions, we quantify encoding capacity by the mutual information between spike count and stimulus value (see Methods). We find that the amount of information the model unit can encode about the n-dimensional stimulus (black markers, Fig 2-1C) exceeds the sum of encoded information about each of the n dimensions separately (magenta markers, Fig 2-1C). We define a positive difference

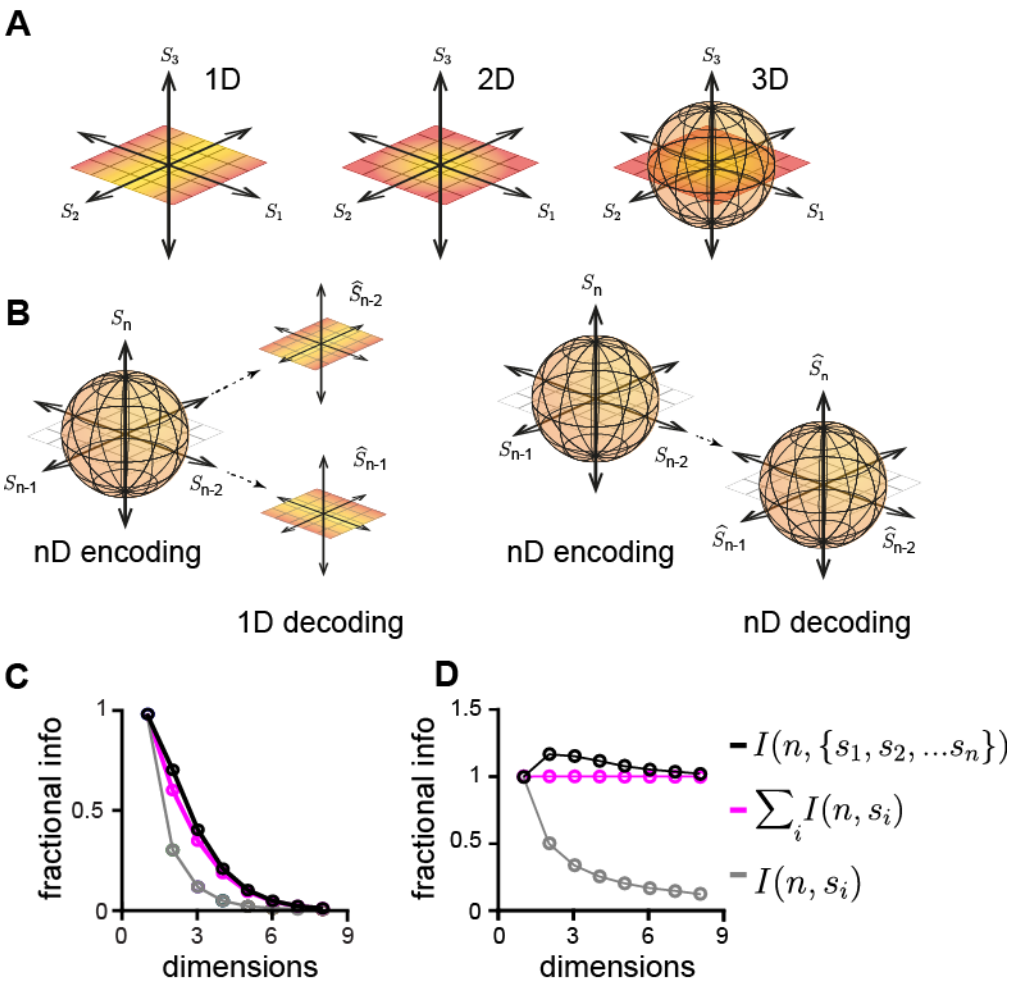

Figure 2-1. Encoding ability of Gaussian-tuned neurons peaks at 2-4 stimulus dimensions.

(A) Cartoon of dimensionality and encoding. Gradients indicate dimensions along which a tuned model unit modulates its response.

(B) The responses of a neuron tuned to *n* stimulus dimensions can be read out with respect to each dimension individually (left) or all dimensions together (right).

(C) The fraction of information that can be encoded about each dimension separately, relative to the total information encoded by the unit about one stimulus dimension, decreases with more simultaneously encoded dimensions.

(D) Fractional synergy $\left[I(\vec{\mathrm{v}}, n) - \left(I(\theta, n) + I(v, n)\right)\right]/I(\vec{\mathrm{v}}, n)$, shown as the difference between black and magenta symbols, peaks at 2-3 dimensions for SD = 0.16, the average bandwidth of our MT sample as a percentage of stimulus range, consistent with reports that MT neurons are tuned for direction, speed, and binocular disparity (see text). All quantities are normalized to the sum of information encoded about all dimensions (magenta symbols).

between the information encoded jointly about all stimulus dimensions with the sum of that encoded about each 1D component as "stimulus synergy". The total amount of information that the model neuron encodes decreases with the number of dimensions (for D>2; green markers, Fig 2-1D), as others have reported [49,50]. What we care about is the fractional advantage of encoding all dimensions together vs. individually, i.e. $\{I_{nD} - \Sigma(I_{1D})\}/ \Sigma(I_{1D})$. Fractional synergy is maximized at 2-3 dimensions (difference between black and magenta markers, Fig 2-1D) when we select a tuning bandwidth corresponding to the mean bandwidth observed in our, and others, cortical sample.

The term synergy implies that the whole -- the total encoded information about the multidimensional stimulus -- is more than the sum of its component parts. The fact that a Poisson model neuron displays synergy indicates that the coding advantage does not arise from correlations between spike times that allow a pattern of spikes to encode more stimulus information that the total count [34,35,37,38] or individual differences that allow a pattern of activation across neurons encode more than their summed count [34,35]. Nor does the model's synergy arise from interactions between dimensions (inseparability) or differences in tuning functions along multiple dimensions. Both were absent by design. Rather, stimulus synergy appears to be inherent to multidimensional representation. If so, cortical sensory representations should also display stimulus synergy, with implications for how downstream targets should decode those spikes most efficiently. We tested this hypothesis by recording from cortical neurons that respond to multiple independent

features of visual motion and measuring the information encoded about the multidimensional stimulus vector compared to its components.

Neurons in the middle temporal cortical area (MT) respond selectively to retinal image motion, and are tuned to varying degrees for multiple motion features such as direction, speed, binocular disparity, and spatial frequency [1,8,51,52]. We isolated two motion features, direction and speed, to study how stimulus information is multiplexed in area MT. While the monkeys fixated, we recorded extracellular activity from isolated units responding to 200ms-steps of coherent random dot patterns moving at a fixed direction and speed (Fig 2-2A,B; see Methods). Ninety-six motion stimuli (12 directions, 8 speeds) were repeated an average of 33 times, which allowed us to compute entropies directly from the recorded spike counts. We measured the cumulative spike count, *n(T)*, as a function of time since motion onset at 1ms intervals (Fig 2-2A). Spike counts increased quickly for preferred stimuli (red trace), more slowly for non-preferred stimuli (gold trace), and spiking was suppressed for directions in the anti-preferred direction (blue trace) (Fig 2-2C). As expected, the firing rates of all neurons in our sample were strongly modulated by both the direction and speed of motion, which is apparent in the 6 example direction-speed tuning functions in Figure 2-2D. We plot direction-speed tuning functions, i.e. the conditional mean spike count $\langle n(\vec{s}) \rangle$ measured 200ms after motion onset in Fig 2-2D for six example neurons. The direction-speed tuning functions are ovoid in shape, oriented such that direction tuning does not change as a function of stimulus speed, or vice versa. The shape suggests that the stimulus conditioned spike count distribution can be described as the outer product of two independent 1D tuning

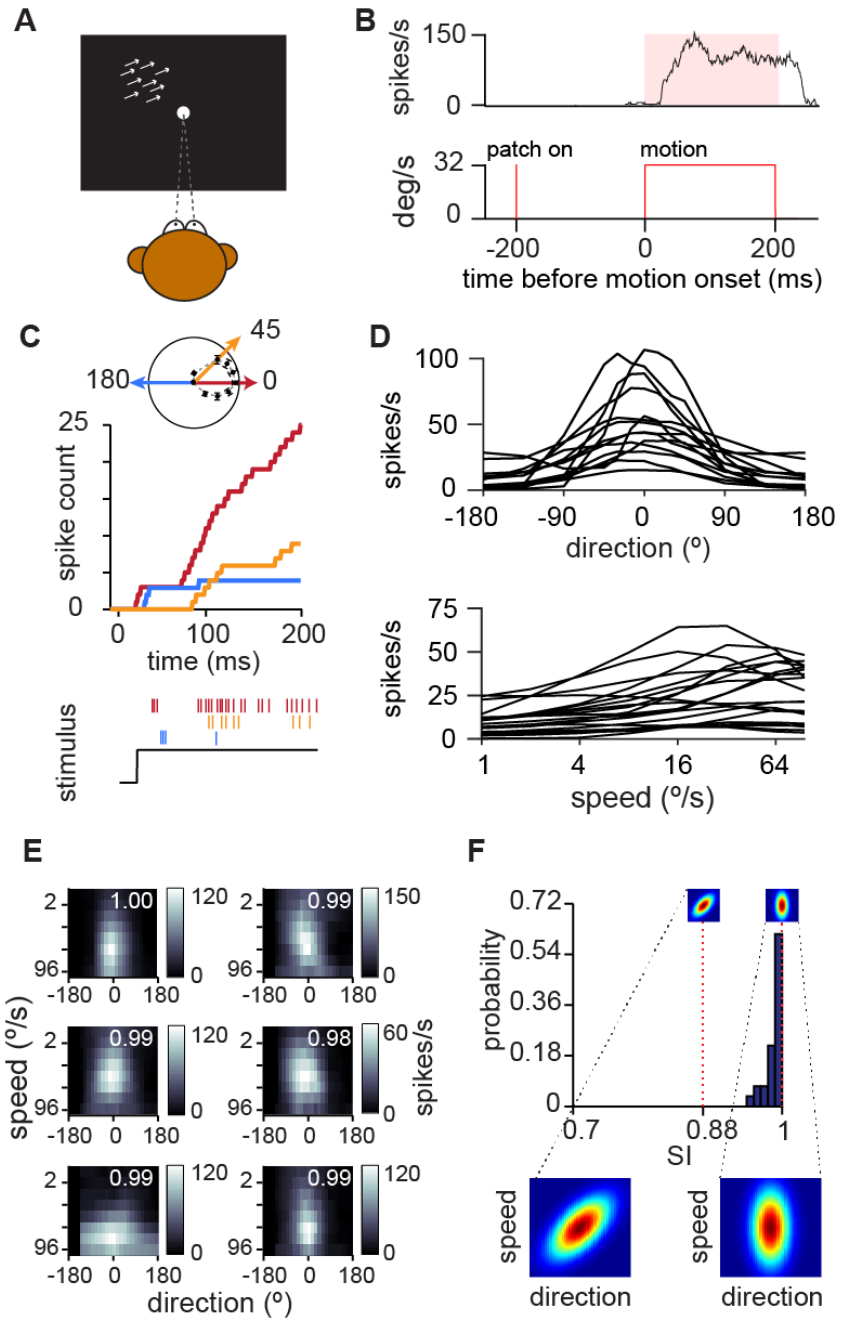

Figure 2-2. Separable direction-speed tuning functions for direction and speed in MT.

(A) Cartoon of an MT experiment. Monkeys fixated while random dot kinematograms moved coherently in the receptive field. Dots appeared and remained stationary for 200ms, then moved in one of 12 or 16 directions and 8 speeds for 200ms, then were stationary for another 300ms.

(B) Example peri-stimulus-time-histogram (PSTH) for one motion condition sampled at 1000 Hz and summed over sliding 10ms bins.

(Fig 2-2 continued)

(C) We used cumulative spike count to quantify MT responses over time, shown for 3 directions for an example unit (see tuning curve, upper inset). Cumulative spike counts were computed from motion onset from the spike times (lower panel).

(D) Sample of direction (top) and speed (bottom) tuning curves from recorded MT units.

(E) 2D tuning functions for 6 MT units. Panels show the conditional mean spike count $\langle n(\vec{\boldsymbol{s}})\rangle$ measured 200ms after motion onset. Separability indices (SI, see text) listed in upper right corner.

(F) Histogram of separability indices across MT sample. A perfectly separable tuning function (lower right inset) has an SI index of 1. Rotating the tuning function by 45° (lower left inset) creates an inseparable 2D tuning function, corresponding to SI = 0.88. Index values that deviate from unity by small amounts can indicate inseparability.

---

functions, $p(n|\vec{\boldsymbol{s}}) = f(n(\theta))g(n(v))^T$ [53]. A singular value decomposition (SVD) of the 2D tuning functions confirms that MT direction and speed tuning functions are separable [54]. We computed a separability index (SI), defined as ${s_1}^2/\sum_i {s_i}^2$, which represents the fraction of variance captured by a single SVD mode (see Methods;[40,41]). The SI values for the 6 example neurons are indicated in the upper right corner of each panel in Figure 2-2E, and the distribution across our sample in Figure 2-2F. All are clustered near complete separability, with second SVD mode values below statistical significance. On average, a single mode describes 98±1% (SD, n=30 neurons) of the variance in the conditional response distributions. A perfectly separable two-dimensional tuning curve (SI=1) is shown on the lower right of Figure 2-2F. Rotating that function by 45° creates a direction tuning curve that depends on motion speed, and vice versa - i.e., an inseparable tuning function (lower left panel, Fig 2-2F). The SI of the rotated, inseparable tuning function is 0.88, therefore small deviations from unity can indicate substantial interactions between stimulus

dimensions. SI values for direction-speed tuning are higher than reported for other tuning dimensions in MT, such as speed-spatial frequency [55] or direction-disparity [40].

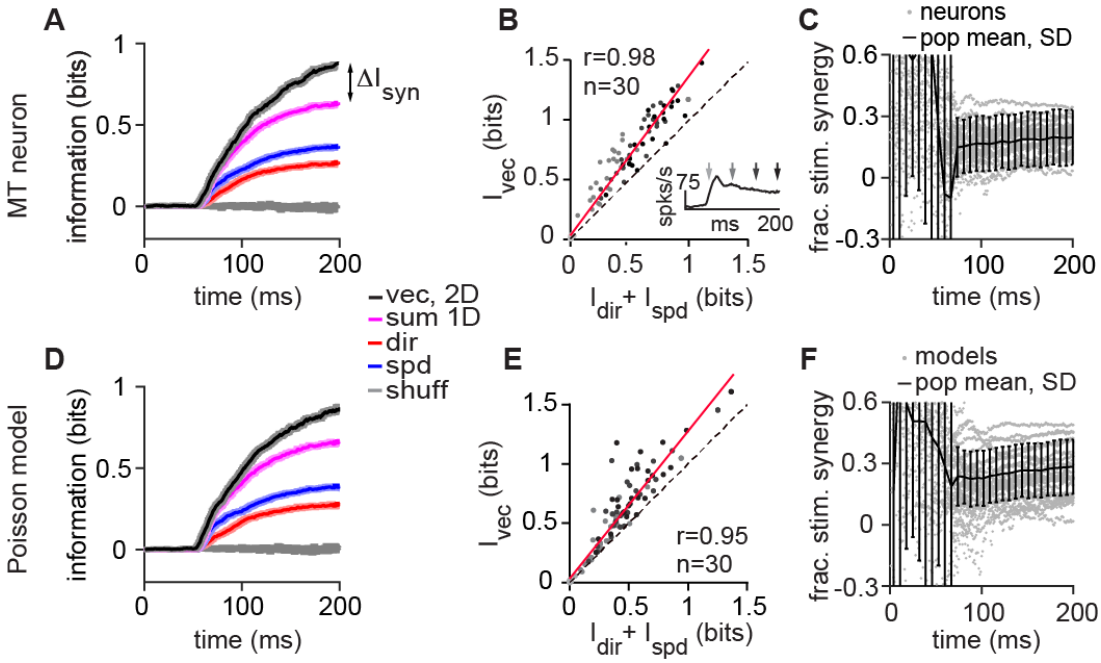

Figure 2-3. MT neurons encode stimulus components synergistically even when temporal spike patterns are disrupted.

(A) Time course of information about stimulus components from cumulative spike count in an example MT unit. Mean and errorbars (SD) have been corrected for sample size (see Methods). Information about the 2D motion vector (black) is greater than the sum (magenta) of the 1D information about direction (red) and speed (blue). Gray trace indicates the same calculation applied to stimulus label shuffled-data as a control.

(B) Population data from 30 units (dots) sampled at 4 times relative to motion onset. Most neurons encode stimulus dimensions synergistically. A linear fit (red) to the data has a slope greater than unity (dashed) ($I_{vec} = 1.18*I_{sum}$).

(C) Fractional stimulus synergy for all units (gray dotted lines), population mean, SD (black) is approximately stable over time after response onset of neurons (~65ms from motion onset).

(D), (E), (F). Same analyses applied to Poisson models of each unit, created by randomizing trials at each time step to break within-trial temporal correlations without altering the PSTH (see text). The randomization creates heterogeneous Poisson spiking statistics but preserves the features of stimulus synergy in the MT

(Fig 2-3 continued) sample. Stimulus synergy therefore does not arise from temporal patterning of spike times.

MT neurons encode motion direction and speed synergistically

The independence of direction and speed tuning functions does not indicate that MT neurons encode direction and speed information independently. For each unit, we compared information about the 2D motion vector, $\vec{\mathbf{v}} = ve^{i\theta}$, to the information represented about direction (θ) and speed (v) individually. Starting from motion onset, we measured the cumulative spike count distribution at 1ms intervals and computed the mutual information between the cumulative spike count and motion direction $I_{dir} = I(n(T), \theta)$), speed ($I_{spd} = I(n(T), v)$), or the 2D motion vector ($I_{vec} = I(n(T), \vec{\mathbf{v}})$) (see Methods, Equation 3). Figure 2-3A shows the information time courses for each term in Equation 3 for an example MT unit. Traces represent the extrapolated information values at infinite sample size, and the errorbars are extrapolated standard deviations [39,17,56]. Information about motion speed (blue trace) and direction (red trace) both increase quickly upon response onset and thereafter more slowly. Information levels off over time not because all stimulus information has already been encoded -- the stimulus entropy is $\log_2(96)$ = 6.6 bits, more information than we observe here from single neurons -- but rather because temporal correlations in spike count fluctuations increase the noise entropy over time [17,57]. After 200ms of stimulus motion, the information encoded about the 2D motion vector (black trace) is greater than the sum of the direction and speed information (magenta trace) by 0.12 bits or 14% of the summed 1D

information levels, which was near the sample mean of 14.3±13.6% (SD, n=30 neurons; $p < 0.0001$, 1-tailed t-test) (Figs 2-3A, B). One of thirty neurons did not display statistically significant stimulus synergy (Figs 2-3B, C). For the rest of the sample, stimulus synergy reached statistical significance 67±16ms (SD, n=29; $p<0.05$; one-tailed t test) after motion onset, or ~11ms after each neuron's response onset, and increased to a steady value after ~150ms of motion (~95ms of response) (Fig 2-3C).

We disrupted the temporal correlations within MT responses to determine the impact on the time course of stimulus information and synergy. We binned spike times at 1ms resolution and then created synthetic trials by randomly shuffling bins between trials while maintain the temporal position of the bin in the response ([17]; see Methods). The shuffling operation created an inhomogeneous Poisson-like model of each neuron that preserved the PSTH, latency, and tuning, but eliminated any temporal patterning of spikes within trials that might give rise to synergistic coding. The model neurons produced nearly identical information results to the recorded data (Figs 2-3D, 2-3A), although the cumulative count distributions were not identical. The model neurons also displayed nearly the same level of stimulus synergy as MT neurons (Figs 2-3E, 2-3B) and the same dynamics (Figs 2-3C, 2-3F). After 200ms, the model-averaged stimulus synergy was 14.8 ± 9.4% (SD, n=30 models; $p<0.0001$, 1-tailed t-test), which was not statistically different from the neural data ($p<0.0001$; two tailed t-test). These results confirm that while temporal relationships between spikes contribute to coding synergy [38,58], they are not necessary for stimulus synergy.

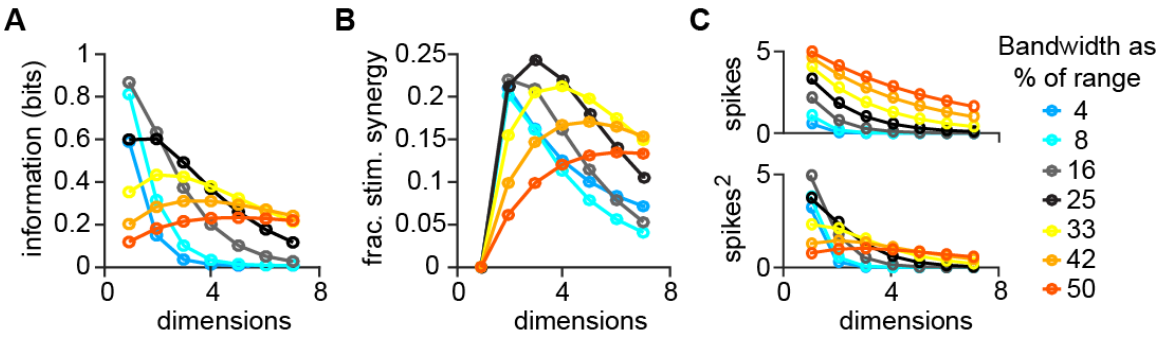

Figure 2-4. Optimal encoding dimensionality and level of stimulus synergy depend on stimulus tuning bandwidth.

(A) Mutual information between spike count and an arbitrary stimulus feature from a homogeneous Poisson model unit with identical response parameters for each stimulus dimension (see Methods for details). Model unit tuning bandwidth expressed as percentage of the tested range. Dotted bars in each panel indicate the mean of observed range-normalized bandwidths of the MT sample, as a fraction of 360° (direction tuning) or 10 (speed range from 0.25-256°/s, in $\log_2$ units).

(B) Fractional stimulus synergy peaks at lower dimensionality at narrow tuning bandwidths (blue) than at wider bandwidths (orange).

(C) Mean spike count across stimuli increases with wider bandwidth at all dimensionalities (top panel). Variance of spike count across stimuli is greater at narrow bandwidths than wide bandwidths at low dimensionality, but this trend reverses at high dimensionality (bottom panel).

MT tuning bandwidths maximize stimulus synergy

A sensory neuron's tuning curve determines how well it discriminates between different stimulus values, i.e. the amount of information it encodes. The tuning function that maximizes information at the population level is not a fixed value, but rather depends on the number of encoded stimulus dimensions [49], whether the stimulus is periodic (direction, orientation) or not (speed) [6], the size of the activated coding pool [22], pairwise correlations [5,20,49,59]. Poisson models simplify the analysis of the interdependence between discriminability, dimensionality, and tuning

bandwidth, and so we returned to the idealized model described in Figure 2-1 to determine how MT tuning bandwidths impact both encoded stimulus information and the degree of stimulus synergy. We parametrically changed the tuning bandwidth and number of encoding dimensions in the idealized model simulations, and computed the mutual information between count and stimulus as well as the fractional stimulus synergy for each combination. As expected from previous studies, we found that higher levels of information are encoded with narrow tuning functions, <30% of the stimulus range, but only for a single dimension (Fig 2-4A). Increasing the dimensionality of a neuron's selectivity requires broader tuning functions to avoid a steep information roll-off [6,22,49,50,60]. Models with tuning functions similar to our MT sample (gray and black traces, Fig 2-4) are well-suited to encoding 2-3 dimensions which is consistent with MT's role in encoding motion in depth [40,61]. MT-matched models also display high levels of stimulus synergy in 3 dimensions (Fig 2-4B). As with information, broader tuning is necessary to maintain stimulus synergy for more 4 or more dimensions, even when synergy is expressed as a fraction the total information for each condition (Fig 2-4B). The simulation results in Figure 2-4B predict that MT neuron responses should encode 20-25% more information about motion vectors than about direction and speed separately, which is what we observe.

Less intuitive is why increasing the number of encoded dimensions impacts information and fractional stimulus synergy so differently based on tuning bandwidth. Adding coding dimensions decreases information and stimulus synergy in narrowly tuned model responses (blue curves, Fig 2-4A, B) but increases

information and stimulus synergy for broadly tuned neurons (orange-red curves, Fig 2-4A, B). The reversal in the relationship between tuning sharpness and information or stimulus synergy can be explained by changes in the spike count distribution with the number of stimulus dimensions. The number of stimulus values increases exponentially with the number of coding dimensions, but because the peak firing rate remains fixed, the maximum number of coding symbols remains the same (0 to the maximum count). Generally speaking, spreading the same number of coding symbols across a larger stimulus space lowers the average count (Fig 2-4C, top), and decreases count entropy and coding capacity. Particularly with narrow tuning functions, the effect of increasing stimulus dimensionality is a steep decline in variance (blue curves, Fig 2-4C, bottom). However, the drop off in variance is more gradual for broadly tuned models, and even increases slightly from 1 dimension to 3 dimensions (red curves, Fig 2-4C, bottom). Broad tuning restricts the range of response values because all stimulus conditions elicit non-zero firing rates. However, with each added stimulus dimension, the minimum rate falls, increasing the response range (variance) and mitigating the tendency for the drop off in mean rate to lower the entropy. The amount of information encoded, and the degree of stimulus synergy reported in Figures 2-4A, B reflect the balance of the trends in Figure 2-4C. The MT tuning bandwidths in our sample correspond to models that maximize information and stimulus synergy for 2-3 dimensions.

Statistical origin of stimulus synergy

More information can be encoded about a multidimensional stimulus if the entropy of $p(\vec{\mathbf{s}}, n)$ is lower than the entropy of $p(\theta, n)\, p(v, n)$. Indeed the entropy difference determines the degree of stimulus synergy we observe in each MT neuron (Fig 2-5A). In MT, the interaction between stimulus dimensions in $p(\vec{\mathbf{s}}, n)$ that creates the potential for stimulus synergy is not apparent in the structure of $p(n|\vec{\boldsymbol{s}})$, so we consider the form of the posterior distribution, $p(\vec{\mathbf{s}}|n)$, from which the brain must estimate the stimulus most likely to have generated the observed neural activity [33].

For neurons with Gaussian or cosine-like tuning functions, the stimulus giving rise to the maximal firing rate is well specified, but many stimuli lying on a torus in direction-speed space are equally likely to produce an intermediate response. We plot $p(\vec{\mathbf{s}}|n = n_i)$ in Figure 2-5B for the 6 example MT neurons in Figure 2-2B, where n_i is a mid-range count value for each unit. The donut-like shape of the posterior specifies motion vectors – combinations of directions and speeds – that are likely to give rise to the observed spike count. Ignoring the dimensionality of the stimulus space by decoding the direction and speed independently from the distributions in Figure 2-5B would give an erroneous result. The expected values of the direction, $E(\theta|n = n_i) \equiv \sum_i \theta_{\boldsymbol{i}}\, p(\theta|n = n_i)$, and speed specify a motion vector with a low probability of eliciting that count. The donut shape makes it apparent that the marginal distributions of directions $p(\theta|n)$ and speeds $p(v|n)$ that give rise to a count *n* cannot be multiplied to yield $p(\vec{\mathbf{s}}|n)$, i.e. $p(\vec{\mathbf{s}}|n) \neq p(\theta|n)\, p(v|n)$. We quantify the deviation from separability by computing a separability index for $p(\vec{\mathbf{s}}|n = n_i)$

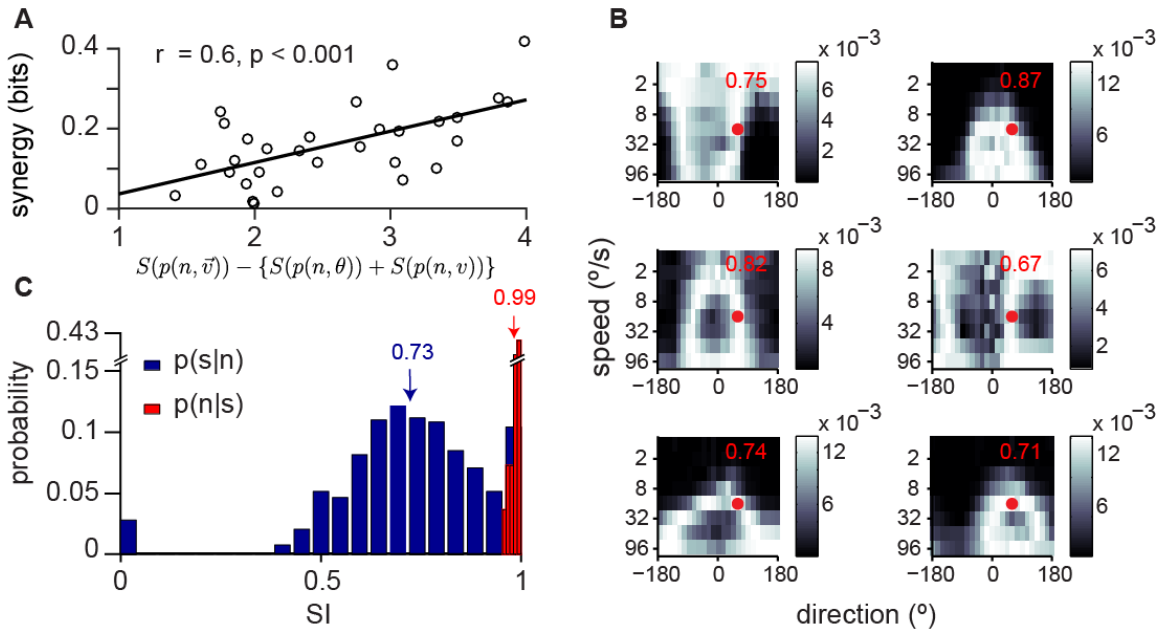

Figure 2-5. Response conditioned stimulus (posterior) distributions are not separable.

(A) The difference between the entropy of $p(n, \vec{\mathbf{s}})$ and the entropy of $p(n,\theta)p(n,v)$ predicts levels of stimulus synergy in MT neurons.

(B) The response conditioned stimulus distributions, $p(\vec{\mathbf{s}}|n)$, for the same 6 MT neurons shown in Figure 2-2B, conditioned on the trial-averaged count observed for a stimulus of 60° and 16°/s (red dot). Directions are plotted with respect to each neuron's preferred direction. For intermediate response levels, a nonlinear combination of directions and speeds can give rise to the same neural response.

(C) The structure of $p(\vec{\mathbf{s}}|n)$is higher dimensional than $p(n|\vec{\mathbf{s}})$, reflected in a broader distribution of separability index ($SI_{s|n}$) values for in the MT sample (blue) compared to the $SI_{n|s}$ re-plotted from Figure 2-2F (red). The number of samples in the distribution of $SI_{s|n}$ (blue) represents neurons and particular count values, i.e. $SI[p(\vec{\mathbf{s}}|n = n_i)]$for each value of *i*.

($SI_{s|n}$) for each neuron and cumulative count value n_i measured 200ms after motion onset. The distribution of $SI_{s|n}$ values (blue bars, Fig 2-5C), is much broader than the distribution of the SI values for $p(n|\vec{\mathbf{s}})$ (red bars, Fig 2-5B, data replotted from Fig 2-2F). The sample mean index value is 0.87±0.09 (SD, n=30), significantly different from both unity (p<0.0001, one-tailed t-test) and from the distribution of $SI_{n|s}$ (p <10-

[5], Kruskal-Wallis test). The inseparable form of the posterior distribution (blue bars, Fig 2-5C) provides a substrate for stimulus synergy that is not apparent in the tuning function.

Not all sensory neurons will have separable tuning functions, in which case stimulus synergy might arise from the forms of both $p(n|\vec{\mathbf{s}})$ and $p(\vec{\mathbf{s}}|n)$. To consider more generally how $p(n|\vec{\mathbf{s}})$ and $p(\vec{\mathbf{s}}|n)$ contribute to stimulus synergy, we used simulations to parametrically change the conditional distributions. We started with a Poisson model with separable Gaussian direction and speed tuning functions using parameters that approximated the average of our MT sample. The conditional response for each stimulus value, $\langle n(\theta, v)\rangle$ is given by $\sum_i n_i\, p(n = n_i|\theta, v)$ (upper panel) and one of the conditional stimulus distributions, $p(\vec{\mathbf{s}}|n = 40)$ (lower panel) are shown in Figure 2-6A. Rotating $p(n|\vec{\mathbf{s}})$ in the direction-speed coordinate frame modulates the degree of separability between direction and speed tuning (blue trace, Fig 2-6B), and likewise the separability of the posterior $p(\vec{\mathbf{s}}|n)$ (red trace, Fig 2-6B) which rotates along with $p(n|\vec{\mathbf{s}})$. Separability is lowest at oblique orientations in direction-speed space ($SI_{n|s}$ = 0.88; $SI_{s|n}$ = 0.23) and highest values at cardinal orientations ($SI_{n|s}$ = 1; $SI_{s|n}$ = 0.75) (red and blue traces, Fig 2-6C), as expected, but the separability of $p(n|\vec{\mathbf{s}})$ is always greater than that of posterior $p(\vec{\mathbf{s}}|n)$. Information about direction (red trace, Fig 2-6D) and speed (blue trace, Fig 2-6D) also rise and fall with rotation angle because direction and speed tuning bandwidths vary. Information about the 2D motion vector (black trace, Fig 2-6D) remains constant for all rotation angles, but the sum of the information about each 1D stimulus component does not (magenta trace, Fig 2-6D). The difference creates maximal stimulus synergy

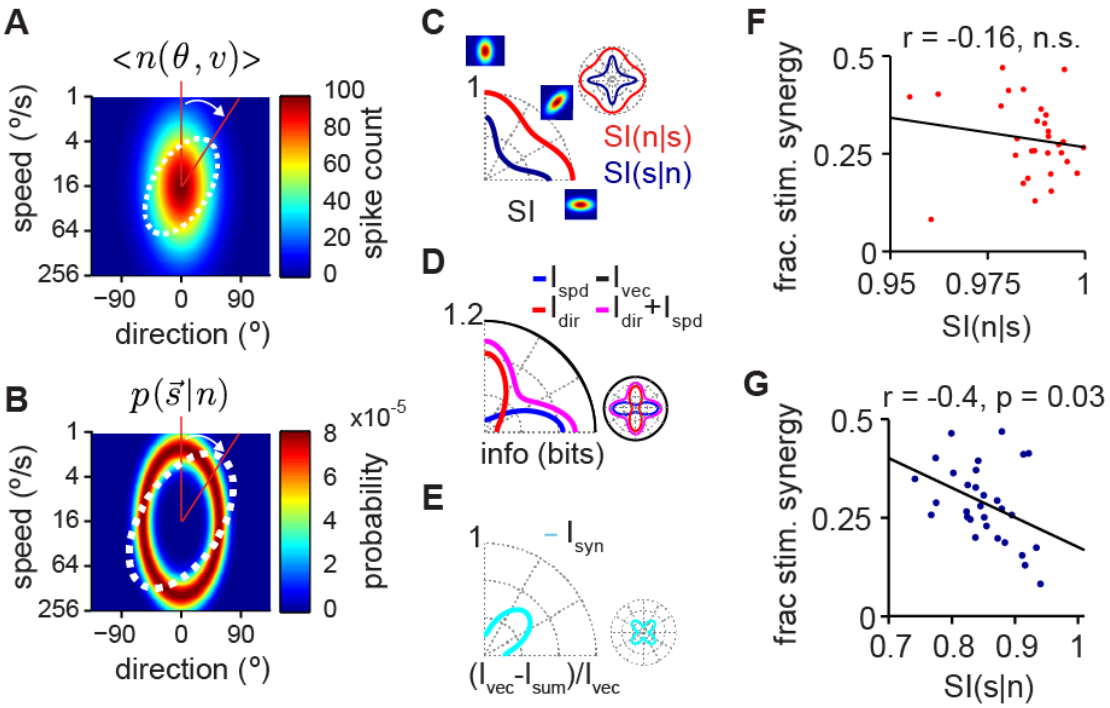

Figure 2-6. Contributions of conditional response and stimulus distributions to stimulus synergy

(A) An idealized 2D direction-speed tuning function, $\langle n(\theta, v)\rangle$. When the long axis of the function is oriented along cardinal directions, direction and speed tuning functions are separable. At intermediate angles, the response to each motion component is not independent of the other.

(B) As the tuning function is rotated, the conditional stimulus distributions, $p(\vec{\mathbf{s}}|n = n_i)$ rotate with it, changing their separability.

(C) The separability index (SI, see text) is modulated as a function of rotation angle. The SI of $p(n|\vec{\mathbf{s}})$ (red) is consistently higher than the SI of $p(\vec{\mathbf{s}}|n)$ (blue).

(D) Mutual information between Poisson spike counts, generated with the tuning function in A, and stimuli. Information about direction (red) and speed (blue) are modulated by tuning bandwidth, which changes as a function of rotation angle. The information about the 2D motion vector (black) is constant under rotation, and is always larger than the sum of the information about each stimulus component (magenta). Radial axis has been normalized such that the vector information is unity.

(E) Fractional synergy as a function of rotation angle. Stimulus synergy is maximal when the separability of both $p(n|\vec{\mathbf{s}})$and $p(\vec{\mathbf{s}}|n)$ are at their minima, but stimulus synergy is non-zero around the circle.

(F) SI of $p(n|\vec{\mathbf{s}})$is not predictive of fractional synergy.

(G) <SI>, defined as $\sum SI[p(\vec{\boldsymbol{s}}|n)]p(n)$, is correlated with fractional synergy in model units generated from recorded MT neurons.

values at oblique orientations (cyan trace, Fig 2-6E) when the conditional distributions are least separable. $SI_{n|s}$ and $SI_{s|n}$ are both anti-correlated with the level of stimulus synergy, but $\langle SI_{s|n} \rangle$ over all Poisson model count values accounts for a greater share of the variance (R = -0.16, not significant, red symbols Fig 2-6F, vs. R = -0.4, p = 0.03, blue symbols Fig 2-6G). The greater predictive power of the mean separability of the posterior stimulus distributions is consistent with the fact that stimulus synergy is non-zero even when $p(n|\vec{\mathbf{s}})$ is oriented along cardinal axes and fully separable (cyan trace, Fig 2-6E; Fig 2-6A). We find that some degree of inseparability in $p(\vec{\mathbf{s}}|n)$ is a necessary condition for stimulus synergy.

Stimulus synergy is amplified in MT population responses

For stimulus synergy to be a behaviorally relevant feature of the sensory code, it must also be measurable in population responses. We used both recorded data and data based simulations to test the degree of stimulus synergy at the population level. We assumed that the MT population could represent motion information in one of two ways, either as the total number of spikes fired, or the pattern of counts within a cell group.

Pooling spikes in a population can be an effective way of reducing noise if the neurons in the pool are selective for similar stimulus features. The preferred stimuli of the recorded units spanned a wide range of directions and speeds, so we created a more similar coding pool by aligning the preferred directions of our units prior to counting spikes. Direction alignment created a pool of responses with overlapped direction selectivity but retained all other aspects of neural individuality, such as

speed tuning, PSTH dynamics, peak rate, and direction tuning bandwidth (Fig 2-7A). We elected not to shift speed tuning curves because that would involve discarding a substantial portion of data from neurons whose preferred speeds were not centered within the stimulus range. Otherwise, our population count analysis paralleled that of individual neurons. We counted spikes over the first 200ms of stimulus motion for each stimulus condition. We created population responses from our recorded data by randomly selecting trials recorded for that stimulus, and then computed the total spike count conditioned on the stimulus value, i.e. $\langle N(\vec{\mathbf{s}})\rangle = \frac{1}{K}\sum_{j=1}^{K} N_j(\vec{\mathbf{s}})$ where j is one of K random draws from the MT trialset.

Figure 2-7A plots the conditional mean pooled count in a 16-cell group, for each motion stimulus, the population analog of the single unit examples in Figure 2-2E. Because we aligned the units by preferred direction, the pooling operation sharpens population-level direction tuning compared to single units; speed tuning is little effected. Pooling did not affect direction and speed tuning separability. Like single units, the population level separability indices were near unity, $SI_{n|s}$. = 0.99±0.007 (SD, 1000 random draws). Figure 2-7B plots a conditional stimulus distribution, $p(\vec{\mathbf{s}}|N = n_i)$, for the same cell-group as Figure 2-7A for a mid-range value of the pooled count. As with the single units (see Fig 2-5B), the conditional stimulus distribution of the population response is not separable, averaging $SI_{s|n}$. = 0.46±0.01 (SD, 1000 cell groups, difference from 1: $p < 10^{-10}$; one-tailed t-test) which was statistically significantly lower than the separability indices of single units ($p< 10^{-10}$, independent-samples t-test).

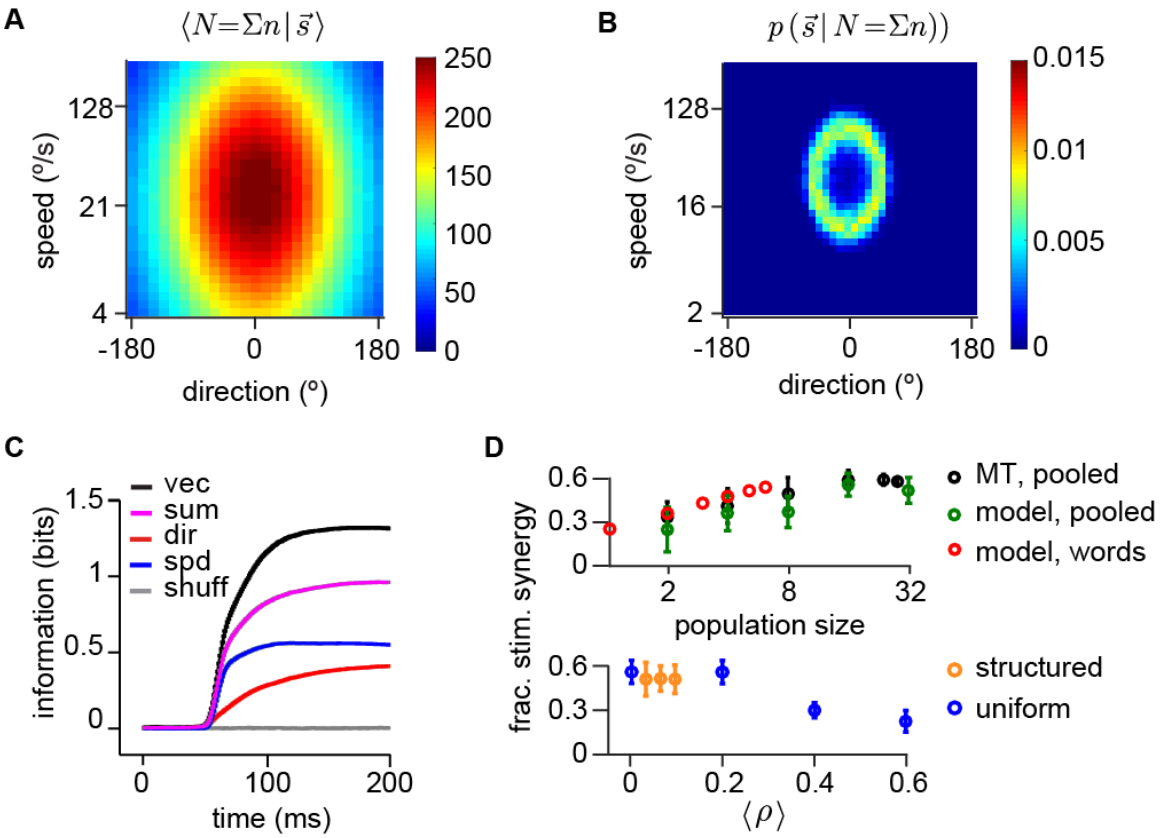

Figure 2-7. Stimulus synergy is enhanced in MT and model populations compared to individual units.

(A) We created population data from the recorded MT units by treating cells as if their preferred directions were aligned. For each motion stimulus, we randomly drew trials with replacement and summed spike counts. Conditional population response distributions for 4 16-cell groups. Colors represent the cumulative spike count 200ms after motion onset.

(B) Conditional stimulus distributions for the same example MT populations in **A** for a spike count of 53, compared to a maximum spike count of 107. This conditional distribution has a separability value of 0.54.

(C) Time course of motion information from the cumulative pooled spike count. Values represent the mean, SD over 100 random 16-cell groups, corrected for finite sample size (see text).

(D) **Top panel:** Fractional stimulus synergy from pooled spike counts increases with population size up to ~30 in data and model responses. Average fractional stimulus synergy measured 200ms after motion onset over 100 randomly generated population groups of different sizes. Symbols indicate the mean, SD of all *n*-cell groups drawn from (black) recorded MT cells, (green) Poisson model responses. Stimulus synergy is also present in a combinatorial population code based on Poisson simulations (red). **Bottom panel:** Fractional stimulus synergy

(Fig 2-7 continued) from pooled count in 16-cell populations of Poisson neurons as a function of mean pairwise correlation. Correlations were imposed uniformly (blue), or were structured to decay with increasing separation in preferred stimulus values (orange). Pairwise correlations in the observed physiological range (≤0.2) do not affect levels of stimulus synergy.

Lower separability suggests that population responses have an enhanced capacity for stimulus synergy compared to single neurons, and that is what we found. Figure 2-7C plots the time course of information about the motion vector and its components averaged over 16-cell groups using the same convention as the single unit in Figure 2-3A. Information about the motion vector (black trace, Fig 2-7C) is greater than the summed information about the motion components (black trace, Fig 2-7C) indicating substantial stimulus synergy in population responses. On average, 16-cell groups encode half again as much information about the motion vector as they encode about the components (fractional synergy = 0.55±0.11, mean ± SD, n=10 16-cell groups, difference from 0: $p < 10^{-7}$; two-tailed t-test), higher than the stimulus synergy observed in single units (n=30, difference from single units $p < 10^{-7}$; two-tailed t-test). Fractional synergy levels increase with population size up to group sizes of 16 (black symbols, Fig 2-7D), rising 2.1-fold with an 8-fold increase in pool size (2 vs. 16 cells). To ensure that our limited data sample did not bias estimates of population stimulus synergy, we repeated the analysis using Poisson-model neurons for which we could generate arbitrarily large sample sizes. We found that simulation results were within error bars of the MT data (green symbols, Fig 2-7D, top panel) for all pool sizes.

Cortical neuron responses are not independent but display a range of pairwise correlation levels, which might impact the level of stimulus synergy available in cortical populations. Using published MT data as a guide, we added pair-wise correlations to our Poisson model simulations and computed the effect on stimulus synergy [48,30,31]. We generated spikes with uniform levels of count correlation from 0-0.6 [30] and structured correlations that decayed as a function of the squared difference in preferred speeds [48,30] (see Methods). We plot the average level of fractional stimulus synergy as a function of pairwise correlation level in 7D (bottom panel) for 16-cell groups. Stimulus synergy levels are within errorbars for independent (ρ = 0, bottom panel, Fig 2-7D), uniform (blue symbols), and structured (orange symbols) correlations for $<\rho> \leq 0.2$ (see Methods), which is the likely physiological range [30,62,63]. This result suggests that ignoring pairwise interactions in constructing cell groups from our MT data did not strongly bias our estimates of fractional stimulus synergy. However, higher levels of pairwise correlations ($<\rho> \geq 0.4$) have been observed between cells with similar tuning preferences [27,30]. We simulated tuned correlations with a peak value up to 0.6 (mean value of 0.1) without any impact the calculated levels of stimulus synergy (orange symbols).

If multidimensional feature tuning exists in nature to increase sensory information recovery via stimulus synergy, then the brain might also exploit other mechanisms of information savings such as combinatorial coding. Patterns of responses across neurons encode substantially more information than the pooled count [34], but does a combinatorial code also exhibit stimulus synergy? Poisson

models allowed us to construct the probability of observing spike patterns exactly, allowing us to measure stimulus synergy in a combinatorial code without the data limitations imposed by experiments. We used aligned direction preferences and a range of speed preferences to create homogeneous, independent Poisson model neurons (see Methods). We used the tuning functions to construct analytically the probability of observing each pattern of count values for a given stimulus. In the absence of pairwise noise correlations between neurons, the probability of observing a pattern of counts, or spike "word" $\{n_1, n_2, \ldots, n_N\}$ is the product of count probabilities in each unit (see Methods, Fig 2-8B). There are $(n^{max}+1)^N$ observable words in an N-cell population, from {000 … 0} to $\{n_1{}^{max} n_2{}^{max} n_3{}^{max} \ldots n_N{}^{max}\}$, where n^{max} is the maximum observed spike count in each neuron. We constrained the time window and maximum spike rate such that counts greater than 15 were rare, so for a 6-cell group there were 16^5 possible words. Figure 2-8C plots the probability of observing words in rank order for groups from 2-9 units. For each group size, the most likely word has no spikes, which is also observed in cortical data [34]. The joint distribution of words and stimuli had an entropy of 8.3 bits (2 cell groups) to 16.2 bits (9 cell groups) which ranges from 73% (2 cells) to 55% (9 cells) of the maximum entropy condition of equally frequent words. Like the pooled count, population words encode stimulus features synergistically, encoding more information about the vector stimulus than about its 1D components (Fig 2-8D). The level of encoded information and of stimulus synergy was lower in our word simulations compared to the pooled count analysis because we restricted the firing rate to limit the total number of patterns. As we observed in the pooled count analysis, fractional synergy

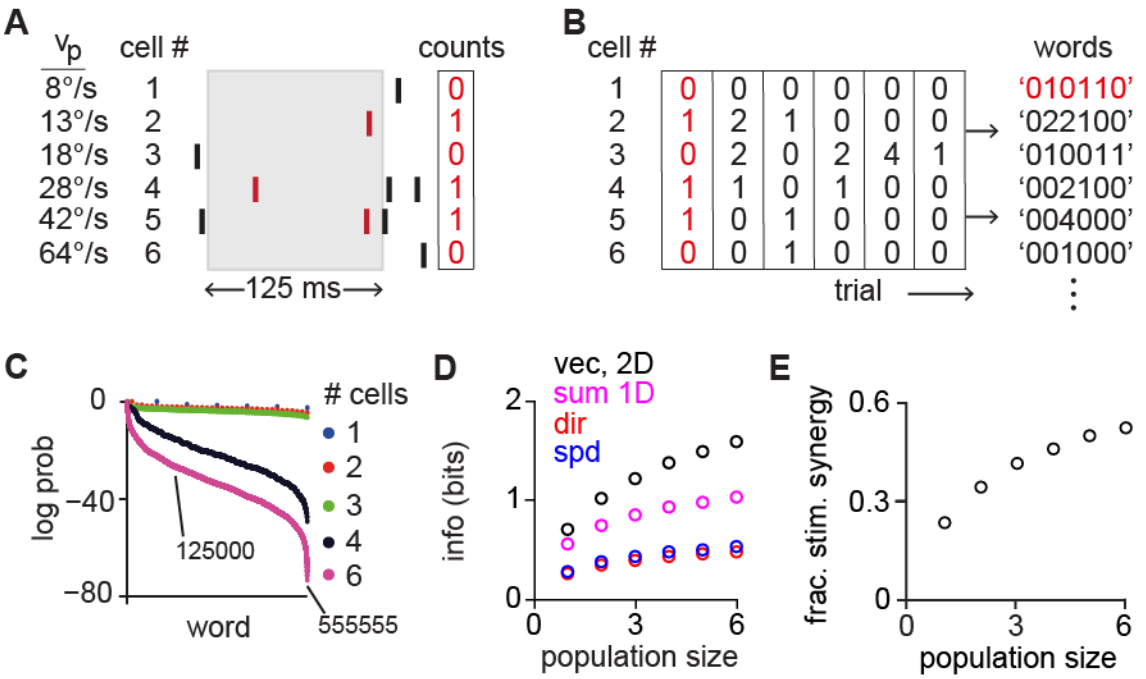

Figure 2-8: A combinatorial population code displays stimulus synergy

(A) We use patterns of spike counts in a 125ms window across Poisson model neurons (see Figure 2-7) as a coding symbol. With homogeneous Poisson spiking, sliding the window through time is equivalent to repeating trials.

(B) We considered spike patterns across up to 6-cell groups. To restrict the combinatorial scale, we set a cut-off of 15 spikes per cell such that there were 16^N possible words, where N is the population size.

(C) We constructed the probability of occurrence of each spike word for each population size. X axis is normalized to the number of observable words: 36 points are plotted for a 2-cell population, while ~10^6 words are plotted for a 9-cell population.

(D) Mutual information between words and stimulus increases with population size.

(E) Stimulus synergy, expressed as a fraction of the summed 1D information values, increases with the number of dimensions.

---

increases with population size (Fig 2-8E). Overall we find that stimulus synergy levels are preserved at the population level under several different assumptions about the nature of the cortical sensory code.

Pursuit eye movements reflect the stimulus synergy observed in MT

The preservation of synergistic coding at the population level suggests that stimulus synergy may be relevant to behaviors guided by tuned sensory populations. We tested this hypothesis by analyzing the information about stimulus motion encoded in the monkeys' smooth pursuit eye movements. In order to stabilize the retinal image of a moving target, the pursuit system translates motion estimates from MT activity into commands to the extra-ocular muscles to smoothly accelerate and rotate the eye. Because the behavior is precise, pursuit provides a window into ongoing internal estimates of target motion, at least until extraretinal signals become available >125ms after pursuit onset to complicate interpretation. Figure 2-9B shows horizontal and vertical components of eye velocity over time for a single dataset. Monkeys tracked targets that translated across the screen with pseudorandomly selected directions and speeds (0°, 45°, 135°, 180°, 225°, 315° at speeds of 14, 16, 18, 20, 22, 24, 26, and 28°/s) (Fig 2-9C). Because purely vertical pursuit tends to be poor, we did not include tracking for 90° and 270° target motions in the analysis. The entropy of analyzed stimuli was $\log_2(24)$ or 4.6 bits for all 3 monkeys.

We computed the mutual information between eye and target velocity components to determine if stimulus synergy affects the quality of motion-driven movement. We averaged horizontal (H) and vertical (V) eye velocity components in 10ms windows, stepping the window at 1ms intervals through the trial. We discretized the component eye velocities into 24 bins and then computed the mutual information quantities in Equation 1, correcting for finite sample size as with the

neural recordings (see Methods). As with MT responses, the information about direction rises quickly after pursuit onset, ~90ms after the target begins to move (red trace, Fig 2-9A). Information about target speed accumulates more slowly in the pursuit response because the eye accelerates from rest for all target speeds (blue trace, Fig 2-9E). Also consistent with MT, more information is encoded about the target motion vector (black trace, Fig 2-9A), than the sum of the information about direction and speed (magenta trace, Fig 2-9A). We observed stimulus synergy in all 3 monkeys. Measured 200ms after stimulus onset, percentage synergy values were 25±0.3% (M1), 21±0.8% (M2) and 14±0.04% (M3) (SD, n=50 draws of 70% of total data sample). These levels are lower than both individual MT units and population estimates of stimulus synergy. Stimulus synergy appears ~40ms after pursuit onset and increases thereafter for all monkeys (Fig 2-9B). In comparison, synergy appears in MT responses within 15ms of response onset.

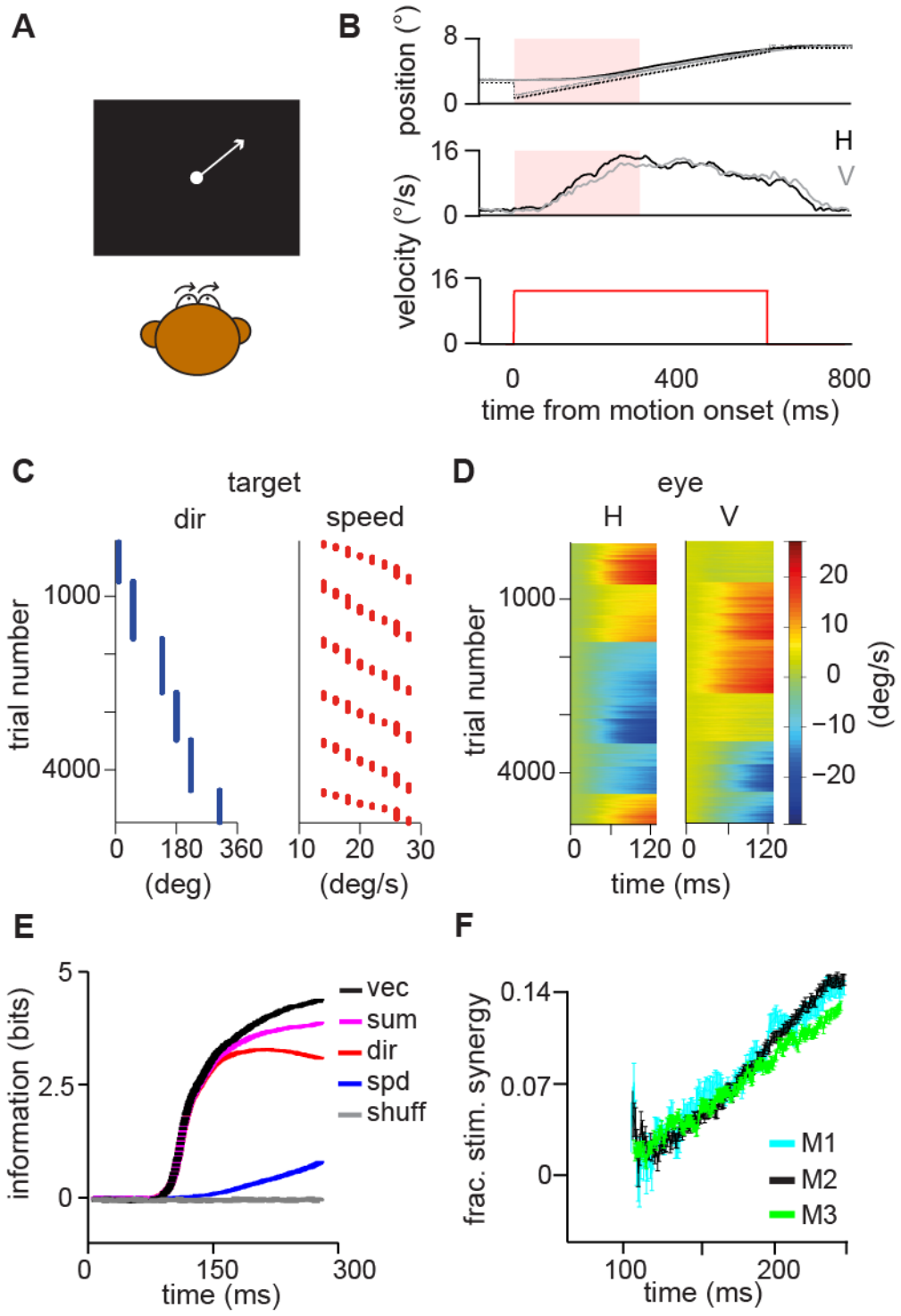

Figure 2-9. Stimulus synergy is apparent in pursuit behavior.

(A) Cartoon of a pursuit experiment. Monkeys pursued spot targets that appeared eccentrically as the fixation point was extinguished then immediately began to translate toward the fixation position. Target directions matched the MT recording experiments and speeds ranged from 1 to 96°/s.

(Fig 2-9 continued)

(B) Horizontal (H) and vertical (V) eye positions and velocities over time for a single pursuit trial for a 14°/s target moving at 45° relative to rightward.

(C) Target direction (left panel) and speed (right panel) for each trial in A. Target directions ranged in 45° increments around the circle. Target speeds were 14-28°/s.

(D) Each row of the color density plot represents the horizontal (H, left panel) and vertical (V, right panel) eye velocity on a single trial during the first 125ms of pursuit from a day's experiment with M1.

(E) Mutual information between H,V eye velocity and target motion over time for M1. Information about the 2D motion vector (black) is greater than the sum of the information about direction (red) and speed (blue) individually. Speed information increases slowly as the eye accelerates smoothly from rest. Times are relative to target motion onset.

(F) Fractional stimulus synergy increases over time during pursuit initiation. Data from 3 monkeys.

Discussion

From a coding perspective, the prevalence of multidimensional sensory maps in the brain is perplexing because they create a credit assignment problem – along which dimension did a stimulus change to create the observed modulation in sensory activity? Yet at many levels of the visual system, and throughout the brain, multidimensional maps are the rule rather than the exception [8,64–66,7,52,67–71]. We show that multi-dimensional tuning functions have a computational advantage. More information can be encoded about a multidimensional stimulus than its individual components, even when those stimulus features are independent. Stimulus synergy has implications for how cortical responses should be decoded to provide sensory estimates for behavior: sensory stimuli should be decoded in the dimensionality of their representation to maximize the recovered information. The fact that stimulus synergy is apparent in the initiation of smooth pursuit suggests that MT activity is read out as a motion vector, rather than as independent estimates of target direction and speed. These results add to a growing body of work demonstrating efficient information transmission from visual motion estimates to pursuit eye movements [72,15,18,19,73,74].

Unlike more familiar forms of coding synergy, stimulus synergy does not depend on subtle features of feature selectivity or spike timing, but rather emerges from multidimensional tuning itself. Therefore we expect that stimulus synergy will impact information representation in any area of the brain with tuned responses. Like MT, neurons in primary visual cortex (V1) are tuned for a small number of visual

features. Grunewald and Skoumbourdis reported that V1 neurons tuned for binocular disparity and orientation encoded more information about the features jointly than singly [41], although their focus was the impact of tuning diversity within V1 on coding. Recent studies of prefrontal cortical neurons credit their high-dimensional representations with enhanced cognitive performance on decision-related tasks [75–78]. Our work provides a theoretical framework for understanding how multidimensional representations, whether in sensory or higher association areas, could benefit the many behaviors that depend on multidimensional estimates from cortical populations [46,67,79,80].

Origins of stimulus synergy

A nonlinearity forms the basis of any form of synergy. Coding synergies can arise from neural diversity within nominally redundant coding pools [34,36,37,43,45], or from temporal patterning in spike trains [35,38] such that the pattern encodes more information than the summed response. MT neurons do demonstrate coding synergy, largely arising from diversity in rate dynamics among neurons with the same preferred direction [34]. We have described a distinct form of synergy that arises from the multidimensional tuning functions that exist throughout the brain, and we show that shown that it enhances information representation at the level of individual neurons, populations, and in sensory-driven behavior. Multidimensional tuning creates a divergence between the conditional response distribution for an n-dimensional stimulus and its component parts, and it

is this nonlinearity, rather than response diversity or high-dimensional feature selectivity, that creates stimulus synergy. MT neurons have highly separable tuning functions for motion direction and speed, surpassing separability levels for ocular disparity and motion direction in MT [40] and values reported elsewhere in cortex [46,41]. The fact that MT displays substantial direction-speed synergy despite separable tuning functions indicates that a coding advantage to multidimensional sensory representation should be accessible to most, if not all, brain areas.

Implications for decoding multidimensional stimuli

A potential downside to multiplexing sensory signals is that decoding multidimensional maps can lead to systematic estimation errors. In one dimension, a vector average operation can recover unbiased estimates of a stimulus feature by weighting neural responses by their preferred stimulus, which under some conditions is an ideal estimator [48,59,81–86]. Applying the same decoder to a multidimensional stimulus representation introduces large, systematic errors [23,83]. For example, a vector average decoder underestimates motion speed when neurons are direction and speed tuned and stimuli have multiple directions [81,83]. Our results suggest that a decoder that operated in the same dimensions as the stimulus representation could recover more information than independent decoders for each stimulus component (e.g. a motion vector decoder could recover more information than independent direction and speed decoders combined). The fact that pursuit eye movements show evidence of stimulus synergy is suggestive that the

visual drive for pursuit is a 2D motion vector. One study of correlations between MT activity and eye movement fluctuations supports 2D motion decoding [87], but another does not [48], although we note that neither of the previous studies employed motion stimuli of multiple directions and speeds, which complicates interpretation in this context.

Several theoretical studies have considered how tuning along multiple dimensions competitively affects feature discriminability. Sharpened tuning generally decreases per-spike errors for stimulus estimation along that dimension, with the caveat that if tuning functions become so narrow as to lower the size of the coding pool, noise increases to offset the signal increase [5,49]. Broadened tuning along an independent stimulus dimension can reduce estimation errors by increasing the pool size activated by a stimulus along another dimension, but at the expense of reducing the discriminability of that stimulus dimension [22,23,50]. Errors in discriminating a stimulus feature from a homogeneous population are therefore proportional to the tuning bandwidth of the stimulus feature itself but inversely proportional to the tuning bandwidths of other mapped dimensions [5,22]. Correlations between neurons can modulate how estimation errors depend on dimensionality, but we and others show that the dependence persists in the independent case [5,22,88]. It is an interesting idea, if questionable from an efficiency standpoint, that sensory neurons might encode less important stimulus features to improve discrimination of important ones. For pursuit behavior, which tries to minimize the difference between eye and target motion to eliminate retinal slip,

motion direction and speed are equally important and discriminability along one motion dimension cannot be sacrificed to optimize the other.

Are sensory responses tuned to maximize multidimensional stimulus information and stimulus synergy?

If information enhancement is the primary objective in sensory map design, are cortical sensory neurons encoding the ideal number of stimulus features? That is a difficult question to answer because it is unclear whether we have fully described feature selectivity in any cortical area, and the predicted level of stimulus synergy will depend critically on that tuning. Most MT neurons display strong, separable tuning for 2-3 motion dimensions: direction, speed and binocular disparity, a cue for motion in depth [1,40,61,89–91]. While MT responses can be modulated by other features such as spatial frequency [9,55], and acceleration [92], firing rates are consistently tuned for the first three. For the average tuning bandwidth we measured in our MT sample (0.16, as a fraction of the tested stimulus range), 2-3 dimensions correspond to a peak in total stimulus information and to stimulus synergy. While this result is suggestive, a larger comparative study of stimulus synergy in neurons with a large variety of feature selectivity and dimensionality will be needed to draw any conclusion about its generality. Because the highest levels of stimulus information are encoded by neurons with sharp tuning to a single stimulus dimension, if maximizing stimulus information were the brain's sole objective, we should observe a preponderance of single feature maps of very selective neurons in the brain. To the

contrary, many if not most sensory maps represent more than one stimulus dimension. The reason is likely that neurons and the spikes they generate are metabolically expensive [93], and cranial space is at a premium [69,94], such that energy and wiring savings may outweigh the modest information loss. It is also possible that multidimensional tuning could have computational benefits such as simplifying hierarchical processing [95,96]. Certainly at the population level, the tuning bandwidths that optimize encoding depend on other factors such as response overlap, heterogeneity, pairwise correlations, and the coding symbol of interest [5,22,25,49,50].

Our work makes a strong prediction that stimulus multiplexing in sensory areas can confer a computational advantage, and it shows that behavior can benefit. Stimulus synergy should influence how we think about sensory representations and their readout, and it highlights what fundamental coding features neuroscientists can miss when isolating single stimulus features in experimental design.

Acknowledgments

We thank S.E. Palmer and D.J. Schwab for helpful discussions about the analysis and N Brunel and S Lisberger for comments on the manuscript. We also thank T. Mukherjee for assistance with animal care and data collection, and the veterinary staff of the Animal Resources Center at University of Chicago. Research was supported by grants to LCO from the Alfred P Sloan Foundation, Whitehall Foundation, Brain Research Foundation, NIH NEI EY023371, and NSF IOS 145704.

References

1. DeAngelis GC, Uka T. Coding of horizontal disparity and velocity by MT neurons in the alert macaque. J Neurophysiol. 2003;89: 1094–1111. doi:10.1152/jn.00717.2002

2. Rushton WAH. Review Lecture. Pigments and signals in colour vision. J Physiol. 1972;220: 1P–31P. Available: http://www.ncbi.nlm.nih.gov/pmc/articles/PMC1331666/

3. Huk AC. Multiplexing in the primate motion pathway [Internet]. Vision Research. 2012. pp. 173–180. doi:10.1016/j.visres.2012.04.007

4. Dokka K, DeAngelis GC, Angelaki DE. Multisensory Integration of Visual and Vestibular Signals Improves Heading Discrimination in the Presence of a Moving Object. J Neurosci. 2015;35: 13599–607. doi:10.1523/JNEUROSCI.2267-15.2015

5. Brunel N, Nadal JP. Mutual information, Fisher information, and population coding. Neural Comput. 1998;10: 1731–57. Available: http://www.ncbi.nlm.nih.gov/pubmed/9744895

6. Montemurro M a, Panzeri S. Optimal tuning widths in population coding of periodic variables. Neural Comput. 2006;18: 1555–1576. doi:10.1162/neco.2006.18.7.1555

7. Zohary E. Population coding of visual stimuli by cortical neurons tuned to more than one dimension. Biol Cybern. 1992;66: 265–72. doi:10.1007/BF00198480

8. Maunsell JHR, Van Essen DC. Functional properties of neurons in middle temporal visual area of the macaque monkey . I . Selectivity for stimulus direction, speed, and orientation. J Neurophysiol. 1983;49: 1127–1147.

9. Priebe NJ, Cassanello CR, Lisberger SG. The neural representation of speed in macaque area MT/V5. J Neurosci. 2003;23: 5650–5661. doi:23/13/5650 [pii]

10. Lagae L, Raiguel S, Orban G a. Speed and direction selectivity of macaque middle temporal neurons. J Neurophysiol. 1993;69: 19–39.

11. Britten KH, Newsome WT, Shadlen MN, Celebrini S, Movshon J a. A relationship between behavioral choice and the visual responses of neurons in macaque MT. Vis Neurosci. 1996;13: 87–100. doi:10.1017/S095252380000715X

12. Newsome WT, Paré EB. A selective impairment of motion perception following lesions of the middle temporal visual area (MT). J Neurosci. Society

for Neuroscience; 1988;8. doi:http://www.ncbi.nlm.nih.gov/pubmed/3385495

13. Groh JM, Born RT, Newsome WT. How Is a Sensory Map Read Out? Effects of Microstimulation in Visual Area MT on Saccades and Smooth Pursuit Eye Movements. J Neurosci . 1997;17: 4312–4330. Available: http://www.jneurosci.org/content/17/11/4312.abstract

14. Newsome WT, Wurtz RH, Komatsu H. Relation of cortical areas MT and MST to pursuit eye movements. II. Differentiation of retinal from extraretinal inputs. J Neurophysiol. 1988;60: 604–20. Available: http://www.ncbi.nlm.nih.gov/pubmed/3171644

15. Osborne LC, Lisberger SG, Bialek W. A sensory source for motor variation. Nature. 2005;437: 412–6. doi:10.1038/nature03961

16. Lisberger SG, Westbrook LE. Properties of visual inputs that initiate horizontal smooth pursuit eye movements in monkeys. J Neurosci. 1985;5: 1662–73. Available: http://www.ncbi.nlm.nih.gov/pubmed/4009252

17. Osborne LC, Bialek W, Lisberger SG. Time course of information about motion direction in visual area MT of macaque monkeys. J Neurosci. 2004;24: 3210–22. doi:10.1523/JNEUROSCI.5305-03.2004

18. Osborne LC, Hohl SS, Bialek W, Lisberger SG. Time course of precision in smooth-pursuit eye movements of monkeys. J Neurosci. 2007;27: 2987–98. doi:10.1523/JNEUROSCI.5072-06.2007

19. Mukherjee T, Battifarano M, Simoncini C, Osborne LC. Shared Sensory Estimates for Human Motion Perception and Pursuit Eye Movements. J Neurosci. 2015;

20. Wilke SD, Eurich CW. Representational accuracy of stochastic neural populations. Neural Comput. United States; 2002;14: 155–189. doi:10.1162/089976602753284482

21. Kayser C, Montemurro M a, Logothetis NK, Panzeri S. Spike-phase coding boosts and stabilizes information carried by spatial and temporal spike patterns. Neuron. Elsevier Ltd; 2009;61: 597–608. doi:10.1016/j.neuron.2009.01.008

22. Eurich CW, Wilke SD. Multidimensional encoding strategy of spiking neurons. Neural Comput. 2000;12: 1519–1529. doi:10.1162/089976600300015240

23. Liu X, Xing Z, Guo W. Encoding and Decoding Neural Population Signals for Two-Dimensional Stimulus. Neural Process Lett. Springer US; 2017; doi:10.1007/s11063-017-9602-x

24. Wu S, Amari S, Nakahara H. Population Coding and Decoding in a Neural Field: A Computational Study. Neural Comput. 2002;14: 999–1026. doi:10.1162/089976602753633367

25. Yarrow S, Series P. The influence of population size, noise strength and behavioral task on best-encoded stimulus for neurons with unimodal or monotonic tuning curves. Front Comput Neurosci. 2015;9: 1–20. doi:10.3389/fncom.2015.00018

26. Lehky SR, Sereno AB. Population coding of visual space: modeling. Front Comput Neurosci. 2011;4: 155. doi:10.3389/fncom.2010.00155

27. Ecker AS, Berens P, Tolias AS, Bethge M. The effect of noise correlations in populations of diversely tuned neurons. J Neurosci. 2011;31: 14272–83. doi:10.1523/JNEUROSCI.2539-11.2011

28. Shamir M. Emerging principles of population coding: in search for the neural code. Curr Opin Neurobiol. England; 2014;25: 140–148. doi:10.1016/j.conb.2014.01.002

29. Shamir M, Sompolinsky H. Implications of neuronal diversity on population coding. Neural computation. United States; 2006. pp. 1951–1986. doi:10.1162/neco.2006.18.8.1951

30. Huang X, Lisberger SG. Noise correlations in cortical area MT and their potential impact on trial-by-trial variation in the direction and speed of smooth-pursuit eye movements. J Neurophysiol. 2009;101: 3012–30. doi:10.1152/jn.00010.2009

31. Cohen MMR, Kohn A. Measuring and interpreting neuronal correlations. Nat Neurosci. 2011;14: 811–819. doi:10.1038/nn.2842.Measuring

32. Shannon CE. A mathematical theory of communication. Bell Syst Tech J. 1948;27: 379–423. doi:10.1145/584091.584093

33. Bialek W, de Ruyter van Steveninck R, Rieke F, Warland D. Spikes: Exploring the Neural Code. Boston: MIT Press; 1997.

34. Osborne LC, Palmer SE, Lisberger SG, Bialek W. The neural basis for combinatorial coding in a cortical population response. J Neurosci. 2008;28: 13522–13531. doi:10.1523/JNEUROSCI.4390-08.2008

35. Schneidman E, Puchalla JL, Segev R, Harris RA, Bialek W, Berry MJ. Synergy from silence in a combinatorial neural code. J Neurosci. 2011;31: 15732–15741. doi:10.1523/jneurosci.0301-09.2011

36. Reich DS, Mechler F, Victor JD. Independent and Redundant Information in

Nearby Cortical Neurons. Science (80-). 2001;294: 2566 LP-2568. Available: http://science.sciencemag.org/content/294/5551/2566.abstract

37. Schneidman E, Bialek W, Berry MJ. Synergy, Redundancy, and Independence in Population Codes. J Neurosci. 2003;23: 11539 LP-11553. Available: http://www.jneurosci.org/content/23/37/11539.abstract

38. Brenner N, Strong SP, Koberle R, Bialek W, de Ruyter van Steveninck RR. Synergy in a neural code. Neural Comput. 2000;12: 1531–1552. doi:10.1162/089976600300015259

39. Strong SP, Koberle R, de Ruyter van Steveninck RR, Bialek W. Entropy and Information in Neural Spike Trains. Phys Rev Lett. 1998;80: 197–200. Available: http://arxiv.org/abs/cond-mat/9603127v2

40. Smolyanskaya A, Ruff DA, Born RT. Joint tuning for direction of motion and binocular disparity in macaque MT is largely separable. J Neurophysiol. 2013;110: 2806–16. doi:10.1152/jn.00573.2013

41. Grunewald A, Skoumbourdis EK. The integration of multiple stimulus features by V1 neurons. J Neurosci. 2004;24: 9185–9194. doi:10.1523/JNEUROSCI.1884-04.2004

42. Cover TM, Thomas JA. Information Theory and Statistics. Elements of Information Theory. John Wiley & Sons, Inc.; 2005. pp. 347–408. doi:10.1002/047174882X.ch11

43. Gawne TJ, Richmond BJ. How independent are the messages carried by adjacent inferior temporal cortical neurons? J Neurosci. 1993;13: 2758–71. Available: http://www.ncbi.nlm.nih.gov/pubmed/8331371

44. Gat I, Tishby N. Spotting Neural Spike Patterns via Decomposition Into Types. Time.

45. Panzeri S, Schultz SR, Treves A, Rolls ET. Correlations and the encoding of information in the nervous system. Proc Biol Sci. 1999;266: 1001–12. doi:10.1098/rspb.1999.0736

46. Sunkara A, DeAngelis GC, Angelaki DE. Joint representation of translational and rotational components of optic flow in parietal cortex. Proc Natl Acad Sci U S A. 2016;113: 5077–82. doi:10.1073/pnas.1604818113

47. Mazer J a, Vinje WE, McDermott J, Schiller PH, Gallant JL. Spatial frequency and orientation tuning dynamics in area V1. Proc Natl Acad Sci U S A. 2002;99: 1645–1650. doi:10.1073/pnas.022638499

48. Hohl SS, Chaisanguanthum KS, Lisberger SG. Sensory population decoding for

visually guided movements. Neuron. Elsevier Inc.; 2013;79: 167–79. doi:10.1016/j.neuron.2013.05.026

49. Zhang K, Sejnowski TJ. Neuronal Tuning: To Sharpen or Broaden? Neural Comput. 1999;11: 75–84. doi:10.1162/089976699300016809

50. Brown WM, Bäcker A. Optimal neuronal tuning for finite stimulus spaces. Neural Comput. 2006;18: 1511–1526. doi:10.1162/neco.2006.18.7.1511

51. Nadler JW, Nawrot M, Angelaki DE, DeAngelis GC. MT neurons combine visual motion with a smooth eye movement signal to code depth-sign from motion parallax. Neuron. 2009;63: 523–32. doi:10.1016/j.neuron.2009.07.029

52. Sanada TM, DeAngelis GC. Neural Representation of Motion-In-Depth in Area MT. J Neurosci. 2014;34: 15508–15521. doi:10.1523/JNEUROSCI.1072-14.2014

53. Rodman HR, Albright TD. Coding of visual stimulus velocity in area MT of the macaque. Vision Res. 1987;127: 2035–2048.

54. Kumano H, Uka T. Quantification of direction-speed tuning and its relationship with pattern motion selectivity in macaque area MT. Neurosci Res. 2010;68: e270. doi:https://doi.org/10.1016/j.neures.2010.07.1202

55. Priebe NJ, Lisberger SG, Movshon JA. Tuning for spatiotemporal frequency and speed in directionally selective neurons of macaque striate cortex. J Neurosci. 2006;26: 2941–2950. doi:10.1523/JNEUROSCI.3936-05.2006

56. Panzeri S, Treves A. Analytical estimates of limited sampling biases in different information measures. Netw Comput Neural Syst. 1996;7: 87–107. doi:doi: 10.1088/0954-898x/7/1/006

57. Lombardo J, Macellaio M, Liu B, Palmer SE, Osborne LC. State Dependence of Stimulus-Induced Variability Tuning in Macaque MT. Preprint. 2017; Available: https://arxiv.org/abs/1710.10548

58. Panzeri S, Treves A, Schultz S, Rolls ET. On Decoding the Responses of a Population of Neurons from Short Time Windows. Neural Comput. 1999;11: 1553–1577. doi:10.1162/089976699300016142

59. Lakshminarasimhan KJ, Pouget A, Deangelis GC, Angelaki DE. Inferring decoding strategies for multiple correlated neural populations. 2017; 1–41.

60. Bethge M, Rotermund D, Pawelzik K. Optimal Short-Term Population Coding: When Fisher Information Fails. Neural Comput. 2002;14: 2317–2351. doi:10.1162/08997660260293247

61. Czuba TB, Huk AC, Cormack LK, Kohn A. Area MT Encodes Three-Dimensional Motion. J Neurosci. Society for Neuroscience; 2014;34: 15522–15533. doi:10.1523/JNEUROSCI.1081-14.2014

62. Ponce-Alvarez A, Thiele A, Albright TD, Stoner GR, Deco G. Stimulus-dependent variability and noise correlations in cortical MT neurons. Proc Natl Acad Sci U S A. 2013;110: 13162–7. doi:10.1073/pnas.1300098110

63. Nienborg H, Cumming B. Correlations between the activity of sensory neurons and behavior: how much do they tell us about a neuron's causality? Curr Opin Neurobiol. Elsevier Ltd; 2010;20: 376–81. doi:10.1016/j.conb.2010.05.002

64. Nishimoto S, Gallant JL. A Three-Dimensional Spatiotemporal Receptive Field Model Explains Responses of Area MT Neurons to Naturalistic Movies. J Neurosci. 2011;31: 14551–14564. doi:10.1523/JNEUROSCI.6801-10.2011

65. Gu Y, Cheng Z, Yang L, DeAngelis GC, Angelaki DE. Multisensory Convergence of Visual and Vestibular Heading Cues in the Pursuit Area of the Frontal Eye Field. Cereb Cortex. 2015; doi:10.1093/cercor/bhv183

66. Angelaki DE, Gu Y, DeAngelis GC. Multisensory integration: psychophysics, neurophysiology, and computation. Curr Opin Neurobiol. 2009;19: 452–8. doi:10.1016/j.conb.2009.06.008

67. Neri P, Levi DM. Evidence for joint encoding of motion and disparity in human visual perception. J Neurophysiol. 2008;100: 3117–3133. doi:10.1152/jn.90271.2008

68. Haxby J V, Gobbini MI, Furey ML, Ishai a, Schouten JL, Pietrini P. Distributed and overlapping representations of faces and objects in ventral temporal cortex. Science. 2001;293: 2425–30. doi:10.1126/science.1063736

69. Van Essen DC. Behind the optic nerve: an inside view of the primate visual system. Trans Am Ophthalmol Soc. American Ophthalmological Society; 1995;93: 123–133. Available: http://www.ncbi.nlm.nih.gov/pubmed/8719674

70. Van Essen DC, Gallant JL. Neural mechanisms of form and motion processing in the primate visual system. Neuron. 1994;13: 1–10. doi:10.1016/0896-6273(94)90455-3

71. Desimone R, Schein SJ. Visual properties of neurons in area V4 of the macaque: sensitivity to stimulus form. J Neurophysiol. 1987;57: 835–868. doi:doi.org/10.1152/jn.1987.57.3.835

72. Liu B, Macellaio M V., Osborne LC. Efficient sensory cortical coding optimizes pursuit eye movements. Nat Commun. Nature Publishing Group; 2016;7:

12759. doi:10.1038/ncomms12759

73. Medina JF, Lisberger SG. Variation, signal, and noise in cerebellar sensory-motor processing for smooth-pursuit eye movements. J Neurosci. 2007;27: 6832–6842. doi:10.1523/JNEUROSCI.1323-07.2007

74. Stephens GJ, Osborne LC, Bialek W. Searching for simplicity in the analysis of neurons and behavior. Proc Natl Acad Sci U S A. 2011;108 Suppl: 15565–71. doi:10.1073/pnas.1010868108

75. Gao P, Trautmann E, Yu BM, Santhanam G, Ryu S, Shenoy K, et al. A theory of multineuronal dimensionality, dynamics and measurement. bioRxiv. 2017; 214262. doi:10.1101/214262

76. Lopes-dos-Santos V, Ribeiro S, Tort ABL. Detecting cell assemblies in large neuronal populations. J Neurosci Methods. Elsevier B.V.; 2013;220: 149–166. doi:10.1016/j.jneumeth.2013.04.010

77. Kobak D, Brendel W, Constantinidis C, Feierstein CE, Kepecs A, Mainen ZF, et al. Demixed principal component analysis of population activity in higher cortical areas reveals independent representation of task parameters. 2014; Available: http://arxiv.org/abs/1410.6031

78. Rigotti M, Barak O, Warden MR, Wang XJ, Daw ND, Miller EK, et al. The importance of mixed selectivity in complex cognitive tasks. Nature. 2013;497: 585–590. doi:10.1038/nature12160

79. Pack CC, Born RT, Livingstone MS. Two-dimensional substructure of stereo and motion interactions in macaque visual cortex. Neuron. 2003;37: 525–535. doi:10.1016/S0896-6273(02)01187-X

80. Qian N, Freeman RD. Pulfrich phenomena are coded effectively by a joint motion-disparity process. J Vis. NIH Public Access; 2009;9: 24 1-16. doi:10.1167/9.5.24\r/9/5/24/ [pii]

81. Priebe NJ, Lisberger SG. Estimating target speed from the population response in visual area MT. J Neurosci. 2004;24: 1907–1916. doi:10.1523/JNEUROSCI.4233-03.2004

82. Lisberger SG, Ferrera VP. Vector averaging for smooth pursuit eye movements initiated by two moving targets in monkeys. J Neurosci. 1997;17: 7490–7502.

83. Johnston A, Scarfe P. The role of the harmonic vector average in motion integration. Front Comput Neurosci. 2013;7: 146. doi:10.3389/fncom.2013.00146

84. Salinas E, Abbott LF. Vector reconstruction from firing rates. J Comput

Neurosci. 1994;1: 89–107. doi:10.1007/BF00962720

85. Seung HS, Sompolinsky H. Simple models for reading neuronal population codes. ProcNatlAcadSci. 1993;90: 10749–10753. doi:10.1073/pnas.90.22.10749

86. Qian N, Andersen RA. A physiological model for motion-stereo integration and a unified explanation of Pulfrich-like phenomena. Vision Res. 1997;37: 1683–98. doi:10.1016/S0042-6989(96)00164-2

87. Lee J, Yang J, Lisberger SG. Control of the Gain of Visual-Motor Transmission Occurs in Visual Coordinates for Smooth Pursuit Eye Movements. J Neurosci. 2013;33: 9420–9430. doi:10.1523/JNEUROSCI.4846-12.2013

88. Zavitz E, Yu H-H, Rosa MGP, Price NSC. Correlated Variability in the Neurons With the Strongest Tuning Improves Direction Coding. Cereb Cortex. 2017; doi:10.1093/cercor/bhx344

89. Krekelberg B. Interactions between Speed and Contrast Tuning in the Middle Temporal Area: Implications for the Neural Code for Speed. J Neurosci. 2006;26: 8988–8998. doi:10.1523/JNEUROSCI.1983-06.2006

90. Butts DA, Goldman MS. Tuning curves, neuronal variability, and sensory coding. PLoS Biol. 2006;4: e92. doi:10.1371/journal.pbio.0040092

91. Yamane Y, Carlson ET, Bowman KC, Wang Z, Connor CE. A neural code for three-dimensional object shape in macaque inferotemporal cortex. Nat Neurosci. 2008;11: 1352–1360. doi:10.1038/nn.2202

92. Lisberger SG, Movshon JA. Visual motion analysis for pursuit eye movements in area MT of macaque monkeys. J Neurosci. 1999;19: 2224–2246.

93. Laughlin SB, de Ruyter van Steveninck RR, Anderson JC. The metabolic cost of neural information. Nat Neurosci. Nature Publishing Group; 1998;1: 36–41. doi:10.1038/236

94. Varshney LR, Sjöström PJ, Chklovskii DB. Optimal information storage in noisy synapses under resource constraints. Neuron. 2006;52: 409–23. doi:10.1016/j.neuron.2006.10.017

95. Rust NC, DiCarlo JJ. Selectivity and Tolerance ("Invariance") Both Increase as Visual Information Propagates from Cortical Area V4 to IT. J Neurosci. 2010;30: 12978–12995. doi:10.1523/JNEUROSCI.0179-10.2010

96. DiCarlo JJ, Zoccolan D, Rust NC. How does the brain solve visual object recognition? Neuron. Elsevier Inc.; 2012;73: 415–434. doi:10.1016/j.neuron.2012.01.010

CHAPTER III

Correlations in smooth pursuit errors

are predicted by vector decoding

Abstract

Behavior is a useful tool to discover how brain circuits are organized, and how they manipulate sensory information to generate motor outputs. Here, we take advantage of the tight link between extrastriate area MT and smooth pursuit eye movements, finding that correlated errors in the eyes' direction and speed can be predicted by vector decoding estimates from a simulated MT population. We recorded smooth pursuit eye movements to repeated presentations of multiple directions and speeds of target motion, allowing us to describe single trials' eye movements in terms of their errors in direction, speed, and onset time from the mean. Because the scale of these errors is comparable to perceptual thresholds, smooth pursuit can be interpreted as a faithful representation of the estimate of the MT population, and makes a strong prediction that MT neurons' responses are read out not as direction and speed separately, but as a unified movement vector. To test this, we simulated MT responses and estimated direction and speed jointly using a vector decoder or using separate decoders for each feature. We find that only the vector decoder results in correlated output estimates, suggesting that MT responses are transformed to drive eye movements by being treated as a single movement vector.

Introduction

Despite decades of research performed on the middle temporal area of the macaque (MT) and visual motion processing [1–16], the literature remains inconclusive as to exactly how MT responses are read out to drive behavior and perceptual judgments. MT neurons are tuned for a variety of stimulus parameters, including object direction, speed, depth in the visual field, and binocular disparity [1,17–22]. Typically, MT neurons' responses are modeled as being decoded separately according to each stimulus parameter to drive both perception and behavior [15,23–25]. Single-trial fluctuations in single neurons' spike rates would therefore weight a neuron's preference more strongly, no matter which parameter was being decoded. If multiple parameters were decoded simultaneously, spike count fluctuations could cause correlated deviations in the behavioral output.

The decoding methods that have been the most successful at replicating behavior based on simulated MT responses are vector-averaging methods, which weight the responses of neurons by their preferred stimulus parameters to generate an estimate of the stimulus speed and direction $(\hat{s}, \hat{\theta})$[26–29]:

$$\hat{s} = \frac{\sum_i s_i \theta_i}{\sum_i R_i};\ \hat{\theta} = \tan^{-1}\left(\frac{Im\left(R_i e^{i\theta_i}\right)}{Re(R_i e^{i\theta_i})}\right), \quad (1)$$

where R_i, s_i, and θ_i are the response, preferred speed, and preferred direction of neuron *i*. Basic labeled-line vector averaging methods like Equation 1 have recently

been enhanced by variations on the manner of normalization used to mimic lateral inhibition within cortex, producing more accurate and biologically plausible predictions[15,29–31]. Opponent vector averaging computes the difference of the responses from a neuron pair with identical preferred speeds but opposite preferred directions. It also adds log-tuning for the speed calculation, as speed-tuning functions in MT are well-described by a log-normal distribution[11]:

$$\hat{\theta} = \tan^{-1}\left(\frac{\hat{V}}{\hat{H}}\right);\ \hat{s} = 2^{\sqrt{\hat{H}^2+\hat{V}^2}}; \tag{2}$$

$$\hat{H} = \frac{\sum_i \log_2(s_i)\cos(\theta_i)R_i}{\epsilon + \sqrt{R_h^2 + R_v^2}};\ \hat{V} = \frac{\sum_i \log_2(s_i)\sin(\theta_i)R_i}{\epsilon + \sqrt{R_h^2 + R_v^2}},$$

where

$$R_h = \sum_i \cos(\theta_i)\, R_i\ ;\ R_v = \sum_i \sin(\theta_i)\, R_i \tag{3}$$

and ε is a parameter that serves to stabilize the estimate when model neuron responses are near zero. A further improvement, opponent vector averaging with uncorrelated normalization[15], decorrelates the numerator and denominator by using responses from two separate populations (*i* and *j*) for the numerator and denominator. Responses *within* each population are correlated in a physiologically plausible manner, but there is no explicit correlation *between* the populations:

$$\hat{\theta} = \tan^{-1}\left(\frac{\hat{V}}{\hat{H}}\right);\ \hat{s} = 2^{\sqrt{\hat{H}^2+\hat{V}^2}}; \tag{4}$$

$$\hat{H} = \frac{\sum_i \log_2(s_i)\cos(\theta_i)R_i}{k\sum_j R_j};\ \hat{V} = \frac{\sum_i \log_2(s_i)\sin(\theta_i)R_i}{k\sum_j R_j},$$

Other decoding methods have been used to probe a wide array of sensory computations, including the optimal linear estimator[32], the maximum likelihood estimate [33], and multiple correlation codes that maximize information coding[34]. We aim to test these different classes of decoding methods to determine which are best able to match behavioral accuracy and precision, along with any constraints we are able to place on them through analysis of pursuit behavior error. Although the means by which these decoding methods generate estimates are not necessarily biologically plausible mechanisms, these methods are widely used to match the mean stimulus direction and speed. We compare the statistics of pursuit behavior as a readout of cortical activity to estimates from competing decoding models. By doing so, we rule out specific decoding models.

We calculate errors in the direction and speed estimates of smooth pursuit eye movements on single trials, and observe that single-trial errors in the direction and speed are correlated. We also create testbeds of simulated MT population responses, and apply vector-average decoding to generate estimates from the population. We find that the errors of these estimates are correlated, suggesting that spike count fluctuations in a population jointly tuned to multiple stimulus parameters can cause correlated errors in the behavioral readout of the population response.

Materials and Methods

Behavioral recording

We trained animals to fixate and perform basic pursuit tasks for a juice or water reward before collecting all data. The horizontal and vertical position of one eye was sampled at 1 kHz, then filtered, differentiated, and digitized [35]. During the pursuit task, animals were required to maintain fixation within 2° of the target to begin a trial and during the final 200ms of the pursuit interval and for 400ms at the end of the trial. Accuracy windows were relaxed during pursuit initiation. Experiments were organized into trials 1-2 seconds long. The fixation point appeared at the center of the screen for 500-1000ms to cue fixation. The fixation point then disappeared, and a target appeared ~3° eccentric to screen center. The eccentricity of target appearance was selected to minimize the occurrence of saccades during pursuit initiation. The target then moved towards the center of the screen with a constant direction and speed for 500ms, followed by a jump of 1° in the direction of motion and stopped for a final fixation period of 300ms (Fig 3-1B). For one experiment, target directions were 0°, 45°, 135°, 180°, 225°, and 315° relative to rightward motion, and target speeds were 14, 16, 18, 20, 22, 24, 26, or 28°/s (Fig 3-1D, bottom). We also collected data at 72 directions around the circle in increments of 5° for M1 and M2 at 20°/s. Prior to analysis, we inspected each pursuit trial record for saccades or eye blinks during the fixation period and the first 500ms after the onset of target movement. We did not analyze trials containing saccades or blinks during these time periods.

We measured the onset of closed-loop pursuit, the time that extra-retinal contributions become measurable, by comparing eye speed during normal pursuit vs. the response to a retinally stabilized target [36–38]. We defined the open loop duration as the time point with respect to pursuit onset when eye speeds diverged by 1 SD. The open-loop interval was 146ms (M1), 135ms (M2), and 138ms (M3), consistent with past studies [37,38].

Direction and speed errors from eye movements

We sampled the horizontal (H) and vertical (V) components of eye velocity at 1ms intervals, so the eye movements are vectors in time and space of dimension 2*T*, where *T* is the duration of the time window in milliseconds (Fig 3-1C). We analyzed the first 150ms of pursuit during which the eye movement expresses visual estimates of target motion direction and speed [37,38,35]. We analyzed equal numbers of leftward/rightward, upward/downward trials to minimize any H, V bias in the data sample, 20-176 repetitions (average 49) for each of the target motions.

Errors in visual estimates of target direction or speed should be small, ~2-3° and 8-10% based on psychophysical thresholds for motion discrimination on comparable time scales [37,38,35,39–41]. In the absence of other sources of variation, these errors should introduce small deviations from the mean eye trajectory until visual feedback allows for a course correction. We express the impact of errors in motion estimation as a first order expansion around the mean eye

trajectory for a given target motion. The eye trajectory on trial i to a target with direction θ and speed v is:

$$\mathbf{v_i}(t) = (v(t + \delta t_i) + \delta v_i)e^{i(\theta + \delta\theta_i)} = \tag{5}$$

$$\mathbf{v}_{\text{mean}}(t) + \delta\theta_i \cdot \frac{\partial \mathbf{v}_{\text{mean}}(t)}{\partial \theta} + \delta v_i \cdot \frac{\partial \mathbf{v_{mean}}(t)}{\partial v} + \delta t_i \cdot \frac{\partial \mathbf{v}_{\text{mean}}(t)}{\partial t},$$

where $\delta\theta_i$, δv_i, and δt_i represent scalar errors in estimating the direction, speed and time of motion onset with respect to the trial-averaged mean trajectory, $\mathbf{v}_{\text{mean}}(t)$, for a target moving in direction θ at speed ν. The partial differentials represent vector operators that describe how the eye's trajectory transforms based on small perturbations in the direction, speed and onset timing of target motion, or of the brain's estimates of target motion. Equation 5 will not predict fluctuations in eye movements arising from other sources such as jitter arising from background motor noise. Equation 5 predicts that the covariance of velocity fluctuations around the mean should have 3 dominant dimensions. We confirmed this to be the case by forming the covariance matrix of eye velocity fluctuations about the mean, whose elements are

$$C_{ij}(t, t') = \langle \delta\mathbf{v}_i(t)\delta\mathbf{v_j}(t') \rangle + \langle \delta\mathbf{v}_i^{\text{back}}(t)\delta\mathbf{v}_j^{\text{back}}(t') \rangle \tag{6}$$

where i and j can each represent horizontal or vertical components, t and t' represent a pair of time points in the 250D eye vectors, and $\delta\mathbf{v}_{i,j}^{\text{back}}$ represents the small background jitter. The angle brackets $\langle \ldots \rangle$ denote the average over multiple trials. We subtracted that term from Equation 6 to form a difference matrix, $\Delta C_{ij} =$

$\langle \delta \mathbf{v}_i(t) \delta \mathbf{v_j}(t') \rangle$. Equation 5 predicts that the covariance of velocity fluctuations during pursuit initiation should be given by:

$$\Delta C_{ij} = \begin{bmatrix} \frac{\partial \mathbf{v_i}(t)}{\partial \theta} \\ \frac{\partial \mathbf{v_i}(t)}{\partial v} \\ \frac{\partial \mathbf{v_i}(t)}{\partial t} \end{bmatrix}^T \cdot \begin{bmatrix} \langle \delta\theta\delta\theta \rangle & \langle \delta\theta\delta v \rangle & \langle \delta\theta\delta t \rangle \\ \langle \delta v\delta\theta \rangle & \langle \delta v\delta v \rangle & \langle \delta v\delta t \rangle \\ \langle \delta t\delta\theta \rangle & \langle \delta t\delta v \rangle & \langle \delta t\delta t \rangle \end{bmatrix} \cdot \begin{bmatrix} \frac{\partial \mathbf{v_j}(t')}{\partial \theta} \\ \frac{\partial \mathbf{v_j}(t')}{\partial v} \\ \frac{\partial \mathbf{v_j}(t')}{\partial t} \end{bmatrix} \quad (7)$$

where $\langle \delta\theta\delta\theta \rangle, \langle \delta\theta\delta v \rangle, \ldots$ are the covariances of the sensory errors across trials. The fact that ΔC can be written as the outer product of 3 vectors predicts that the 250x250 covariance matrix should only have 3 non-zero eigenvalues. We confirmed that to be the case by measuring the covariance of H and V eye velocity fluctuations for the first 125ms of pursuit (first term in Equation 6) and a 125ms period when the monkeys were fixating.

We determined the form of the partial differentials in Equation 5 from the pursuit data itself, by determining how pursuit trajectories differ on average for targets moving at different speeds and different directions. We analyzed data sets with multiple directions (0°, 45°, 135°, 180°, 225°, and 315° relative to rightward motion) and speeds (14, 16, 18, 20, 22, 24, 26, or 28 °/s) of target motion, described above under *Behavioral recording*. We used singular value decomposition (SVD) to represent the mean eye trajectories, averaged over many repetitions, as the weighted sum of orthonormal modes, i.e.

$$\mathbf{v}_{\text{mean}}(\theta, v, t) = \sum_{i=1}^{K} A_i(\theta, v)\, \mathbf{v_i}(t) \quad (8)$$

where K represents the number of unique target trajectories in a dataset (48), $\mathbf{v}_{\text{mean}}(\theta, v, t)$ represents the trial-averaged mean eye movement for the corresponding target trajectory, $A_i(\theta, v)$ is a scalar weight that minimizes errors in capturing the i^{th} trajectory, and $\mathbf{v_i}(t)$ represent orthonormal modes. We found that the array of K= 48 250-dimensional vectors were well represented by two modes, $\mathbf{v_1}$ and $\mathbf{v_2}$ such that

$$\mathbf{v}_{\text{mean}}^{(\text{H})}(t) = A_1(\theta, v)\, \mathbf{v}_1^{(\text{H})}(t) + A_2(\theta, v)\, \mathbf{v}_2^{(\text{H})}(t) \quad (9)$$

$$\text{v}_{\text{mean}}^{(\text{V})}(t) = A_1(\theta, v)\, \mathbf{v}_1^{(\text{V})}(t) + A_2(\theta, v)\, \mathbf{v}_2^{(\text{V})}(t) \quad (10)$$

where our notation decomposes the vectors into their horizontal (H) and vertical (V) components (Fig 3-2A, top row). The 2 modes, $\mathbf{v}_1$(t) and $\mathbf{v}_2$(t), captured ~90% of the variance in the shapes of the mean eye trajectories across target conditions: 93% for M1, 89% for M2, and 91% for M3. In practice the first mode ($\mathbf{v}_1$) was dominated by horizontal and the second ($\mathbf{v}_2$) by vertical motion. With appropriate normalization of the SVD modes, the coefficients $A_{1,2}(\theta, v)$ correspond to the sines and cosines of target direction. For a single target speed, Equation 6 corresponds exactly to a rotation operation. For multiple target speeds, the coefficients combine a scaling operation and rotation operation. The scaling is $v/\, v_0$, where v_0 is the average target speed in the set of trajectories and v is the target speed of the particular eye movement being reconstructed. In the middle row of Fig 3-2A, we have scaled the SVD modes with scalar parameters S_1 and S_2 to reconstruct the average eye movement for a target moving with speed v in direction θ. Thus:

$$\frac{v}{v_0}\cos(\theta - \theta_0) = S_1 A_1$$

$$\mathrm{v}_1^{(\mathrm{H})}(t) = S_1\, \mathbf{v}_{\mathrm{mean}}^{(\mathrm{H})}(t)$$

$$\mathrm{v}_1^{(\mathrm{V})}(t) = S_1\, \mathbf{v}_{\mathrm{mean}}^{(\mathrm{V})}(t)$$

$$\frac{v}{v_0}\sin(\theta - \theta_0) = S_2 A_2$$

$$\mathrm{v}_2^{(\mathrm{H})}(t) = S_2\, \mathbf{v}_{\mathrm{mean}}^{(\mathrm{V})}(t)$$

$$\mathrm{v}_2^{(\mathrm{V})}(t) = -S_2\, \mathbf{v}_{\mathrm{mean}}^{(\mathrm{H})}(t) \qquad (11)$$

where the H and V superscripts refer to the horizontal and vertical vector components and the numeric subscripts (1,2) indicate the first or second SVD mode. We used Equation 11 to construct the vector operators shown in Equation 5: a vector rotation operation to represent the effect of small errors in direction estimates on pursuit, a vector scaling operation to represent small speed errors, and a time shift operation that could represent either motion onset time detection errors or trial-to-trial differences in movement latency:

$$\frac{\partial \mathbf{v}_{\mathbf{mean}}(t)}{\partial \theta} = \cos(\theta - \theta_0)\, S_2 \mathbf{v_2}(t) - \sin(\theta - \theta_0)\, S_1 \mathbf{v_1}(t) \qquad (12)$$

$$\frac{\partial \mathbf{v}_{\mathbf{mean}}(t)}{\partial v} = \frac{1}{v_0}[\cos(\theta - \theta_0)\, S_1 \mathbf{v_1}(t) + \sin(\theta - \theta_0)\, S_2 \mathbf{v_2}(t)] \qquad (13)$$

$$\frac{\partial \mathbf{v}_{\mathbf{mean}}(t)}{\partial t} = -\cos(\theta - \theta_0)\, S_1 \frac{\partial \mathbf{v_1}(t)}{\partial t} - \sin(\theta - \theta_0)\, S_2 \frac{\partial \mathbf{v_2}(t)}{\partial t} \qquad (14)$$

Equations 12-14 describe how small errors in motion estimation should affect the eye trajectory for a target moving in direction θ_0 at speed v_0. Because direction errors

are less than a few degrees, $|\sin(\theta - \theta_0)| \ll 1$ and $|\cos(\theta - \theta_0)| \sim 1$ and thus Equations 12-14 simplify to:

$$\frac{\partial \mathbf{v}(t)}{\partial \theta} = S_2 \mathbf{v_2}(t) \tag{15}$$

$$\frac{\partial \mathbf{v}(t)}{\partial v} = \frac{1}{v_0} S_1 \mathbf{v_1}(t) \tag{16}$$

$$\frac{\partial \mathbf{v}(t)}{\partial t} = -S_1 \frac{\partial \mathbf{v_1}(t)}{\partial t} \tag{17}$$

Equations 15-17 are vectors that form a basis onto which we can project individual eye movements to recover the direction, speed and timing error $(\delta\theta, \delta v, \delta t)$ for each trial. The error distributions are well fit by Gaussian functions (see Fig 3-2D) with zero mean.

For each target motion, we computed the angular-linear correlation coefficient between the direction error, $\delta\theta$, and speed error, δv, across repeated movements with the MATLAB function circ_corrcl in the Circular Statistics Toolbox [42]:

$$\rho(\delta\theta, \delta v) =$$

$$\sqrt{\frac{[(\rho(\delta v,\sin(\delta\theta))^2 + \rho(\delta v,\cos(\delta\theta))^2 - 2\rho(\delta v,\sin(\delta\theta)\rho(\delta v,\cos(\delta\theta))\rho(\sin(\delta\theta),\cos(\delta\theta)))]}{(1-\rho(\sin(\delta\theta),\cos(\delta\theta))^2)}} \tag{18}$$

where $\rho(X, Y) = \text{cov}(X, Y)/\sigma_X \sigma_Y$. We randomly resampled draws of 50% of the total repeats for each condition and computed the mean and standard deviation of the correlation coefficient across samples.

Population models

We constructed populations of direction and speed-tuned neurons with homogeneous Poisson spiking statistics and stimulus-conditioned (noise) correlations that were tuned based on the similarity of feature selectivity of the neurons. The firing rates had a Gaussian tuning profile in direction and $\log_2$ speed. The preferred directions and speeds were spaced uniformly around the circle and from the measured data by centering Gaussian direction tuning functions at equally spaced increments around the circle (10-25 directions) and the speed tuning functions with base-2 logarithmic spacing from 0.5 to 256°/s (10-25 preferred speeds). Each of the combinations of preferred direction and speed was represented once in the model population. A model unit with a preferred speed of v_p and preferred direction θ_p has a firing rate of:

$$r(\theta, v) = r_0 + r_{\max} e^{-\left(\frac{\log_2(v - v_p)}{2\sigma_v}\right)^2} e^{-\left(\frac{\theta - \theta_p}{2\sigma_\theta}\right)^2}, \quad (19)$$

where r_0 is the baseline firing rate of the unit (1 spikes/s), $r_{\max}$ is the maximum firing rate (100 spikes/s), and σ_v and σ_θ scale the tuning bandwidth. We used Equation 19 to generate spike counts with Poisson statistics in a 200ms window for each stimulus condition.

We simulated conditionally independent populations, constant pairwise correlation values from 0.05-0.6, and stimulus-dependent correlation structures. Tuned correlations peaked for neurons with the same preferred direction and speed and decreased with distance between preferred stimuli. To add between-neuron correlations to the mean spike counts, trial spike counts with the desired correlations were generated by drawing single-trial spike counts from the multivariate normal

distribution defined by a covariance matrix, Σ_{ij}, of pair-wise stimulus-conditioned (i.e. noise) correlations in spike counts:

$$\rho_{ij} = \rho_{\max} e^{-\left(\frac{\log_2(v_i - v_j)}{\tau_v}\right)^2} e^{-\left(\frac{\theta_i - \theta_j}{\tau_\theta}\right)^2}, \quad (20)$$

where v_i and $\theta_i$are the preferred speed and direction of neuron i, $\rho_{\max}$ is the maximum pairwise correlation, and τ_v = 1.35 and τ_θ = 60° scale the widths of the correlation tuning function [15,43]. We tested a range of parameters: from 100 to 3125 units, from 10 to 25 preferred speeds (separated evenly in $\log_2$ space from 0.5 to 256 °/s, from 10 to 25 preferred directions, from 1 to 3 units with identical preferences, from r_{max}= 0.05 to 0.6. For each model architecture we simulated 30,000 responses.

Decoding models

We compared the estimates from two decoding models: a scalar, or "separate" decoder, and a vector, or "joint" decoder (Fig 3-4B). The separate decoding model is a basic vector-averaging model [15,23,27,44] that estimates the stimulus direction and speed $(\hat{\theta}, \hat{v})$ independently by weighting each cell's preferred direction and speed (θ_i, v_i for cell i) by its spike count in a 200ms window (R_i), then summing over the population. The population estimates are recovered from normalizing by the summed population response:

$$\hat{\theta} = \frac{\sum_i R_i \theta_i}{\sum_i R_i}; \quad \hat{v} = 2^{\frac{\sum_i R_i v_i}{\sum_i R_i}} \quad (21)$$

In practice we estimated the horizontal and vertical components of the population response separately using the sine and cosine of each cell's preferred direction and then computed the arctangent to recover a direction estimate. We also created a vector decoder that estimates the stimulus motion vector directly. The vector decoder weights each neuron's preferred stimulus vector $\boldsymbol{v}_p = v_p e^{i\theta_p}$ by its response *R* defined as above:

$$\widehat{\boldsymbol{v}} = \frac{\sum_i R_i \boldsymbol{v_p}}{\sum_i R_i} \tag{22}$$

The estimated stimulus direction and speed are recovered after the averaging operation from the modulus and angle of $\widehat{\boldsymbol{v}}$.

We compared decoder performance across many repeated simulated responses from the population architectures described above, using motion stimuli spaced at 36° intervals in direction and 5 log2 units of speed from 16 to 64°/s. We computed the linear correlation between the direction and speed estimates with the MATLAB function circ_corrcl in the Circular Statistics Toolbox [42]. We randomly resampled fractions of the simulated population responses to generate estimates of the average direction-speed correlation and the estimation errors.

Results

To study motion decoding, we performed a series of behavioral experiments in which monkeys tracked moving targets that had closely spaced directions and speeds. We sampled the horizontal and vertical components of eye position every millisecond as targets underwent a position step and subsequent velocity ramp back toward the gaze position (see Fig 3-1; Methods). We presented target motions in a pseudo-random order and presented balanced target motions (leftward/rightward, upward/downward) to minimize anticipatory eye movements. Our analysis focused on the first 125ms of pursuit, the "open-loop" interval, a period when extra-retinal inputs are not available and the eye movement is driven by feed-forward visual estimates of target motion formed during the ~100ms latency period before the eye begins to track the target [37,38,36]. In previous work, we found that on average, the form of the eye's trajectory over time could be predicted by a rotation of a basic movement trajectory to the new target direction. We also found that trial-to-trial fluctuations in pursuit have the same low-dimensional form, at least for near horizontal target motions at a single speed [37,45]. Here we extend our analysis across a broad range of directions and different motion speeds to determine whether trial-to-trial fluctuations in eye direction and speed are correlated in pursuit as a proxy for the internal sensory estimates decoded from visual cortex.

Correlated fluctuations in eye speed and direction

We used dimensionality reduction to assign a direction error and speed error for each pursuit movement. We represented the eye velocity as a 250-element vector

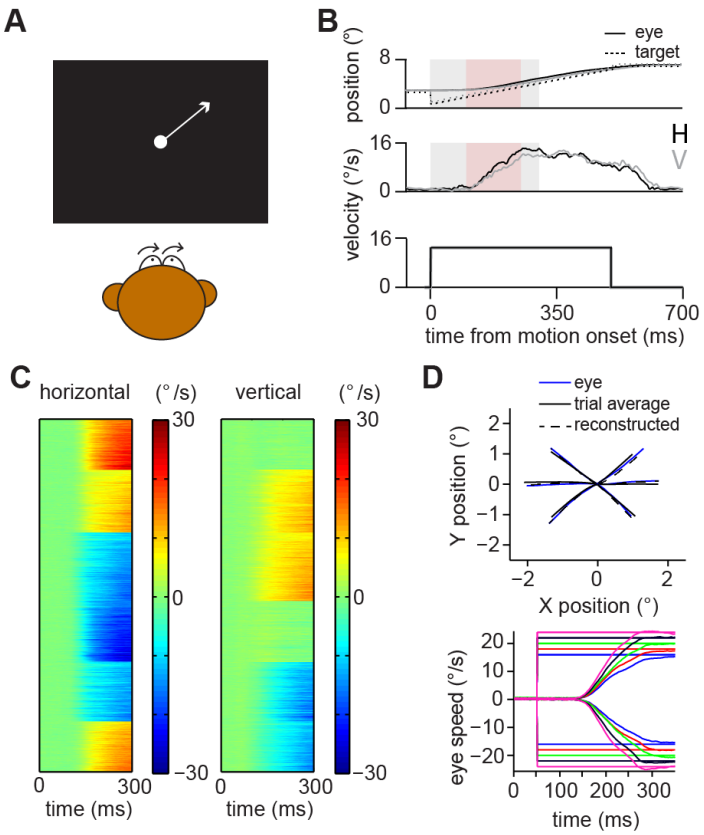

Figure 3-1. Experimental procedure.

(A) The monkey fixated a central spot briefly, then a motion step initiated smooth pursuit eye movements.

(B) Time course of single pursuit trial, with the dot moving 45° relative to horizontal rightward motion, at 14°/s. Dashed lines indicate horizontal (black) and vertical (gray) dot motion, while solid lines indicate eye movements. Top panel: Horizontal (black) and vertical (gray) position of dot target and eyes relative to fixation. Target steps backward approximately 3 degrees and translates toward the fixation location to initiate pursuit (see Methods). Middle panel: Horizontal and vertical velocity of eyes during one trial of smooth pursuit. Analysis window (125ms) shaded in red, time window shown in panel C shaded in gray. Bottom panel: Dot translates across the screen at 20 °/s for 500ms.

(C) Horizontal (left) and vertical (right) velocity of eye for all trials at all directions for M1.

(D) Top panel: Position of eye over time during the analysis period for all tested directions and one speed. Solid black lines indicate the average of all trials for each direction. Blue lines indicate eye position on one trial for each direction. Dotted black lines indicate reconstructed eye position on the same trials using noise analysis (see Fig 2, Methods). Bottom panel: Mean eye speed over time to rightward and leftward motion steps at 16°/s, 18°/s, 20°/s, 22°/s, and 24°/s.

comprising the first 125ms of the horizontal and vertical eye velocities at movement initiation. We measured the open-loop interval to be 146ms (M1), 135ms (M2), and 138ms (M3) for these monkeys (see Methods), thus pursuit is dominated by feed-forward visual inputs rather than non-retinal inputs during the analysis window. Figure 3-2A shows the set of horizontal and vertical components of the eye velocity from an example dataset that had 6 directions (0, 45, 135, 180, 225, and 315°) and 8 speeds (14, 16, 18, 20, 22, 24, 26, and 28°/s). To create a model of how sensory errors in estimating target direction or speed alter the eye movement, we determined how changes in target motion direction and speed affected the movement vectors on average. For each target motion, we formed a 250-element trial-averaged velocity vector and then performed singular value decomposition on the 48 vectors. We found that 2 modes, one almost purely horizontal and the other vertical, could reproduce ~90% of variation in the trial-averaged eye movements across 48 target conditions in two monkeys, and the weights of those modes needed to reconstruct the average pursuit response for each target motion were proportional to the cosine and sine of the target direction (Fig 3-2A, top row). The weights represent a static rotation and scaling operation, moving every element in the pursuit vector to the new direction and re-scaling each element to a new speed. Using the SVD weights to scale the modes predicts the trial averaged eye velocity within errorbars (Fig 3-2A, middle row). The small residuals have a Gaussian distribution (Fig 3-2A, bottom right). Analysis of the average eye movements suggests that pursuit can be described as a basic movement vector – a time course of smooth eye acceleration from rest, that the motor system rotates for different target directions and

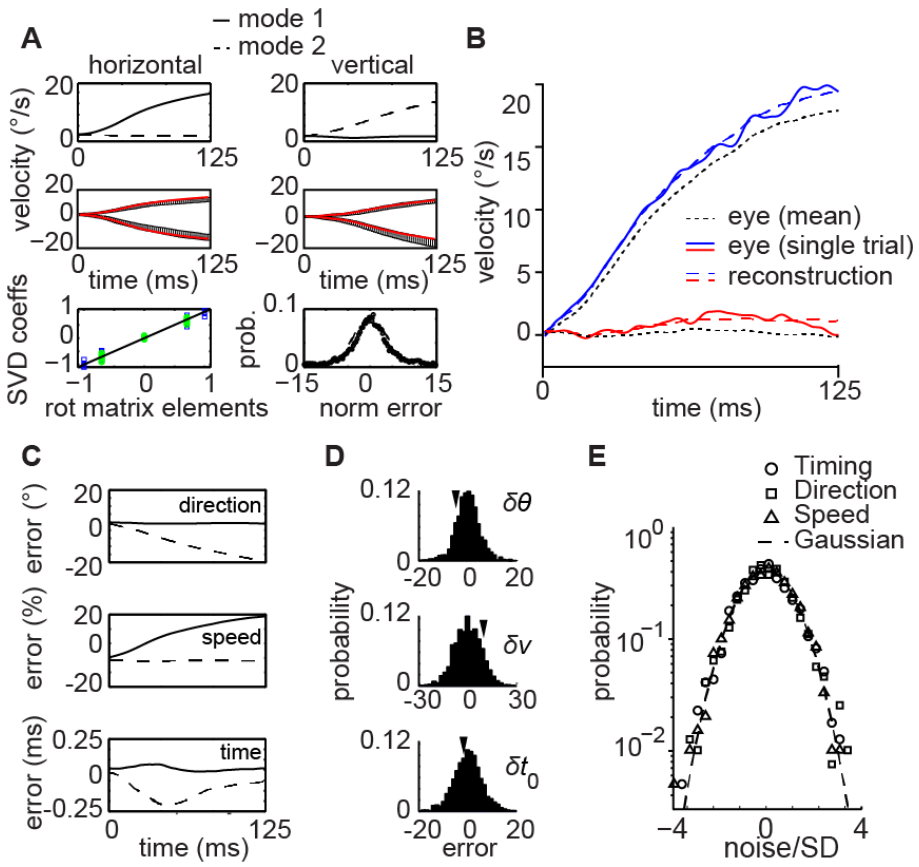

Figure 3-2. Analysis of noise in smooth pursuit eye movements.

(A) Top row: Velocity over time of eigenmodes corresponding to horizontal (mode 1) and vertical (mode 2) aspects of eye movements. Left panel calculated from horizontal eye velocity, right panel from vertical eye velocity. Middle row: Trial-averaged eye velocity for target directions of 45° and 225° relative to rightward motion (black errorbars) and reconstructions from eigenmodes (red), calculated from horizontal (left) and vertical (right) eye velocity. Bottom row, left panel: Weights of SVD coefficients corresponding to the sine (green circles) and cosine (blue squares) of target directions. Bottom row, right panel: Distribution of errors between reconstructed and recorded trials.

(B) Horizontal and vertical velocity of eyes to a rightward-moving stimulus. Dotted lines indicate mean eye velocity over all trials at this motion direction. Solid traces indicate eye velocity on a single trial. Dashed lines indicate reconstructed eye movement using single-trial errors in direction, speed and timing. Reconstructed traces match closely to the actual eye movement, aside from typical levels of eye jitter.

(C) Eigenmodes corresponding to direction (top), speed percentage (middle) and timing (bottom) errors. Single-trial errors are used to weight these eigenmodes to reconstruct eye movements.

(Fig 3-2 continued)
(D) Distribution of direction (top), speed (middle), and timing (bottom) errors on single trials to the same target direction and speed. Arrowheads note the trial in panel B.
(E) Distribution of single-trial errors, when normalized by their standard deviation, are Gaussian-distributed.

---

scales for different target speeds, at least in the tested range. Our model assumes that small errors in visual estimates of target motion will affect the basic response in the same manner.

To analyze trial-to-trial fluctuations in pursuit, we used the basis functions obtained from the trial-averaged responses to construct a rotation, scaling, and time-shift operator (see Methods; [37]). If trial-to-trial fluctuations in pursuit are well described by small sensory errors in estimating the target direction and speed, then each eye movement should look like the pursuit response to a slightly different direction and speed than expected, plus some movement to movement jitter in response latency. Because sensory estimation errors are small, we keep only first-order corrections and model the pursuit response on trial *i* to a target with direction θ and speed *v* as:

$$\mathbf{v_i}(t) = (v(t + \delta t_i) + \delta v_i)e^{i(\theta + \delta\theta_i)} = \mathbf{v_{mean}}(t) + \tag{23}$$

$$\delta\theta \cdot \frac{\partial \mathbf{v_{mean}}(t)}{\partial \theta} + \delta v \cdot \frac{\partial \mathbf{v_{mean}}(t)}{\partial v} + \delta t_0 \cdot \frac{\partial \mathbf{v_{mean}}(t)}{\partial t_0} + \delta v_{\text{back}}(t)$$

where $\delta\theta_i$, δv_i, and δt_i represent scalar errors in estimating the direction, speed and time of motion onset for this trial and $v_{mean}(t)$ is the trial-averaged eye movement for the target. The partial differentials represent vector operators that rotate, scale, and

shift the trial-averaged eye movement vector. The last term, $\delta v_{\text{back}}(t)$, represents jitter arising from background motor noise that is not specific to pursuit but also present during fixation [37]. We modeled single movements without the jitter term, and then confirmed that the model's prediction errors were well captured by the velocity jitter during fixation (see below). Equation 23 makes a strong prediction about the structure of fluctuations of pursuit movements about their means – that they have three dimensions exclusive of background jitter. To test the model, we subtracted the trial-averaged eye movement from each trial, and projected the resulting vector onto the 3 modes derived above (see Methods; Fig 3-2B). Each projection generates the value of the corresponding sensory error ($\delta\theta$, δv, δt). Over all trials, the errors have a Gaussian distribution, with means near zero and standard deviations of 6.0° (M1) (5.1°, M2; 6.5°, M3) in direction, 8.0% (M1) (8.4%, M2; 17.5%, M3) in speed; and 5.5ms (M1) (6.7ms, M2; 6.5ms, M3) in time (Fig 3-2D). The scale of trial-to-trial variation in pursuit eye movements is consistent with visual motion discrimination thresholds over similar viewing durations [3,46] and previous studies of pursuit with more restricted stimulus sets [37,38,35,45]. Reconstructions of eye movements on single trials can be recovered by weighting each mode in Equation 5 by its error and adding to the mean (red, blue traces Fig 3-2D). The residuals of the single trial reconstructions have a Gaussian distribution whose variances matches that of the velocity fluctuations during fixation – an estimate of background motor noise (Fig 3-2E).

We find that direction and speed errors are correlated from trial to trial. Each black dot in the scatter plot (Fig 3-3A) represents a single trial's direction and speed

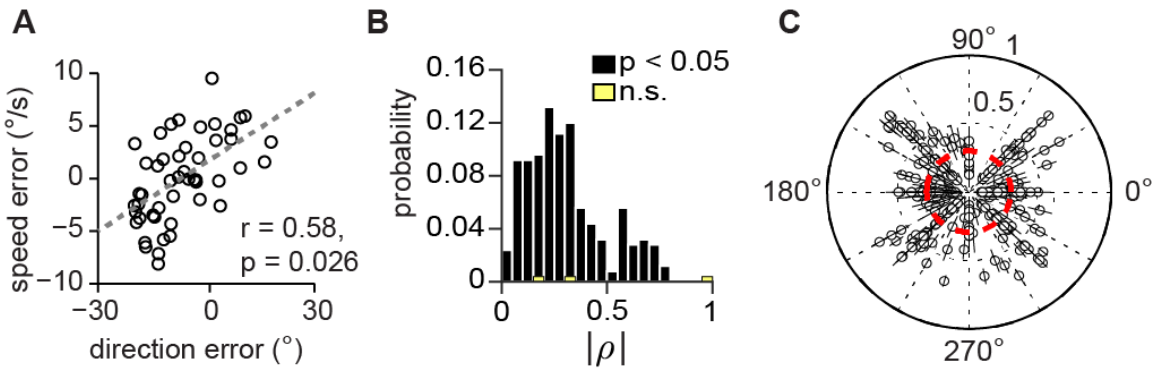

Figure 3-3. Single-trial errors in direction and speed of smooth pursuit are correlated.

(A) Scatter plot of single-trial direction and speed errors for one target trajectory.
(B) Significant correlations observed across all monkeys and all target conditions, with a mean of 0.31 ± 0.19.
(C) Absolute value of correlations plotted as function of target direction.

---

for a target moving at 20°/s, 45° counter-clockwise from rightward for the example experiment in Figure 3-2. The Pearson correlation coefficient for the example data in Figure 3-3A is 0.18, significantly different from 0 ($p<0.05$; 1-tailed t-test). We plot the absolute value of correlation coefficient for all target trajectories and all monkeys in Figure 3-3B, finding that the overwhelming majority of conditions exhibit correlations. These correlations are only apparent if we consider each target vector singly; when combined across target directions the direction-speed correlations average to zero [37]. The pattern of correlations we observe is unlikely to arise from motor noise. Extra-ocular recti muscles pull along Cartesian axes, driven by separate oculomotor nuclei [47–50]. We simulated the result of up to 20% horizontal and vertical channel motor noise on the target velocity, finding that single-trial errors in direction and speed were not significantly correlated, suggesting that purely motor noise is not sufficient to generate our results.

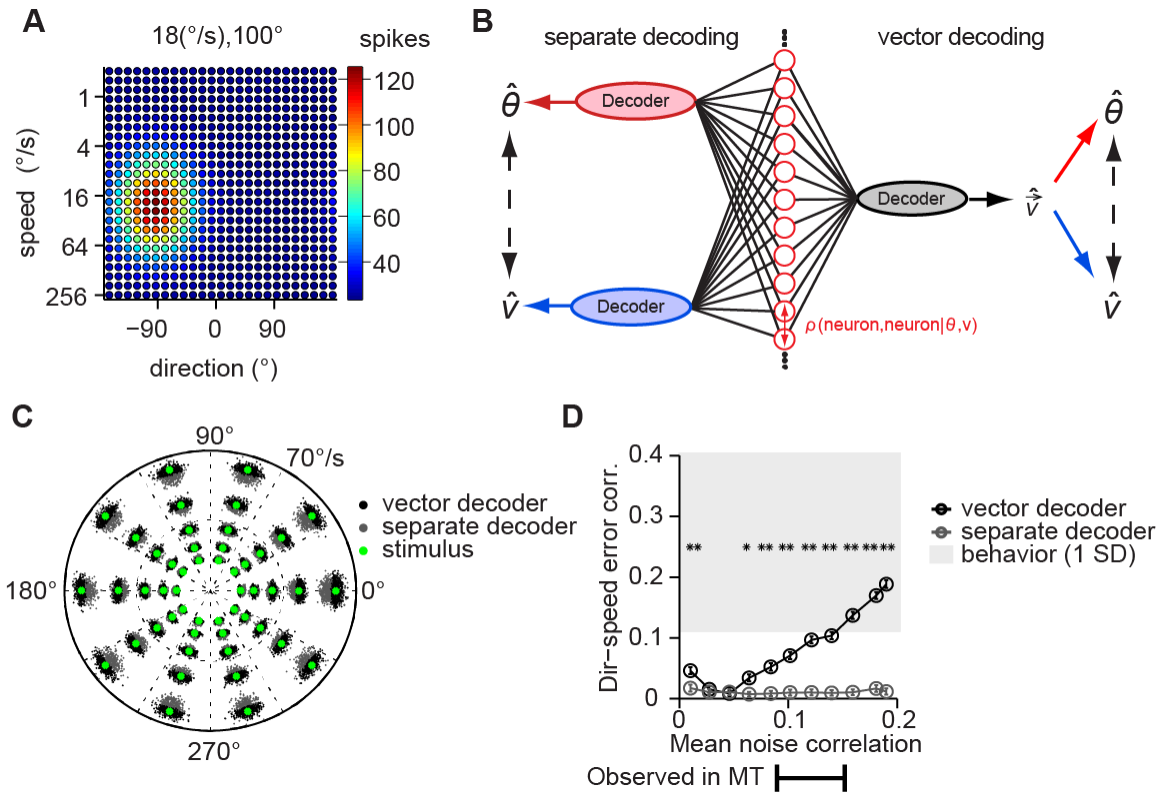

Figure 3-4. Direction and speed estimates from a vector decoder, but not a separate decoder, exhibit error correlations.

(A) Mean rate across a 3125-unit simulated population to a stimulus of 18°/s at an angle of 100°. Unit direction preferences range evenly around the circle, and speed preferences range evenly in $\log_2$ °/s.

(B) Decoders generate estimates of direction (red) and speed (blue) separately (left) or as a motion vector (right) from a simulated MT population with varying interneuronal correlations ρ. Noise correlations between units are applied that decay as a function of the difference between unit preferences, then spike counts are drawn based on the covariance matrix between units (see Methods). Direction and speed errors are calculated relative to the mean estimate.

(C) Vector (black) and separate (gray) decoders, with a mean ρ = 0.2, accurately estimate stimulus (green) at a range of directions and speeds. 30,000 estimates per stimulus from a 3125-unit population shown.

(D) Correlations between direction and speed errors increase as a function of the mean noise correlation in the population for a vector decoder (black), but not a separate decoder (gray). * = p < 0.05, ** = p < 0.01. Mean noise correlations observed in MT by others range from 0.09 to 0.15 (bottom). Correlations from smooth pursuit shaded in gray, with a mean of 0.31 ± 0.19.

Vector decoder predicts observed eye direction-speed error correlations

The correlations between eye direction and speed errors during pursuit suggest that internal visual estimates of direction and speed may themselves be correlated, and the rest of our study was designed to explore the implications of this result for cortical decoding. Presuming that internal motion estimates are decoded from a cortical population of motion-sensitive neurons, we relied on data from recordings of neural responses in cortical area MT to simulate counts from a population of MT neurons [11,15,51], and then analyzed the performance of decoding models applied to this synthetic data to determine which decoders reproduce the direction-speed correlations we observed in pursuit.

Previous work has indicated that the spike counts of MT neurons exhibit correlated variability, or "noise correlations" [52,53] that can significantly impact the outcome of population decoding measures on perception and behavior[54–58]. Noise correlations display a characteristic structure: their magnitude peaks when neurons have the same tuning preferences, and decay with reduced tuning similarity [24,53,59]. By imposing a covariance matrix of noise correlations, we generated simulated counts from a population of MT neurons based on their tuning preferences (Fig 3-4A) while accounting for the impact of correlated variability in cortex. Since the overall level of noise correlations varies across the population, we quantify it with the mean correlation across all pairs of neurons.

We test two types of decoders, finding that the single-trial errors from a vector decoder are correlated, but those from separate direction and speed decoders are not.

The “vector” decoder estimates the vector of a target stimulus by taking into account both the direction and speed of individual units, then decomposes the vector into its component direction and speed (Fig 3-4B, right). In contrast, the “separate” decoder estimates direction and speed individually using only the direction or speed of units (see Methods, Fig 3-4B, left). We generated 30,000 responses for each of 10 directions separated by 36° around the circle and 5 speeds ranging from 16 to 64°/s, and used the same responses for both decoders. Both kinds of decoders can accurately estimate the target vector on average, and exhibit comparable levels of variance (Fig 3-4C). The vector decoder had an RMS direction error of 2.1° and an RMS speed error of 4%, compared to 2.2° and 2.3% for the separate decoder. Their similar performance rules out the possibility that differences between the accuracy or variance of the decoders are a factor in the disparity in the observation of direction-speed error correlations. When we modulate the level of noise correlations in the population, we find that the estimates from the vector decoder become correlated as the decoder approaches the level of noise correlations observed in MT (Fig 3-4D, black symbols). The level of direction-speed error correlations in estimates from the separate decoder fails to become significant at any level of noise correlation. We note that the level of correlations resulting from the vector decoder does not match the level observed in smooth pursuit from our data, and consider that subsequent processing in the visuomotor pathway, including motor noise, adds some variability that could exacerbate error and amplify correlations.

Discussion

Joint encoding in the brain is widespread: spike trains in sensory areas encode information about more than one stimulus feature [19,22,60–65]. Subsequent processing results in joint encoding of multiple sensory streams [66–68]. Fluctuations in the count of a single neuron or a population of jointly-tuned neurons can be interpreted to mean a change in any or all of the stimulus parameters encoded. If this is the case, how do cortical circuits resolve ambiguity about the meaning of trial-to-trial spike count changes, and what effect does the ambiguity have on behavioral variability? We use smooth pursuit eye movements in the macaque as a readout of the cortical estimate of visual motion, finding that trial-to-trial fluctuations in the direction and speed of eye movements are significantly correlated. One interpretation of the correlation between these two stimulus parameters is that they are not only jointly encoded, but jointly decoded to drive oculomotor activity. We also simulate a population of neurons jointly tuned to the direction and speed of motion as a facsimile of the middle temporal area (MT), which we use as a testbed for population decoding methods. We determine that direction-speed error correlations are predicted by decoding visual motion as a vector, instead of in its components of direction and speed. Therefore, vector decoding is a better predictor of motion-driven eye movements from MT population activity than decoding visual motion parameters separately. These results have the potential to improve readout mechanisms of jointly tuned populations, specifically for brain-computer interfaces and neural implants[34,69–73].

Our experiment exploits that MT responses play a large part in driving smooth pursuit [15,24,74] and that MT is known to be tightly coupled to eye movements and perceptual judgments of visual motion [14,75]. It follows that we can use eye movements to elucidate cortical circuitry: previous work has determined that microstimulation of MT [4,26] and adaptation in MT [76,77] can alter smooth pursuit. Perceptual tasks can also shine a light on cortical interactions and mechanisms. The "oblique effect" in perception and behavior may be due to anisotropy in the preferred directions of neurons in MT and V1 [25,78], and attentional modulation that benefits task performance can be traced to modulation of inhibition [54,79]. Further work can expand upon our results by determining if similar correlations between features exist in other systems or in other MT-driven tasks.

A variety of decoding methods have been used to match the responses of MT neurons and predict behavioral and perceptual output. Many of these fall into the category of vector averaging, in which the observed spike count of a single unit is weighted by its tuning preference, and these weighted preferences are summed or integrated to generate an estimate of the stimulus[23,27,80]. These decoding methods tend to report an estimate of only one parameter from a population of neurons that are likely modulating their responses to multiple stimulus parameters, though some have put forth methods such as divisive normalization to stabilize and focus vector averaging estimates in the case of multiparameter tuning[15,44]. Our results, combined with other evidence using information theory [19], suggest that joint decoding of multiple stimulus parameters is a better description of how cortical circuitry transforms sensory information into perception and action.

Although we focus on the vector average method to recapitulate our behavioral results, a number of other methods have gained traction in modeling decoding, especially decoders that use knowledge of the probability distribution of spikes and stimuli [31,32,81–84]. Such decoders are termed Bayesian decoders or maximum likelihood decoders, as they use Bayes' rule to estimate the most likely stimulus $\hat{s}$ that occurred given a spike count n. One advantage that these decoders have is that they are not limited to the structure of one stimulus parameter, as in the circular space of direction or the $\log_2$ space of speed in this study. Another advantage is the growing amount of evidence that the cortex transforms sensory information into perception and action with high efficiency [30,85,86], and probability-based decoding necessarily is optimized to maximally use the information contained in the spike counts at every processing level. These, and other decoding methods, would further benefit from estimating multiple stimulus parameters jointly.

Acknowledgments

We thank T. Mukherjee for assistance with animal care and data collection, and the veterinary staff of the Animal Resources Center at University of Chicago. Research was supported by grants to LCO from the Alfred P Sloan Foundation, Whitehall Foundation, Brain Research Foundation, NIH NEI EY023371, and NSF IOS 145704.

References

1. Maunsell JHR, Van Essen DC. Functional properties of neurons in middle temporal visual area of the macaque monkey . I . Selectivity for stimulus direction, speed, and orientation. J Neurophysiol. 1983;49: 1127–1147.

2. Pack CC, Born RT. Temporal dynamics of a neural solution to the aperture problem in visual area MT of macaque brain. Nature. 2001;409: 1999–2001.

3. Liu J, Newsome WT. Correlation between speed perception and neural activity in the middle temporal visual area. J Neurosci. 2005;25: 711–22. doi:10.1523/JNEUROSCI.4034-04.2005

4. Born RT, Groh JM, Zhao R, Lukasewycz SJ. Segregation of object and background motion in visual area MT: effects of microstimulation on eye movements. Neuron. 2000;26: 725–34. Available: http://www.ncbi.nlm.nih.gov/pubmed/10896167

5. Rust N. Signal transmission, feature representation and computation in areas V1 and MT of the macaque monkey. 2004; Available: http://www.cns.nyu.edu/ftp/eero/rust-phd.pdf

6. Traschütz A, Kreiter AK, Wegener D. Transient activity in monkey area MT represents speed changes and is correlated with human behavioral performance. J Neurophysiol. 2015;113: 890–903. doi:10.1152/jn.00335.2014

7. Krekelberg B, Albright TD. Motion mechanisms in macaque MT. J Neurophysiol. 2005;93: 2908–2921. doi:10.1152/jn.00473.2004

8. Snowden R, Treue S, Andersen R. The response of neurons in areas V1 and MT of the alert rhesus monkey to moving random dot patterns. Exp Brain Res. 1992; Available: http://link.springer.com/article/10.1007/BF02259114

9. Perrone J a, Thiele A. A model of speed tuning in MT neurons. Vision Res. 2002;42: 1035–51. Available: http://www.ncbi.nlm.nih.gov/pubmed/11934454

10. Kohn A, Movshon JA. Adaptation changes the direction tuning of macaque MT neurons. Nat Neurosci. 2004;7: 764–772. Available: http://dx.doi.org/10.1038/nn1267

11. Yang J, Lisberger SG. Relationship between adapted neural population responses in MT and motion adaptation in speed and direction of smooth-

pursuit eye movements. J Neurophysiol. 2009;101: 2693–2707. doi:10.1152/jn.00061.2009

12. Britten KH, Shadlen MN, Newsome WT, Movshon JA. The analysis of visual motion: a comparison of neuronal and psychophysical performance. J Neurosci. 1992;12: 4745–4765. doi:10.1.1.123.9899

13. Cohen MR, Newsome WT. Estimates of the contribution of single neurons to perception depend on timescale and noise correlation. J Neurosci. 2009;29: 6635–48. doi:10.1523/JNEUROSCI.5179-08.2009

14. Newsome WT, Wurtz RH, Komatsu H. Relation of cortical areas MT and MST to pursuit eye movements. II. Differentiation of retinal from extraretinal inputs. J Neurophysiol. 1988;60: 604–20. Available: http://www.ncbi.nlm.nih.gov/pubmed/3171644

15. Hohl SS, Chaisanguanthum KS, Lisberger SG. Sensory population decoding for visually guided movements. Neuron. Elsevier Inc.; 2013;79: 167–79. doi:10.1016/j.neuron.2013.05.026

16. Priebe NJ, Lisberger SG, Movshon JA. Tuning for spatiotemporal frequency and speed in directionally selective neurons of macaque striate cortex. J Neurosci. 2006;26: 2941–2950. doi:10.1523/JNEUROSCI.3936-05.2006

17. DeAngelis GC, Uka T. Coding of horizontal disparity and velocity by MT neurons in the alert macaque. J Neurophysiol. 2003;89: 1094–1111. doi:10.1152/jn.00717.2002

18. Ponce CR, Lomber SG, Born RT. Integrating motion and depth via parallel pathways. Nat Neurosci. 2008;11: 216–223. doi:10.1038/nn2039

19. Smolyanskaya A, Ruff DA, Born RT. Joint tuning for direction of motion and binocular disparity in macaque MT is largely separable. J Neurophysiol. 2013;110: 2806–16. doi:10.1152/jn.00573.2013

20. Born RT, Bradley DC. Structure and function of visual area MT. Annu Rev Neurosci. 2005;28: 157–89. doi:10.1146/annurev.neuro.26.041002.131052

21. Bradley DC, Goyal MS. Velocity computation in the primate visual system. Nat Rev Neurosci. 2008;9: 686–95. doi:10.1038/nrn2472

22. Neri P, Levi DM. Evidence for joint encoding of motion and disparity in human visual perception. J Neurophysiol. 2008;100: 3117–3133. doi:10.1152/jn.90271.2008

23. Salinas E, Abbott LF. Vector reconstruction from firing rates. J Comput Neurosci. 1994;1: 89–107. doi:10.1007/BF00962720

24. Huang X, Lisberger SG. Noise correlations in cortical area MT and their potential impact on trial-by-trial variation in the direction and speed of smooth-pursuit eye movements. J Neurophysiol. 2009;101: 3012–30. doi:10.1152/jn.00010.2009

25. Wong W, Seow N, Price C. Testing Neuronal Accounts of Anisotropic Motion Perception with Computational Modelling. 2014;9. doi:10.1371/journal.pone.0113061

26. Groh JM, Born RT, Newsome WT. How Is a Sensory Map Read Out? Effects of Microstimulation in Visual Area MT on Saccades and Smooth Pursuit Eye Movements. J Neurosci . 1997;17: 4312–4330. Available: http://www.jneurosci.org/content/17/11/4312.abstract

27. Lisberger SG, Ferrera VP. Vector averaging for smooth pursuit eye movements initiated by two moving targets in monkeys. J Neurosci. 1997;17: 7490–7502.

28. Quick RF. A vector-magnitude model of contrast detection. Kybernetik. 1974;16: 65–67. doi:10.1007/BF00271628

29. Churchland MM, Lisberger SG. Shifts in the population response in the middle temporal visual area parallel perceptual and motor illusions produced by apparent motion. J Neurosci. 2001;21: 9387–9402. doi:10.1016/j.bbi.2008.05.010

30. Chaisanguanthum KS, Lisberger SG. A neurally efficient implementation of sensory population decoding. J Neurosci. 2011;31: 4868–77. doi:10.1523/JNEUROSCI.6776-10.2011

31. Yang J, Lee J, Lisberger SG. The Interaction of Bayesian Priors and Sensory Data and Its Neural Circuit Implementation in Visually Guided Movement. J Neurosci. 2012;32: 17632–17645. doi:10.1523/JNEUROSCI.1163-12.2012.The

32. Jazayeri M, Movshon JA. Optimal representation of sensory information by neural populations. Nat Neurosci. 2006;9: 690–6. doi:10.1038/nn1691

33. Deneve S, Latham PE, Pouget a. Reading population codes: a neural implementation of ideal observers. Nat Neurosci. 1999;2: 740–745. doi:10.1038/11205

34. Jacobs AL, Fridman G, Douglas RM, Alam NM, Latham PE, Prusky GT, et al.

Ruling out and ruling in neural codes. Proc Natl Acad Sci U S A. 2009;106: 5936–41. doi:10.1073/pnas.0900573106

35. Osborne LC, Hohl SS, Bialek W, Lisberger SG. Time course of precision in smooth-pursuit eye movements of monkeys. J Neurosci. 2007;27: 2987–98. doi:10.1523/JNEUROSCI.5072-06.2007

36. Lisberger SG, Westbrook LE. Properties of visual inputs that initiate horizontal smooth pursuit eye movements in monkeys. J Neurosci. 1985;5: 1662–73. Available: http://www.ncbi.nlm.nih.gov/pubmed/4009252

37. Osborne LC, Lisberger SG, Bialek W. A sensory source for motor variation. Nature. 2005;437: 412–6. doi:10.1038/nature03961

38. Mukherjee T, Battifarano M, Simoncini C, Osborne LC. Shared Sensory Estimates for Human Motion Perception and Pursuit Eye Movements. J Neurosci. 2015;

39. Kowler E, McKee SP. Sensitivity of smooth eye movement to small differences in target velocity. Vision Res. Pergamon; 1987;27: 993–1015. doi:10.1016/0042-6989(87)90014-9

40. De Bruyn B, Orban G a. Human velocity and direction discrimination measured with random dot patterns. Vision Res. 1988;28: 1323–1335. doi:10.1016/0042-6989(88)90064-8

41. Stone LS, Krauzlis RJ. Shared motion signals for human perceptual decisions and oculomotor actions. J Vis. The Association for Research in Vision and Ophthalmology; 2003;3: 7. doi:10.1167/3.11.7

42. Berens P. CircStat : A MATLAB Toolbox for Circular Statistics. J Stat Softw. 2009;31: 1–21. doi:10.18637/jss.v031.i10

43. Shadlen MN, Britten KH, Newsome WT, Movshon JA. A Computational Analysis of the Relationship between Neuronal and Behavioral Analysis of the Relationship Responses to Visual Motion. 1996;76: 1486–1510.

44. Lee J, Yang J, Lisberger SG. Control of the Gain of Visual-Motor Transmission Occurs in Visual Coordinates for Smooth Pursuit Eye Movements. J Neurosci. 2013;33: 9420–9430. doi:10.1523/JNEUROSCI.4846-12.2013

45. Stephens GJ, Osborne LC, Bialek W. Searching for simplicity: Approaches to the analysis of neurons and behavior. 2011;108: 15565–15571. doi:10.1073/pnas.1010868108

46. Watamaniuk SN., Heinen SJ. Human smooth pursuit direction discrimination. Vision Res. Pergamon; 1999;39: 59–70. doi:10.1016/S0042-6989(98)00128-X

47. Keller EL, Heinen SJ. Generation of smooth-pursuit eye movements: neuronal mechanisms and pathways. Neurosci Res. Elsevier; 1991;11: 79–107. doi:10.1016/0168-0102(91)90048-4

48. Krauzlis RJ. Recasting the Smooth Pursuit Eye Movement System. J Neurophysiol. 2003;91: 591–603. doi:10.1152/jn.00801.2003

49. Grossberg S, Srihasam K, Bullock D. Neural dynamics of saccadic and smooth pursuit eye movement coordination during visual tracking of unpredictably moving targets. Neural Networks. 2012;27: 1–20. doi:10.1016/j.neunet.2011.10.011

50. Fuchs AF, Scudder CA, Kaneko CRS. Discharge Patterns and Recruitment Order of Identified Motoneurons and Internuclear Neurons in the Monkey Abducens Nucleus. JOURNALOFNEUROPHYSIOLOGY. 1988;60. Available: https://pdfs.semanticscholar.org/d54d/33395f195c03c69c34378928eef1bf0a59de.pdf

51. Lee J, Lisberger SG. Gamma Synchrony Predicts Neuron-Neuron Correlations and Correlations with Motor Behavior in Extrastriate Visual Area MT. J Neurosci. 2013;33: 19677–88. doi:10.1523/JNEUROSCI.3478-13.2013

52. Cohen MMR, Kohn A. Measuring and interpreting neuronal correlations. Nat Neurosci. 2011;14: 811–819. doi:10.1038/nn.2842.Measuring

53. Ponce-Alvarez A, Thiele A, Albright TD, Stoner GR, Deco G. Stimulus-dependent variability and noise correlations in cortical MT neurons. Proc Natl Acad Sci U S A. 2013;110: 13162–7. doi:10.1073/pnas.1300098110

54. Cohen MR, Maunsell JHR. Attention improves performance primarily by reducing interneuronal correlations. Nat Neurosci. 2009;12: 1594–600. doi:10.1038/nn.2439

55. Herrero JL, Gieselmann M a, Sanayei M, Thiele A. Attention-induced variance and noise correlation reduction in macaque V1 is mediated by NMDA receptors. Neuron. Elsevier Inc.; 2013;78: 729–39. doi:10.1016/j.neuron.2013.03.029

56. Josić K, Shea-Brown E, Doiron B, de la Rocha J. Stimulus-Dependent Correlations and Population Codes. Neural Comput. MIT Press; 2009;21:

2774–2804. doi:10.1162/neco.2009.10-08-879

57. Zylberberg J, Pouget A, Latham PE, Shea-Brown E. Robust information propagation through noisy neural circuits. Brunel N, editor. PLOS Comput Biol. Public Library of Science; 2017;13: e1005497. doi:10.1371/journal.pcbi.1005497

58. Zohary E, Shadlen MN, Newsome WT. Correlated neuronal discharge rate and its implications for psychophysical performance. Nature. Nature; 1994;370: 140–143.

59. Averbeck BB, Latham PE, Pouget A. Neural correlations, population coding and computation. Nat Rev Neurosci. 2006;7: 358–66. doi:10.1038/nrn1888

60. Fotowat H, Harrison RR, Gabbiani F. Multiplexing of Motor Information in the Discharge of a Collision Detecting Neuron during Escape Behaviors. Neuron. 2011;69: 147–158. doi:10.1016/j.neuron.2010.12.007

61. Huk AC. Multiplexing in the primate motion pathway [Internet]. Vision Research. 2012. pp. 173–180. doi:10.1016/j.visres.2012.04.007

62. Friedrich RW, Yaksi E, Judkewitz B, Wiechert MT. Processing of odor representations by neuronal circuits in the olfactory bulb. Annals of the New York Academy of Sciences. 2009. pp. 293–297. doi:10.1111/j.1749-6632.2009.04010.x

63. Sunkara A, DeAngelis GC, Angelaki DE. Joint representation of translational and rotational components of optic flow in parietal cortex. Proc Natl Acad Sci U S A. 2016;113: 5077–82. doi:10.1073/pnas.1604818113

64. Qian N, Freeman RD. Pulfrich phenomena are coded effectively by a joint motion-disparity process. J Vis. NIH Public Access; 2009;9: 24 1-16. doi:10.1167/9.5.24\r/9/5/24/ [pii]

65. Grunewald A, Skoumbourdis EK. The integration of multiple stimulus features by V1 neurons. J Neurosci. 2004;24: 9185–9194. doi:10.1523/JNEUROSCI.1884-04.2004

66. Dokka K, DeAngelis GC, Angelaki DE. Multisensory Integration of Visual and Vestibular Signals Improves Heading Discrimination in the Presence of a Moving Object. J Neurosci. 2015;35: 13599–607. doi:10.1523/JNEUROSCI.2267-15.2015

67. Drugowitsch J, DeAngelis GC, Klier EM, Angelaki DE, Pouget A. Optimal multisensory decision-making in a reaction-time task. Elife. 2014;2014: 1–19.

doi:10.7554/eLife.03005.001

68. Kim HR, Pitkow X, Angelaki DE, DeAngelis GC. A simple approach to ignoring irrelevant variables by population decoding based on multisensory neurons. J Neurophysiol. 2016; jn.00005.2016. doi:10.1152/jn.00005.2016

69. Serruya M, Hatsopoulos N, Fellows M, Paninski L, Donoghue J. Robustness of neuroprosthetic decoding algorithms. Biol Cybern. 2003;88: 219–28. doi:10.1007/s00422-002-0374-6

70. Delhaye BP, Schluter EW, Bensmaia SJ. Robo-Psychophysics: Extracting Behaviorally Relevant Features from the Output of Sensors on a Prosthetic Finger. IEEE Trans Haptics. 2016;9: 499–507. doi:10.1109/TOH.2016.2573298

71. Willett FR, Suminski AJ, Fagg AH, Hatsopoulos NG. Differences in motor cortical representations of kinematic variables between action observation and action execution and implications for brain-machine interfaces. 2014 36th Annual International Conference of the IEEE Engineering in Medicine and Biology Society. IEEE; 2014. pp. 1334–1337. doi:10.1109/EMBC.2014.6943845

72. Suminski AJ, Fagg AH, Willett FR, Bodenhamer M, Hatsopoulos NG. Online adaptive decoding of intended movements with a hybrid kinetic and kinematic brain machine interface. 2013 35th Annual International Conference of the IEEE Engineering in Medicine and Biology Society (EMBC). IEEE; 2013. pp. 1583–1586. doi:10.1109/EMBC.2013.6609817

73. Balasubramanian K, Vaidya M, Southerland J, Badreldin I, Eleryan A, Takahashi K, et al. Changes in cortical network connectivity with long-term brain-machine interface exposure after chronic amputation. Nat Commun. 2017;8: 1796. doi:10.1038/s41467-017-01909-2

74. Bair W, Zohary E, Newsome WT. Correlated Firing in Macaque Visual Area MT : Time Scales and Relationship to Behavior. 2001;21: 1676–1697.

75. Purushothaman G, Bradley DC. Neural population code for fine perceptual decisions in area MT. Nat Neurosci. 2005;8: 99–106. doi:10.1038/nn1373

76. Liu B, Macellaio M V., Osborne LC. Efficient sensory cortical coding optimizes pursuit eye movements. Nat Commun. Nature Publishing Group; 2016;7: 12759. doi:10.1038/ncomms12759

77. Gardner JL, Tokiyama SN, Lisberger SG. A population decoding framework for

motion aftereffects on smooth pursuit eye movements. J Neurosci. 2004;24: 9035–9048. doi:10.1523/JNEUROSCI.0337-04.2004

78. Li B, Peterson MR, Freeman RD. Oblique Effect: A Neural Basis in the Visual Cortex. J Neurophysiol. 2003;90: 204–217. doi:10.1152/jn.00954.2002

79. Cohen MR, Maunsell JHR. Using neuronal populations to study the mechanisms underlying spatial and feature attention. Neuron. Elsevier Inc.; 2011;70: 1192–204. doi:10.1016/j.neuron.2011.04.029

80. Priebe NJ, Lisberger SG. Estimating target speed from the population response in visual area MT. J Neurosci. 2004;24: 1907–1916. doi:10.1523/JNEUROSCI.4233-03.2004

81. Naselaris T, Prenger RJ, Kay KN, Oliver M, Gallant JL. Bayesian reconstruction of natural images from human brain activity. Neuron. Elsevier Ltd; 2009;63: 902–15. doi:10.1016/j.neuron.2009.09.006

82. Chen X, Beck JM, Pearson JM, Benson P, Rolls E, Paninski L. Neuron's eye view: Inferring features of complex stimuli from neural responses. Park IM, editor. PLoS Comput Biol. MIT press; 2017;13: e1005645. doi:10.1371/journal.pcbi.1005645

83. Samengo I. Information loss in an optimal maximum likelihood decoding. 2001; doi:10.1162/089976602317318947

84. Granot-Atedgi E, Tkačik G, Segev R, Schneidman E. Stimulus-dependent Maximum Entropy Models of Neural Population Codes. PLoS Comput Biol. 2013;9. doi:10.1371/journal.pcbi.1002922

85. Deneve S, Latham PE, Pouget A. Efficient computation and cue integration with noisy. 2001;4.

86. Antonopoulos CG, Srivastava S, Pinto SE d. S, Baptista MS. Do Brain Networks Evolve by Maximizing Their Information Flow Capacity? Bassett DS, editor. PLoS Comput Biol. Public Library of Science; 2015;11: e1004372. doi:10.1371/journal.pcbi.1004372

CHAPTER IV

General Discussion

The work in this thesis reveals that the brain encodes multiple stimulus features at every processing level despite potential ambiguity of the response because it is more efficient and benefits behavioral output. The first study shows that there is a benefit of multidimensional stimulus encoding - stimulus synergy - the magnitude of which depends on the dimensionality of the representation and the tuning bandwidth of the cells. We observe that the benefit accrues also to small populations whether their responses are assessed via pooled rate codes or via spike "words", indicating that there are myriad ways for the brain to take advantage of stimulus synergy. Smooth pursuit behavior also reaps the rewards of stimulus synergy, which suggests that estimates of direction and speed from MT are read out as a motion vector. The second study adds more evidence to that claim by showing that when the cortical readout to drive behavior in the visuomotor pathway estimates a motion vector, it more closely predicts errors in the sensory estimate of motion. Taken together, these two studies form a cohesive story that the visuomotor pathway manipulates retinal image motion as a motion vector instead of in its component features.

In addition, the results at the cellular and small population level can be extrapolated to other areas of the brain that also exhibit joint encoding. Analysis of two-dimensional tuning suggests that the case of separable tuning should exhibit the least stimulus synergy of any two-dimensional tuning curve. Therefore, the benefit of

joint decoding to circuits with non-separable tuning would be even greater than that with separable tuning. The apparent ubiquity of the benefit of stimulus synergy also suggests that it may facilitate the hierarchical nature of processing [1–3]. Stimulus features at the level of the sensory periphery are sequentially combined and transformed as they are processed through recurrent and intracortical connections. Since there is an informational benefit to each step of encoding and decoding jointly, and there are bandwidths that favor single-feature or higher-dimensional encoding, it leads us to believe that cortical circuits could tune those properties to flexibly manipulate sensory information through the cortical hierarchy.

Why sensory neurons are tuned to multiple stimulus features

In Chapter II, I applied information theoretic approaches to determine how information propagates through multiple levels of cortical circuitry in the condition of joint coding. I focused on direction and speed coding in the visual motion system, from encoding in extrastriate area MT to smooth pursuit eye movements. I also examined in depth what properties of MT neuron responses might affect joint encoding. I found that at each level of processing, the mutual information about the joint direction-speed vector exceeded that of the sum of the direction and speed separately, a condition we call stimulus synergy. This result indicates that there was a processing benefit to the system to treating the stimulus as a vector instead of as the two individual components.

An interesting finding that advanced what we know about joint coding was that the level of stimulus synergy can be manipulated by changing the variance of the

stimulus-conditioned count distribution. One way to manipulate the level of stimulus synergy, and thereby the coding advantage, is to change the bandwidth of the neurons. For model neurons encoding only 1-2 features, a narrow bandwidth was ideal. However, as the number of features increased, a wider bandwidth became more beneficial primarily because it increased the response entropy by increasing the variance of the spike count. Therefore, I was able to find the optimal number of features for MT neurons given the observed bandwidths of MT neurons for the two stimulus features we tested, determining that MT gains the most benefit from joint coding when it encodes 2-4 stimulus features [4,5]. I also increased stimulus synergy by making the two-dimensional tuning curve inseparable.

Stimulus synergy also persisted at the level of small populations of MT neurons, simulated units, spike words, and even in smooth pursuit eye movements, suggesting that it provides a reliable benefit to joint coding that is consistent across decoding methods, and that the benefit is evident in the precision of behavior. These results are encouraging, and combined with previous results from other areas and different stimulus features [6,7], they provide a theoretical justification for joint coding that should be applicable to any system with neurons tuned for more than one stimulus feature.

Correlations in smooth pursuit errors are predicted by vector decoding

Chapter III asks the question: since MT neurons encode multiple stimulus features jointly, what is the impact on behavior, and how is the cortical estimate of motion in MT read out? To answer this, I recorded smooth pursuit behavior in

macaques at a range of directions and speeds, and then calculated trial-to-trial errors in the direction, speed, and onset timing of the eye movements [8]. I then simulated responses from a biologically plausible MT population to those directions and speeds, and tested decoders that read out direction and speed either separately or together, as a motion vector. I found that errors in direction and speed are correlated for each target motion, and that only the vector decoder predicts these error correlations.

Correlations between direction and speed errors in smooth pursuit was a novel finding, and one that is puzzling. Although there can be ambiguity in how single neurons' jointly encoded responses would be read out, it is not necessarily intuitive that ambiguity should persist and affect population responses, despite evidence that adding sensory noise to either direction or speed is reflected in the variance of both direction and speed of eye movements [9]. Nevertheless, the population simulations show a significant difference between the vector and separate decoders, illustrating that decoding a joint representation is the only way to recapitulate what is observed from behavior.

These results make a strong prediction that adds to the existing decoding literature, which primarily focuses on one-feature decoding from neural populations that are known to encode multiple features. Most decoders were only tested to match features of the stimulus for which they were created and tuned, so there is a wealth of further analysis to be done to determine which types of decoders maintain their performance and behavioral predictions when faced with decoding multiple features simultaneously. It would also be interesting to find out more about what cortical

circuits may select to decode single stimuli from a multidimensional representation, and what constraints that places on the decoding mechanism and readout.

Concluding remarks

This work focused on the responses of extrastriate area MT and the motion processing pathway to describe processing patterns that can be generalized to other cortical areas. In Chapter II, I found that single MT neurons encode more information about a joint direction-speed vector than about direction and speed separately, and that this stimulus synergy can be manipulated by tuning bandwidth and separability. MT neurons appear to be tuned such that they maximize their stimulus synergy by reliably encoding 2-4 features, which seems to be approximately the number of features MT neurons actually encode reliably. Finally, I find that stimulus synergy is apparent in the readout of the MT population, as assessed by pooled rate code, by spike "words", and by smooth pursuit eye movements. These results strongly suggest that MT responses are both encoded and decoded as a motion vector.

In Chapter III, these claims are further supported by observations of correlated variability between direction and speed of smooth pursuit eye movements, which are known to be a faithful representation of the readout of MT. These direction-speed error correlations would occur if MT responses were decoded as a vector, and indeed a vector decoder mirrors these results. I propose that stimulus synergy underlies cortical coding on a widespread scale, as the informational benefit would be available to most, if not all, types of joint coding. A useful future direction would therefore involve wider testing of cortical areas in different modalities and various

levels of the cortical hierarchy to verify our results, as there is extensive heterogeneity in cortex and cortical responses.

References

1. Zeki S, Shipp S. The functional logic of cortical connections. Nature. Nature Publishing Group; 1988;335: 311–317. doi:10.1038/335311a0

2. Ponce CR, Lomber SG, Born RT. Integrating motion and depth via parallel pathways. Nat Neurosci. 2008;11: 216–223. doi:10.1038/nn2039

3. Antolík J, Hofer SB, Bednar JA, Mrsic-flogel TD. Model Constrained by Visual Hierarchy Improves Prediction of Neural Responses to Natural Scenes. 2016; 1–22. doi:10.1371/journal.pcbi.1004927

4. Zohary E. Population coding of visual stimuli by cortical neurons tuned to more than one dimension. Biol Cybern. 1992;66: 265–72. doi:10.1007/BF00198480

5. Brown WM, Bäcker A. Optimal neuronal tuning for finite stimulus spaces. Neural Comput. 2006;18: 1511–1526. doi:10.1162/neco.2006.18.7.1511

6. Grunewald A, Skoumbourdis EK. The integration of multiple stimulus features by V1 neurons. J Neurosci. 2004;24: 9185–9194. doi:10.1523/JNEUROSCI.1884-04.2004

7. Smolyanskaya A, Ruff DA, Born RT. Joint tuning for direction of motion and binocular disparity in macaque MT is largely separable. J Neurophysiol. 2013;110: 2806–16. doi:10.1152/jn.00573.2013

8. Osborne LC, Lisberger SG, Bialek W. A sensory source for motor variation. Nature. 2005;437: 412–6. doi:10.1038/nature03961

9. Osborne LC, Lisberger SG. Spatial and temporal integration of visual motion signals for smooth pursuit eye movements in monkeys. J Neurophysiol. 2009;102: 2013–25. doi:10.1152/jn.00611.2009